Experimental Investigation and Parametric Optimization of Tungsten Inert Gas Welding Process Parameters during Welding of Similar and Dissimilar Metals

Anteneh Teferi Assefa

A Thesis Submitted to the Department of Mechanical Engineering

School of Mechanical, Chemical, and Materials Engineering

Presented in Partial Fulfillment of the Requirement for the Degree of Master's in Manufacturing Engineering

Office of Graduate Studies
Adama Science and Technology University

June, 2022
Adama, Ethiopia

Experimental Investigation and Parametric Optimization of Tungsten Inert Gas Welding Process Parameters during Welding of Similar and Dissimilar Metals

Anteneh Teferi Assefa

Advisor:
Dr. G. M. Sayeed Ahmed (Ph.D.)

A Thesis Submitted to the Department of Mechanical Engineering
School of Mechanical, Chemical, and Materials Engineering

Presented in Partial Fulfillment of the Requirement for the Degree of Master's in Manufacturing Engineering

Office of Graduate Studies
Adama Science and Technology University

June, 2022
Adama, Ethiopia

DECLARATION

I declare that this thesis entitled "**Experimental investigation and Parametric Optimization of tungsten inert gas welding process parameters during welding of similar and dissimilar metals**" is my original work. That is, it has not been submitted for the award of any academic degree, diploma or certificate in any other university. All sources of materials that are used for this thesis have been duly acknowledged through citation.

Anteneh Teferi Assefa	______________	______________
Name of Student	Signature	Date

RECOMMENDATION

I, the major advisor of this thesis, hereby certify that I have read the revised version of the thesis entitled "Experimental investigation and Parametric Optimization of tungsten inert gas welding process parameters during welding of similar and dissimilar metals" prepared under my guidance by Anteneh Teferi Assefa. Submitted in partial fulfillment of the requirements for the degree of Mater's of Science in Manufacturing Engineering.

Therefore, I recommend the submission of a revised version of the thesis to the department following the applicable procedure.

Dr. G. M. Sayeed Ahmed	_____________	_____________
Main Advisor	Signature	date

APPROVAL SHEET

I, the advisor of the thesis entitled "Experimental investigation and Parametric Optimization of tungsten inert gas welding process parameters during welding of similar and dissimilar metals" developed by Anteneh Teferi Assefa. hereby certify that the recommendation and suggestions made by the board of examiners are appropriately incorporated into the final version of the thesis.

Dr. G. M. Sayeed Ahmed	____________	____________
Major Advisor	Signature	Date

We, the undersigned, members of the Board of Examiners of the thesis by Anteneh Teferi Assefa have read and evaluated the thesis entitled "Experimental investigation and Parametric Optimization of tungsten inert gas welding process parameters during welding similar and dissimilar metals" and examined the candidate during the open Défense. This is, therefore, to certify that the thesis is accepted for partial fulfillment of the requirement of the degree of Master of Science in Manufacturing Engineering.

Dr. Habtamu Beri	____________	____________
Chairperson	Signature	Date
Dr. Melesse Werkineh	____________	____________
Internal Examiner	Signature	Date
Dr. Desalegn Wegasso	____________	____________
External Examiner	Signature	Date

Finally, approval and acceptance of the thesis is contingent upon the submission of its final copy to the Office of Postgraduate Studies (OPGS) through the Department Graduate Council (DGC) and School Graduate Committee (SGC).

Mr. Girmachew Ashagrie	____________	____________
Department Head	Signature	Date
____________________	____________	____________
School Dean	Signature	Date
____________________	____________	____________
Office of Postgraduate Studies, Dean	Signature	Date

ACKNOWLEDGMENT

I've had a lot of ups and downs in the process of finishing this thesis. I've met a variety of generous people, battled a lot, and triumphed in the face of adversity. And it was only because of GOD that I was able to have this experience and learn these life lessons. So, first and foremost, I'd like to express my gratitude to the almighty GOD for his unending blessings and lessons in my life. Dr. G.M. Sayeed Ahmed my thesis advisor, deserve special thanks for his advice, support, and understanding throughout the thesis.

Furthermore, I want to thank Dr. Moera Gutu for providing me with excellent advice and important recommendations and direction during my studies whenever I needed it, and for making me feel hopeful about finishing this thesis.

I also owe a debt of gratitude to Mr. Muluken, and Mr. Tewodros for their relentless advice, suggestion, and support during working at the Center of Excellence for Engineering and MIDI. Furthermore, Mr. Habtamu A. deserves my gratitude for his support and advice during working at Ethiopian Conformity Assessment Enterprise (ECAE).

My heartfelt thanks and affection go out to my one and only Mrs. Senait T. for her unwavering support and understanding. I thank you so much and appreciate you for all those restless days and sleepless nights you spent supporting me. You've been my inspiration throughout this, and I'm confident you'll be my pillar for the rest of my life.

Finally, I would like to acknowledge all my families and friends, for their love, encouragement, appreciation, and endless support which made me stronger each day.

Thank you all

TABLE OF CONTENTS

LIST OF TABLES

LIST OF FIGURES

ACRONYMS

AC	Alternating current
AISI	American Iron and Steel Institute
ANOVA	Analysis of Variance
ASTM	American Society for Testing and Materials
CDI	Composite desirability index
IDI	Individual desirability index
DC	Direct current
DOE	Design of Experiment
GFR	Gas flow rate
GTAW	Gas tungsten arc welding
HAZ	Heat affected zone
HRB	Rockwell hardness
HV	Vickers Hardness
MGB	Migrated grain boundaries
MS	Mild steel
MSS	Mean Sum of Square
OA	Orthogonal Array
S/N	Signal to Noise Ratio
SEM	Scanning electron microscopy
SS	Stainless steel
SST	Total sum of squares
SSTR	Treatment sum of squares
TIG	Tungsten inert gas
TS	Tensile strength
UTM	Universal testing machine
UTS	Ultimate tensile strength

ABBREVIATIONS

A	Ampere
b	width
d	diameter
Dg	composite desirability
di	individual desirability
et.al.	And others
L	Length
t	Thickness

ABSTRACT

Gas tungsten arc welding is one of the most extensively used procedures for joining aluminium alloys, nickel alloys, stainless steel, mild steel, and other metal. The goal of this study was to see how different TIG process parameters (welding current, gas flow rate, root gap, and filler materials) affecting the mechanical properties (tensile, hardness, and flexural strength), bead geometry and microstructural properties of stainless steel 316 (similar) and stainless steel 316 and AISI 1020 (dissimilar), welded metals. The experimental plan was done using Taguchi L16 orthogonal array. These SS316 and AISI 1020 materials were commonly used in industrial applications such as steam power generation, automotive engineering, biomedical engineering, dairy industry, petrochemical engineering, and general engineering products. As a result, the above TIG welding parameters for weld quality of similar and dissimilar welds were optimized in this study using Taguchi-based desirability function analysis and other statistical tools like Analysis of Variance (ANOVA) techniques. From the result it was observed that, the microstructure of weld metal of similar and dissimilar joints consists of a delta ferrite network in an austenite matrix using filler wire ER-316L and ER-309L respectively. The tensile strength experimental results revealed that welding current, followed by GFR, was a highly significant parameter. Hardness result show that the welding current followed by filler metal has a significant effect for similar and welding current followed by root gap for dissimilar welding. Flexural strength experimental result reveals that the GFR has higher effect followed by welding current for similar and welding current followed by filler type for dissimilar welding. The experimental results show that the welding current has a significant impact on the bead width of welded specimens followed by the root gap. From the DFA multi response optimization result it was shown that the similar and dissimilar weld samples was optimized. Percentage improvement of similar welded metals was 8.41% with a parametric setting of (A2B4C3D2). Also, for dissimilar weld the percentage improvement of 22.90% with a parametric setting of (A2B4C3D2). Finally, the confirmation test result reveals that the experimental test result in agreement with predictive optimum setting result with minimum positive validation error (0.622%) for similar and (3.42%) for dissimilar welding.

Keywords: Multi-response optimization, TIG welding, Mild Steel, Weld quality, Stainless Steel, Taguchi method

CHAPTER - 1

INTRODUCTION

1.1. Background

Welding is a system in which two similar or dissimilar metals or nonmetals are joined by applying pressure or non-pressure. It is exceptionally utilized for becoming a member of metal components in manufacturing processes. When there are wishes to be part of portions together or more substantial lengths of trendy sections are required to fabricate the preferred structure. Generally, welding is the technique of joining a member of metals and plastics besides using adhesives or fasteners. Welding is the method of applying heat and pressure to the surface of unique substances such as polymers, metals, and alloys to manipulate the everlasting joining of the process. Gas tungsten arc welding (GTAW), also known as tungsten inert gas welding (TIG), is an arc welding process that creates an electric arc using a non-consumable tungsten electrode. It was created for the duration of WWII. Welding of difficult-to-weld materials like Aluminum (Al) and Magnesium (Mg) became possible because of this discovery (Miller Electric Mfg, 2013).

Nowadays, it is typically used for welding hard-to-weld metals such as Stainless Steel, Magnesium, Aluminum, and Titanium. TIG welding is most, in many instances, used to weld thin sections. Tungsten Inert Gas Welding of dissimilar substances such as stainless steel and mild metal is attainable to keep appropriate mechanical and metallurgical properties. TIG welding is handy to control, fumeless, and spatter less clean method wants minimal finishing or now and again no finishing. TIG welding gives outstanding welding with the coalescence of heat generated through an electric arc between a tungsten electrode and the steel (Karunakaran & Balasubramanian, 2011). Shielding gases like argon or helium protect the weld area. TIG welding process is used to weld material with a non-consumable tungsten electrode. The electrode is either made of pure tungsten or tungsten blended with small amounts of oxides (thorium oxide, zirconium oxide) to enhance the arc's steadiness and make it less complicated to strike. The electrode is linked to an imperative energy source, and shielding fuel is also employed via a welding gun (M. I. Rani & Marpu, 2012).

The workpieces to be joined are melted at the faying surfaces during welding, and a permanent joint can be formed after solidification. In some circumstances, a filler material creates a liquid weld pool that solidifies to establish a strong link between the components. The weldability of a material is influenced by metallurgical changes during welding, such as variations in hardness in the weld zone due to rapid solidification, the degree of oxidation induced by materials reacting with atmospheric oxygen, and the tendency of crack formation at the joint position. He and Ar are employed as shielding gases since they do not react chemically, and the purpose of inert gas is to keep the welding area free of contaminants (Senthil Kumar et al., 2007).

1.2. Overview of TIG welding

Power is supplied from a power source to a tungsten electrode fitted into the welding torch in TIG welding. An electric arc can be created between a tungsten electrode and a workpiece using this power, as shown in Fig 2.

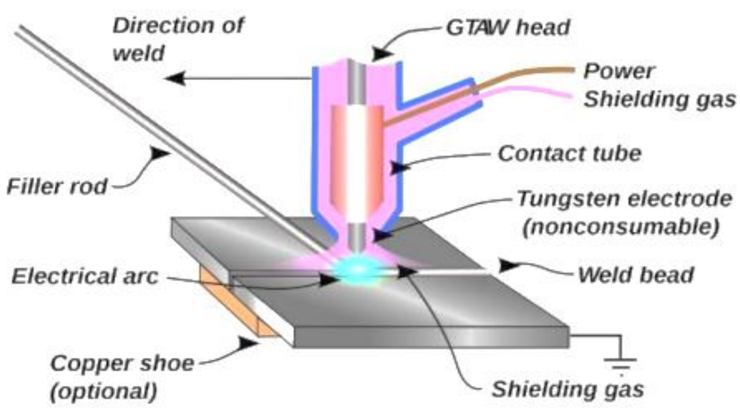

Figure 1.1 Principle of TIG Welding (R. Kumar et al., 2017)

The electric arc may reach temperatures of up to 20,000 degrees Celsius, and this heat can be focused to melt and attach pieces with or without filler. Tungsten electrodes are typically available in diameters ranging from 0.5 to 6.4 mm and lengths ranging from 150 to 200 mm. The current-carrying capability of each electrode size in a DC power source is determined by electrode polarity. For welding stainless steel, direct current with a negative electrode was employed, while a direct current with a positive electrode is far less common and utilized only seldom. There is often a need to study the effect of process parameters while fabricating stainless steel structures and welding stainless steel to low-alloy steels by welding to each other metals either in heat-related systems or space organization, etc., by considering different kinds of process parameters.

TIG welding can also be used for welding with manually applied fillers, like gas welding. TIG welding mechanical tools are used in applications such as connecting tubes and welding tubes to final plates of heat exchangers. These automatic welding tools can incorporate many advanced features, including the mechanical supply of filler wires. This method has the following characteristics:

- Stable ARC
- Excellent control of weld results

The main uses of TIG welding are light metal weldings such as aluminum and magnesium alloy, copper welding, and stainless-steel welding. It is also suitable for welding connections and positions, except for lead and zinc. Additionally, TIG welding is more suitable for thin materials from about 0.5 nm to about 3 nm. In contrast, TIG welding cannot compete with methods such as short arc welding in terms of productivity (Weman, 2011).

1.2.1. Equipment of TIG welding

The main required types of equipment for TIG welding are as follows:

- Power
- High frequency, which is a generator for arc ignition
- Welding gun
- Control equipment
- Shielding gas

1.3. Joining method of dissimilar metals

The intricate functionality of many current industrial applications necessitates the use of different metals for connecting. Multiple material combinations are being employed for various goods as the maker seeks to minimize production and operational costs, improve mechanical and thermal qualities, and create lightweight solutions for sectors such as shipping, aviation, and automobiles (Kah & Jukka Martikainen, 2013). Dissimilar materials can be joined using a variety of approaches. The following are the key approaches employed in industrial applications and in creating the research topic:

a. Fusion,

b. Pressure welding

a. Pressure Welding Methods

Welding takes place at a temperature lower than the melting point of the metal being welded. External pressure can be used to solid-weld the two components together, as long as the pressures are high enough to generate spindle reactions in the surfaces of the two parts to be linked (Lu et al., 2010). For welding, dissimilar metals, friction welding, cold welding, gas welding, pressing, explosion welding, ultrasonic welding, and other methods are utilized.

b. Fusion Welding methods

Melting the edges of the components to be soldered is used to apply welding, which is done without the use of external pressure (Trewiler, 2006; Walak et al., 1992). As shown in Figure 1.2, this group includes various traditional fusion welding methods such as gas tungsten arc welding (GTAW), shielded metal arc welding (SMAW), gas metal arc welding (GMAW), submerged arc welding (SAW), and flux-cored arc welding (FCAW), all of which can be used to weld dissimilar metal combinations. However, fusion welding of various metals comes with a slew of challenges (Chaudhari et al., 2020; Kah & Jukka Martikainen, 2013). These issues stem from metallurgical incompatibility issues, such as the production of brittle phases, the separation of high and low melting phases due to chemical mismatch, and potentially others.

1.4. Research motivation

In today's production industry, quality is the most important factor. According to some sources, quality is defined as client satisfaction when delivering a purchased product. Product quality in various application areas is determined by the requirements attained in the product that meet your functional needs. In the welding area, welding quality has a significant impact on welded metals' mechanical and microstructural properties. On the other hand, the weld's quality is determined by the welding process parameters. Many process parameters can control the mechanical characteristics, weld bead shape, weld chemistry, and metallurgical aspects of the generated weld in a complicated way, resulting in direct or indirect impacts (Greyjevo & Metodo, 2009). Welding process factors, in general, have a significant impact on mechanical and microstructural qualities, as well as weld bead shape. Various researchers experimented by considering some common process parameters such as welding current, welding voltage, speed, and gas flow rate. Other process variables, such as filler wire and root gap, however, have a considerable impact on mechanical and microstructural qualities. Because the chemical and physical properties of materials differed when the base metals to be welded were dissimilar metals, the filler metals utilized compromised this difference. The gap between the roots was also a key determinant in weld penetration, which has an impact on mechanical properties. So, design and production flexibility are substantially needed by the possibility to design new products utilizing various metal and alloy combinations (filler wires). And optimizing the finished properties of a product, such as mechanical, microstructural, and corrosion and heat resistance, while managing its cost, are main motivations for similar and dissimilar metal welding.

1.5. Statement of the Problem

Welding different materials, such as stainless steel and carbon steel, can be more cost-effective than producing a design entirely out of stainless steel because stainless steel is expensive (Kah & Jukka Martikainen, 2013). Welding of multiple substances is commonplace at complementary strength-era facilities like petrochemical refineries and many mining and mineral processing plants. In these applications, carbon metal (mild steel) minimizes the costs of setting up and running these manufacturing operations. When the environment or the service condition permit, this metal can be welded to a considerably less expensive carbon metal by considering weldability and process factors. Weldability determines the welding process parameters and assesses the final weld's suitability for various materials. To be say the weld has a quality or defect free first the process parameters used to be known, because the quality of the weld depending on the parameters **(**Flagg & Krebs, 2004). Because of its high chromium content, stainless steel requires more care in weldability than other steels. Since it needs controlled heat and shielding gas. Austenitic stainless steels, such as (S31600), are the most weldable, but their high coefficient of thermal expansion makes them especially prone to distortion. Stainless steel also has a thermal conductivity of about half that of carbon steel. When welding these different materials, differences in thermal expansion and thermal conductivity coefficient can pose problems (SMI, 2022). This problem can be overtaken (by using a proper filler metal for both base metals.

In light of the issues mentioned above, the goal of this study is to investigate the TIG welding of SS316 stainless steel grade (similar material) and SS316 with AISI 1020 mild steel (dissimilar material) to overcome the issues above when welding similar and dissimilar metals for the prediction and optimization of weld quality (mechanical and microstructure properties, and weld bead geometry) of the joint.

1.6. Research Questions

a) What is the optimum welding parameter setting for welding similar and dissimilar metals and what are the most significant TIG welding parameters?
b) What does the weldment metallography look like for similar and dissimilar metals?

1.7. The objective of the study

1.7.1. General objective

The objective of the present research work is to join S31600 Stainless steel and S31600 with AISI 1020 mild sheets of steel similar and dissimilar metals by TIG (Tungsten Inert Gas) and investigate the influence of process parameters on the weld joint.

1.7.2. Specific objective

The following specific objectives are formulated to get the stated general aim of the study:

- Investigation of welding quality and welding defects using fluid penetrant methods.
- Determination of the most influential controlling parameter.
- Characterize and Analysis of welding metallography (OM and SEM).
- Investigation of welded joint mechanical properties (tensile, hardness, flexural bending)
- Weld bead geometry investigation (bead width).
- Multi-Response optimization at optimum Parametric Setting

1.8. Significance of the Study

Establishing a TIG welding investigation to determine the effect of welding parameters on mechanical properties in a welding operation of similar and dissimilar metals with quality welded joint results in the product having excellent mechanical properties (tensile strength, hardness, and flexural bending), resulting in increased product lifetime and profit.

The thesis has the following significance:

- This study proposes a new method (back purging gas) for conducting an experimental analysis and parametric optimization of tungsten inert gas welding parameters while welding similar (SS316) stainless steel and dissimilar (SS316 with MS-AISI 1020) metals.
- The research focuses on bits that can assist preserve greater mechanical qualities in joints, increase product lifetime, improve weld quality, and eliminate welding flaws in welded joints.

Finally, the thesis can be used as an input for defect-free weld, resulting in improved weld quality in strength and hardness.

1.9. Scope and limitation of the Study

The research was focused on TIG welding equipment and its associated welding parameters and the effect of welding current, root gap, gas flow rate, and filler metal type during the welding of Similar and dissimilar metals. Mechanical properties such as tensile strength (UTS), hardness strength (HV or HRB), and flexural bending strength were utilized to analyze the TIG welded metals. Finally, this research examines and optimizes the effect of welding parameters on the welding quality.

- This study focused on the experimental investigation of TIG welding parameters for welding quality during the welding of similar and dissimilar metals.
- Welding quality and welding defects were determined using visual inspection and fluid penetrant technique (PT).
- By identifying the most significant welding parameters and optimizing which parametric set better welding quality was achieved during welding similar and dissimilar metals.
- Metallographic analysis using OM and SEM microstructures of similar and dissimilar metals welded joints.

Limitation: Other welding characteristics such as welding speed and root metal thickness are not considered. Because some TIG welding machines in Ethiopia are manual or semi-automatic, speed control is difficult. The other issue is that stainless steel is quite expensive to buy in terms of thickness, and as the thickness of mild steel increases, the demand for preheating increases.

1.10. Structure of the Thesis

The thesis consists of five chapters:

Chapter One: Begins with an intention to introduce the overall background of the study, an overview of TIG welding, dissimilar metals welding techniques, research questions, objectives, the problem statement, the significance of the study, and scopes of the study.

Chapter Two: addresses the detailed science behind TIG welding and rules followed during welding similar and dissimilar metals and different optimization techniques by reviewing different kinds of literature. Finally, the summary of the literature and the research gap is described.

Chapter Three: The experimental specifics, such as the materials utilized for the experiment, the experimental protocols, the equipment used, and the methodology that fulfilled the study's aims, are briefly discussed in this chapter.

Chapter Four: The results and discussion of the experimental values are covered in this chapter. It investigates the impact of process parameters on the quality of TIG welds between similar and dissimilar metals. And keeping the parameters settings in optimum condition.

Chapter Five: It is the final chapter that summarizes the research done and proposed the recommendation and future work for further studies.

CHAPTER - 2

LITERATURE REVIEW

2.1. Introduction

A literature review is an essential component of any research project. The effect of process factors on weld quality is explained in a massive volume of material available in journals and books. This chapter examines the research works by addressing different welding methods, studies on TIG welding of stainless steel and purpose of back purging gas for stainless steel, dissimilar weld, characterization of weld, parameter optimization, studies on mechanical properties, studies on weld geometry, and the heat effect, to know and get the work direction.

2.2. Studies on different welding methods

According to the findings of several researchers, the weld quality varies depending on the welding process used.

2.2.1. Gas Tungsten Arc Welding (GTAW)

Inert tungsten gas (GTAW) is another name for GTAW (TIG). A Tungsten electrode is used to produce the weld, and the electrode used doesn't get consumed. The arc that forms between the workpiece and the electrode melts the metals that will be welded together to produce the weld pool (Jeyaprakash et al., 2015). The thickness of the base metals determines whether filler material is used. To avoid oxidation and safeguard the weld pool, argon or helium, or a combination of both, is employed (Balaji et al., 2012). It's best for welding narrow portions because it requires less heat and can be done on a variety of metals.

2.2.2. Gas Metal Arc Welding (GMAW)

The metal-inert gas (MIG) welding technique is another name for GMAW. Metals are melted using an electric arc created between an electrode (filler metal) and base metals in GMAW welding. During the solidification of the molten weld pool, the gas is used to shield the weld from undesired air entrapment. Argon and helium are utilized as inert gases to safeguard the arc and the molten weld pool. Because of the inert shielding gas, the process is spotless, and the weld area is uniform and slag-free (Nagesh & Datta, 2002).

2.2.3. Shielded Metal Arc Welding (SMAW)

This welding process uses a flux-coated electrode to join the metals, and heat is generated by delivering an electric current through the electrode. A gaseous barrier protects the molten metal from atmospheric air, and the electrode is protected by slag, resulting in a clean weld. SMAW welding is primarily used to join high-strength steels that are prone to hydrogen cracking (Nagesh & Datta, 2002)

2.2.4. Frictional Welding

The edges of the two pieces are connected to the heat that is heated by the surface friction of these two pieces when one rotates in contact with the other, which is fixed with an increased axial pressure force, and the welding process is completed once a certain speed of rotation and pressure is reached. Pre-combustion chambers in diesel engines, rotary assemblies, coupling rods, cylinders, axial couplings, motor vehicle front axles, injection shafts, and other applications all require friction welding.

- Following are some pieces of the literature surveyed that discuss a comparative study of different welding techniques.

Msomi & Mabuwa, (2020) studied the bending and tensile strength of a friction stir processed TIG-welded AA5083-H111 joint in an experimental study. The TIG-welded (unprocessed) joint was compared to the FSW processed jointly. Tensile, bending, and microstructure tests were used to assess the joint's quality. As a result, the processed joints' tensile characteristics were found to be higher than the unprocessed joints. The processed joint has a higher bending strength than the unprocessed joint. For both treated and unprocessed joints, the flexural strength of the face was found to be higher than the root of the joint. The microstructural analysis revealed that the coarse grains dominated the friction stir in the unprocessed joint, while the refined grains dominated the friction stir.

The Effects of Welding on the Fatigue Behavior of Commercial Aluminum AA-1100 Joints were investigated by (Uthayakumar et al., 2018). They concluded that the FSW joint had superior qualities over MIG and TIG joints. The yield strength of FS welds is 91.30 percent of the base metal, while MIG and TIG welds are 90.7 percent and 88.9 percent, respectively. The yield strength of the FSW welding method is also found to be 1.3 percent higher than that of MIG and 2.4 percent higher than that of TIG. In addition, several mechanical qualities are superior to those of MIG and TIG welding. The FSW process has roughly 88.88 percent of the base metal life, the TIG process has 77.75 percent, and the MIG method has 66.6 percent of the base metal life in the fatigue test for the notched joints. The FSW has an 11.1 percent improvement over TIG and a 22.2 percent improvement over MIG.

A. K. Singh et al., (2017) investigated a review on Techniques to Improve TIG Weld Penetration. The examined studies are primarily concerned with improving weld penetration and quality while considering the effects of various types of welding procedures such as ATIG (Activated Flux TIG), FBTIG (Flux Bounded TIG), and PCTIG (Pulsed Current Tungsten Inert Gas). The researchers concluded that ATIG (Activated flux TIG) welding achieves significantly better penetration than standard TIG welding. Full penetration is also achieved using FBTIG (Flux Bounded TIG) welding. The disadvantage of this method is that as the distance between the flux coatings on top of the plates across the weld joint grows, so does the weld penetration. When PCTIG (Pulsed Current TIG) welding, it has been discovered that a higher peak current causes higher ripples, resulting in deeper weld penetration. The choice of Welding Parameter by Proper is also crucial.

Naik & Reddy, (2016) used Taguchi's Orthogonal array experimental design on Duplex Stainless Steel (2205) to investigate the Experimental Analysis of TIG Welding and Comparison between A-TIG and TIG on Duplex Stainless Steel (2205). They found the effect of various input parameters on specific performance measures. He concludes that time and current are important factors in tensile strength; tensile strength is highest at 180 seconds and 250 amps, although the gas flow rate is low. The current has a major impact on hardness, and it is complete at 250A, 150 sec, and 6L/min.

In a review of various welding techniques, (Kazi et al., 2015) found that when the speed and current rise, the heat-affected zone increases as well. He also determined that MIG welding has a higher hardness than TIG welding and that MIG welding has a higher ductility than TIG welding based on their findings. TIG welding specimens can withstand higher loads, yield stress, and tensile strength than conventional specimens. According to the findings, all TIG welding parameters are superior and optimal for steel.

Patel & Patel, (2014) conducted an experimental study on The Effect of Activating Flux in TIG Welding and found that most welding parameters, such as welding flux, welding current, welding speed, and depth to width ratio, are commonly utilized in research. TIG welding can be done on a variety of materials, including MS, Titanium alloys, brass, carbon, and stainless steel. He also uses theoretical equations to determine welding penetration, depth to width ratio, and welding joint strength, which he then measures empirically with the use of various input parameters. The austenitic type of stainless steel with grade E321 was chosen as the result of experimental work and the research of several journals, and fluxes were $SiO2$ and $TiO2$.

Aravinth et al., (2012) conducted a study on TIG Welding Process Failure Mode and Effect Analysis. Porosity is the most dangerous fault in TIG welding, according to a Criticality Study, and incorrect shielding is also a serious problem. As a result, before welding, corrective action should be taken, and proper maintenance should be performed for practical welding.

2.3. Studies on TIG Welding of Stainless Steel

Various trials and research on the TIG welding technique on stainless steel have been conducted, considering the grades and process parameters. Following are some research and experimental experiments.

M. Naga Swapna et al., (2021) used the DOE approach to investigate GTA welded SS316L plates with shape memory alloy as a filler material. They used process factors including welding current, welding speed, and tip plate distance. Tensile strength and ferrite number are the response variables, and the model is optimized with the help of a design expert. Finally, it was discovered as a result of the study. Tensile strength was shown to increase as welding speed and welding current (amp) were increased. With increased welding speed (mm/min) and welding current, the ferrite number was shown to decrease. The 10 best solutions and stabilizing runs demonstrate the optimization of the chosen design. Between the model and the test runs, the average error percentage was lower than the similarity.

Saha, (2020) evaluated the effect of TIG welding parameters on welded joints made of stainless steel SS304, considering process parameters including current, gas flow rate, speed, and filler rod diameter. The TAGUCHI method was used to plan the experiment, and the quality of the weld was assessed using tensile, hardness, and depth of penetration tests. The ideal parameter combinations for ultimate tensile strength and hardness differed only in terms of current for optimum UTS, according to the findings. It was necessary to use a greater current (180 amp) a lower current value (150 amp) was, on the other hand, ideal for optimum hardness. However, higher current resulted in improved DOP (Depth of penetration), hence the best UTS combination (A3B3C2D3) was chosen. Using optimum welding settings, the tensile strength improved from 515 MPa to 556 MPa, resulting in a 10.56 percent increase in joint strength. Using optimum welding settings, the hardness improved from 92 HV to 100 HV, a 7.36 percent increase in hardness.

Sanjay Kumar et al., (2019) used ANOVA to experiment with the effect of welding parameters on TIG-welded joints. The influencing parameters were (Voltage, Current, Gas Flow, and Root Gap), with AISI 304 stainless steel as the basis material. The test was carried out using the butt-welded TIG welding process, and the tensile strength of the weldment was used to determine the weld's final quality. The results of the test revealed that:

- ✓ The tensile test demonstrates that the UTS and elongation of all the samples are comparable to the base metal. As a result, the resulting joint has good mechanical qualities.
- ✓ The response value graph shows that current is the most influential parameter in the case of tensile strength. The highest tensile strength was attained at the highest current level (80 A). The voltage at its first level, i.e. (50 V), is the next moving issue, followed by the Root gap (1.5mm R) at its second level, and GFR (18 liter/min) as the fourth satisfying issue.

Mandavia, (2017) used the Design of Experiment Taguchi approach to explore the Experimental Investigation of TIG Welding for Stainless Steel 304, considering process parameters such as current, groove angle, and welding speed. The study's output reaction was Distortion. The welding speed is the most influential parameter for distortion, followed by groove angle and current, according to the results.

Rohit et al., (2017) conducted an Experimental Analysis of TIG Welded 304 Stainless Steel Using the Artificial Intelligence Tool, concluding that the research reveals the successful use of AI-based on the Adaptive Neuro-Fuzzy Inference System for the prediction of the tensile strength of TIG-welded AISI 304 stainless steel specimens, with the obtained results indicating the accuracy over another prediction concept. The specimen's average tensile strength is 638. 5185MPa. However, given the comparable process parameters of voltage 12V, welding current 50A, gas flow rate 12litre per meter, and speed 1mm per minute, the maximum tensile strength obtained is 664MPa.

By selecting current, welding voltage, and gas flow rate as welding parameters, (Jeevahan et al., 2016) evaluated the effect of welding current, voltage, and gas flow rate on welding properties of TIG-welded SS316 material. Tensile, hardness, and impact tests are used to assess the quality of welded joints. Finally, altering the welding current, welding voltage, and gas flow rate improves the welding properties.

- Tensile strength is increased at 160-200 amps, 40-50 volts, and 4-5 L/min.
- Hardness strength is higher at 180 amps, 50 volts, and 5 L/min.
- Impact strength is stronger at 180 amps, 60 volts, and 4 L/min.

Ghadi & S., (2016) used a complete factorial design to explore the Analysis of TIG Welding Process Parameters for Stainless Steel (SS202). The process parameters chosen were current, gas flow rate, and filler wire diameter, and the weld joint was evaluated using tensile, bending, and hardness tests. The results reveal that a combination of high current and inert gas flow rates combined with a smaller filler wire diameter yields the highest tensile strength. Maximum bending strength is achieved by combining low current and smaller diameter with a greater inert gas flow rate. Low current, low inert gas flow rate, and smaller diameter offer the harness maximum toughness.

Ramachandran, (2015) carried out an experimental analysis and investigation of weld properties for SS316L TIG welding. He determined that welding factors such as welding current, voltage, and gas flow rate have a substantial effect on the weld joint after executing numerous destructive and non-destructive tests. For this amp and voltage, the highest penetration depth is achieved with the least amount of failure.

By considering conduction, radiation, and convection effects during both air and inert gas flow rates, (Akbari Mousavi & Miresmaeili, 2008) investigated experimental and numerical studies of residual stress distributions in the TIG welding process for 304L stainless steel. The experiment was carried out with a thermo-elastoplastic constitutive equation and the X-ray diffraction method. According to the findings of the investigation,

- The tensile residual stress peak recorded for the u-grooved configuration is lower than expected for the v-grooved configurations. The estimated residual stresses match the results of the X-ray diffraction investigations quite well. It is further demonstrated that when mechanical limitations are introduced, the amplitude of the transverse residual stresses nearly triples.

- In addition, the confined structure has less Distortion than the unconstrained form. The kinematic and isotropic hardening constitutive equations provide the best agreement between residual stress distributions and X-ray tests.

2.3.1. Purpose of back purging

Back purging is the technique of protecting the inner or back side of the weld with Argon or another inert gas during the welding process to prevent contaminants like sugaring (oxidation), lack of penetration, and other issues, resulting in a stronger weld. As seen from the above surveyed researcher work Stainless steels are susceptible to air, oxygen, hydrogen, and other vapors and gases that may encounter the hot metal during joining. These gases may react with the metal to generate unfavorable compounds that weaken corrosion resistance or contribute to the formation of fissures and other structural flaws in metals. During welding, the rate of oxidation in the metal increases when the temperature rises to a high level. Hence This can be avoided by back purging. Because an inert gas cannot conduct chemical reactions, it inhibits the rapid oxidation of stainless steel while it is still molten (Soul performance Products, 2019).

2.3.1.1. Lack Of Penetration:

The exposed root gap in the butt-welded metal exhibited below is due to a lack of full penetration. During the welding process, this gap can be allowed to allow for a better, stronger weld than the base metal. The section of the gap that isn't filled can attract moisture and corrode faster than the rest of the system this part is part of. The welded part of the material has poor strength and is a site of failure if it is not fully penetrated. The illustration below demonstrates a weld that failed because of a lack of full penetration.

a) 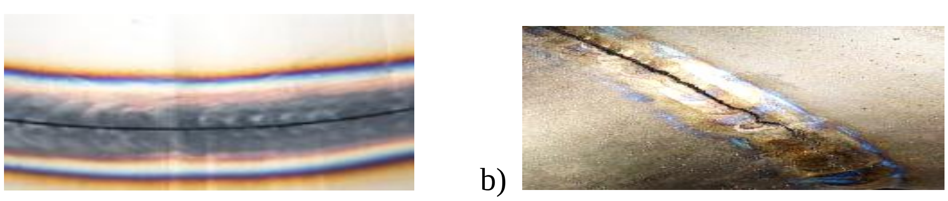 b)

Figure 2.1 a) lack of penetration without back purging b) failure occurred due to lack of penetration (Soul performance Products, 2019)

2.3.1.2. Sugaring (oxidation):

Sugaring is the process of connecting thin stainless steel that warms up quickly in comparison to thicker materials. To keep moisture and oxygen away from the backside of the welding area, purge it with pure Argon. If you don't do this, the chromium in the metal will burn off, making it corrosive. Chromium is a hefty metal with excellent corrosion resistance. Extreme oxidation of the backside of a stainless weld is known as sugaring contamination. The weld has good penetration, but it has also significantly oxidized due to a lack of shielding gas, as seen in figure 2.5 below. While this weld has full penetration, it is not as strong as a back purged weld and can corrode and fail under stress (Soul performance Products, 2019).

Figure 2.2 oxidation (sugaring) (Soul performance Products, 2019).

Argon gas is the most utilized shielding gas in TIG welding because it produces a stable arc that allows for precise control of the weld. The back purging is given tremendous strength, lifespan, and minimum flow influence when the welding operation is completed. Argon was used to back purge the weld illustrated in figure 2.6 below. For a visually different weld, the inert gas prevents scorching and contamination, and there is full penetration with no contamination on the backside.

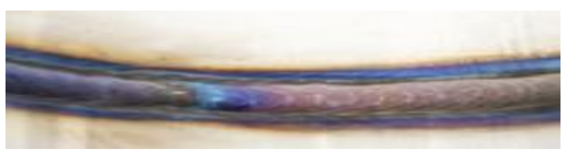

Figure 2.3 back purged weld (Soul performance Products, 2019).

The welding torch is designed to spray shielding gas to protect the front of the weld during the welding process (Soul performance Products, 2019). The back purging tool is designed according to the type and dimension of the weld to be welded.

2.4. Dissimilar metal welding under TIG

Many weld-related problems are associated with dissimilar junctions despite the numerous dissimilar metals joining applications. As a result, extra attention must be paid to dissimilar welds to reduce or eliminate faults throughout the welding process. The composition and characteristics of the weld metal are the most important factors to consider when TIG welding dissimilar metals. They are determined by the compositions of the base and filler metals, as well as their relative dilution and mutual solubility. The relative dilutions and compositional gradients close to each base metal affect the solidification characteristics of dissimilar junctions. When it comes to the warm crackling of the joint during solidification, the solidification attribute is the most important. (Chaudhari et al., 2020; Kah & Jukka Martikainen, 2013). To determine the existence of mutual solubility in TIG welding of dissimilar metals, it is necessary to examine and understand the phase diagrams of the metals involved. Combinations with mutual solubility can be successfully mated if the two base metals are not mutually soluble, and filler metal soluble with both dissimilar base metals can be added. Mutual solubility between the several metals that define the joint's characteristics, such as crack sensitivity, ductility, and corrosion, is used to create the intermetallic compound (IMC) of the final weld metal's microstructural composition (Chaudhari et al., 2020). Melting temperature is an important consideration when TIG welding different metals. There is a lot of heat involved, and one of the base metals' melts faster than the other at the same temperature. Significant variations in melting temperatures between the base metals or the filler metal can cause the metal with a lower melting temperature to rupture. Because the base metal is weak and partially solidified, the solidification and contraction of the metal with a higher melting temperature causes strains in the metal with a lower melting temperature. Buttering the filler metal with an intermediate melting temperature can be employed to solve the problems caused by discrepancies in the melting temperatures of the base metals (Kah & Jukka Martikainen, 2013).

- Under are some of the studies that focus on Welding dissimilar metals**.**

Using DOE Taguchi and ANOVA methodologies (Kausar, 2019) analyzed and studied the weld quality parameters of tungsten inert gas welding on different metal plates SS316L and IS2062. Process parameters such as current, voltage, and gas flow are chosen, and weld quality is determined by tensile strength, hardness, and microstructure. The findings demonstrate that voltage has the most significant impact on stiffness, followed by the gas flow and current. And the most important parameter is tensile current, followed by voltage and gas flow. The optimum parameters for hardness are 130 (Amp), 60 (Volts), and 9 (Liters/min) Airflow, while the optimum parameters for tensile strength are 130 (Amp), 50 (Volts), and 10 (Liters/min) Airflow. Good flow indicates that the connection is vital when it comes to microstructures.

The Analysis and Experimental Investigation of Weld Characteristics for TIG Welding in Dissimilar Metals on SS304 and MS1040 was examined by (Vennimalai Rajan et al., 2020). Tensile strength, hardness, and bend tests inspected the weld quality. The results showed that the tensile strength was 507.902 N/mm2 at a peak load of 49.880 KN, the bending strength was 31.213 N/mm2 at a peak load of 3.140 KN the Rockwell hardness was 78kgf.

Satputaley et al., (2021) evaluated the influence of TIG welding on maximum tensile strength for 4130 Chromoly and 7075T6 aluminum in an experimental investigation. The results demonstrate that Chromoly 4130 has a weld strength of 396.69 MPa, the same as Al 7075T6, resulting in poor weld mechanical properties and poor welding performance. Al 7075T6 has low weld penetration when used for high-strength applications. TIG welding on Chromoly 4130 produces great weld penetration without compromising the material's characteristics.

Anbarasu et al., (2020) used mild steel (IS 2062) as the base material and super Duplex ER2594 as the filler material to investigate the effect of filler material on the hardness of TIG welds. Materials can be created by selecting current, welding speed, and gas flow as process parameters. The Taguchi method of the L9 orthogonal network was used to conduct the test. Micro-hardness and microstructure are two of the weld quality metrics. Finally, their inquiry came to this conclusion. As the welding speed increases, the hardness improves with good surface morphology. A welding current of 120 A, a welding speed of 100 mm/min, and an airflow of 10 liters/min should increase hardness.

Using the TIG welding process**,** (Sayed et al., 2019) conducted a review paper on different metal welds in stainless steel and mild steel. They concluded that to optimize welding output such as strength, tensile strength, hardness of welds, etc., by different input parameters like welding current, voltage, gas flow, welding speed, etc.

Hazari et al., (2019) performed an experimental investigation on TIG welding on AA 6082 and AA 8011 by selecting welding current, electrode diameter, and gas flow rate. The weld's final quality was validated by ultimate strength and hardness. The maximum tensile strength increased dramatically as the amperage was raised, but the yield strength improved significantly. By increasing the effectiveness of the shielding gas, the ultimate tensile strength increases according to the gas flow rate. (The diameter of the filling material changes little; nevertheless, material soldered with a 2.5 mm diameter filler shows a significant difference.)

Sewa Singh et al., (2019) Select process factors such as welding lines and airflow in different heating circumstances to develop similar and dissimilar welding efficiency in towing gravity loads experimental surveys. To ensure maximum pull resistance, the materials utilized in the study are ASME SA 213 GR. T11 and BS 3059: 1987 PT 1 ERW 320. The results reveal that a similar ASME SA 213 Gr. T11 weld produces a maximum tensile strength of 601.63 MPa when welded at 110 A with a 10 L/min inert gas flow and no preheating. When warmed to 150 °C before welding, BS 3059:1987 PT1 ERW 320 showed a maximum tensile strength of 544.17 MPa at 110 A current and 10 l/min inert gas flow. The tensile strength of the material is at its highest.

A. Kumar et al., 2017) used the Taguchi technique to investigate the experimental investigation of TIG welding of stainless steel 202 and stainless steel 410. Current, gas pressure and welding speed are all considered process characteristics, and the final tensile strength determines the quality of the weld. The primary impact graphs revealed that current, gas pressure, and welding speed were the significant influencing elements on the ultimate load. With a welding current of 130 A, a gas pressure of 10 kg/cm2, and a welding speed of 2.8 mm/s, the ideal parameter setting for the ultimate tensile strength of 808.3 N/mm2 was determined experimentally.

Devakumar et al., (2016) investigated GTAW welds in duplex stainless steel and hot-rolled steel (DSS / HRS) by characterizing the weld microstructure, examining the micro composition part using power dispersive X-ray evaluation (EDAX) to determine metallurgical properties and microhardness test, tensile test, and bending test to determine mechanical properties. In contrast to the DSS parent metal, which has long grain austenitic with ferrite, and the HRS parent metal, which has long grain austenitic, the results show the production of a triangular ferritic microstructure. The DSS/HRS weld is more efficient with fine ferrite grain. The creation of the dendritic delta ferrite microstructure appears to be the result of energy-dispersive X-ray analysis (EDAX).

L. S. Kumar et al., (2011) used the Taguchi technique for TIG and MIG welding to investigate the welding features of AISI 304 and 316. They discovered that when welding austenitic stainless steels using the TIG method, the hardness value (BHN) at 40A for TIG is 162.3 and 196.54 for MIG. As a result, he concluded that the MIG technique is appropriate for low currents. He also concluded that the TIG welding pattern could sustain a final load of 57600N, whereas the MIG welding pattern can withstand 56160N. As a result, the TIG welding pattern can withstand more load than the MIG welding pattern. He also concluded that the heat-affected region would

2.5. Characterization Of Welded joints

The characterization of TIG-welded metal joints has been the subject of much research. They primarily focus on microstructure qualities, mechanical properties, and the impact of various input parameters on weld quality. Cores-columnar grains are common in weld fusion zones because of the prevailing heat conditions during weld metal solidification. As a result, weld mechanical characteristics and resistance to hot cracking are frequently compromised. The quality of welded joint is usually controlled by the solidification behaviors of the welded metal. It manages weld metal microstructure, grain structure, mechanical properties, etc.

The (Cr_{eqv} / Ni_{eqv}**)** ratio helps explain the solidification mode of weld metal (Lippold & Kotecki, 2005). Based on the chemical composition of the studied weld metal, nickel and chromium equivalents can be calculated. The Schaeffler formula is used to compute the Creqv. / Nieqv ratio (Kou, 2003).

$$Creqv. = Cr + Mo + 1.50xSi + 0.50xNb \quad (2.1)$$

$$Nieqv. = Ni + 30xC + 0.50xMn \quad (2.2)$$

Table 2.1 shows three methods utilized for determining the metal composition of a weld (Avery, 1991). The second approach is easily applied from them, as seen in Figure 2.2.

Table 2.1: Determination of weld metal chemical composition (Avery, 1991)

s.no	Method	Advantages	Limitation
1	Chemical analysis	Most accurate determination	Time-consuming
2	Approximation of base metal dilution by weld-cross-section and composition	Less expensive and usually shorter than chemical analysis	Estimating the percentage often difficult in welds such as multi-pass welds
3	Approximate dilution figures for common welding processes and composition calculated	Very fast way of estimating “rough” composition. No laboratory work involved	Welding technique can have a strong influence on dilution in some processes, e.g., GMAW, GTAW.

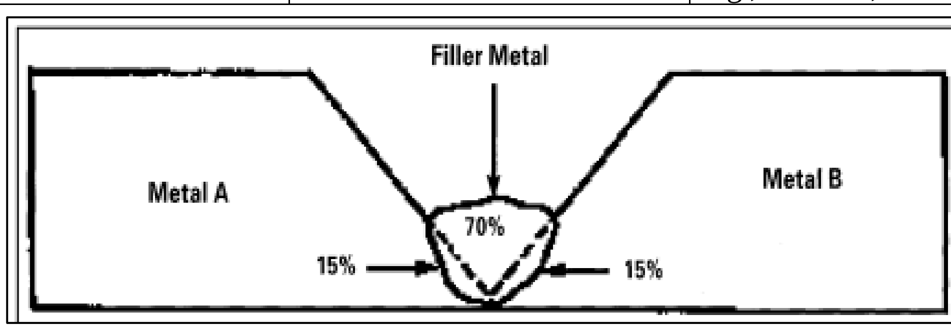

Figure 2.4 determining weld metal composition by using Method 2: approximation of base metal dilution (15% from metal A and 15% from metal B) (Avery, 1991)

An experimental study (Dak & Pandey, 2021) investigated dissimilar welded joints of P92 and AISI 304L austenitic stainless steel. This research aims to look at the material's microstructure, mechanical characteristics, and residual stresses. The welding was done using an optical, multi-pass gas tungsten arc welding (GTAW) procedure to determine the weldment's microstructure and mechanical properties (tensile, Charpy impact, and microhardness) microscope and scanning electron microscope. To homogenize this heterogeneous microstructure generated toward the P92 side, a post-weld heat treatment (PWHT) at 760 °C for two h followed by air cooling was carried out. As a result, the weld fusion zone and heat-affected zone (HAZ) of SS304L microstructure were not affected by this PWHT.

- ✓ The findings of the tensile tests revealed that specimens made of 304L stainless steel (SS) base metal (BM) in as-welded and PWHT conditions were under predicted.
- ✓ In comparison to the P92 (190J) and SS 304L (285J) BM, the hardness of the weld junction was significantly low in as-welded and PWHT circumstances (47J).
- ✓ Due to its lower micro-hardness value than the other regions, the inter critical HAZ (ICHAZ) was the weakest zone among the other zones during the microhardness examination.

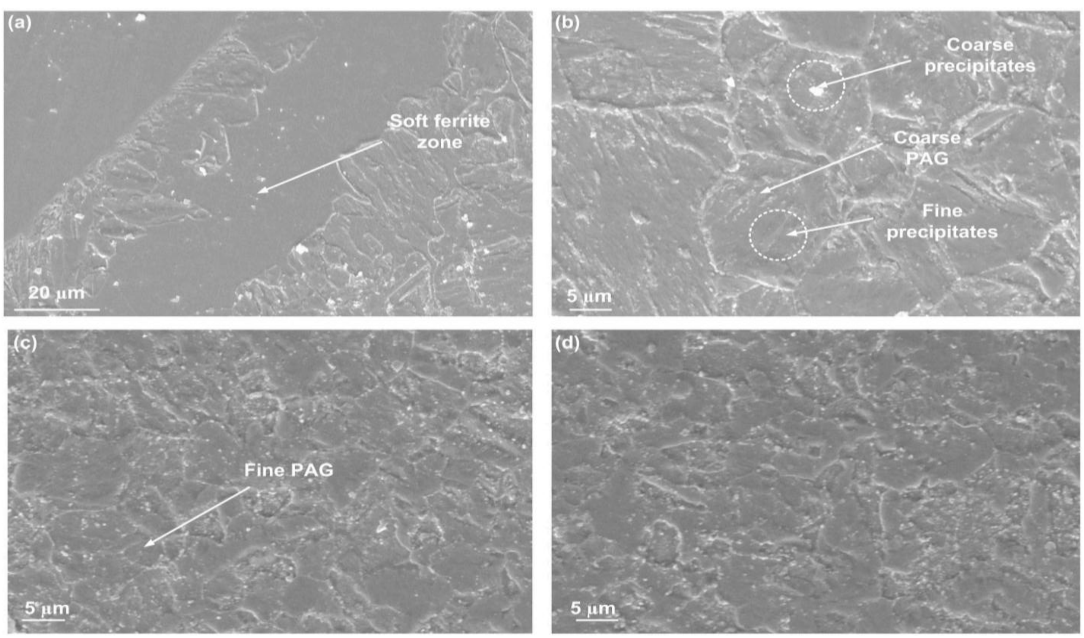

Figure 2.5 SEM images showing the microstructure of the WM and P92 interface and P92 HAZ (PWHT at 760 °C for 2 h) (a) P92 and WM interface, (b) CGHAZ, (c) FGHAZ, (d) ICHAZ. (Dak & Pandey, 2021)

Arora et al., (2020) used the Taguchi technique to investigate the mechanical and morphological properties of inert tungsten gas welded SS304 thin pipe joints, selecting important parameters such as welding speed, welding current, and shielding gas flow rate. Micro-hardness, the breadth of the heat-affected zone, residual stresses, and microstructural characteristics were used to assess weld quality. The hardness of the weld bead decreases with maximum welding current and low welding speed, and the optimal settings for minimal Hardness and minimum HAZ are current (90A), speed (2mm/s), and gas flow rate (5 L/min), according to the results. In this case study, minimal welding heat input resulted in the development of equiaxed grains, whereas high input resulted in dendrite formation. It has also been

Taban et al., (2007) studied the microstructure's microstructure, toughness, and mechanical characteristics. The 6mm thick X2CrNi12 stainless steel arc weld metal properties were altered using two variable heat input Shock resistances. Although grain expansion does not influence tensile or bending properties, it does reduce the heat-affected region's sub-zero impact strength. This is determined by the amount of precipitate present and the coarse grain structure.

Microstructural and Transient Thermal Analysis of TIG Welded Joint SAE 2205 With AISI 304 was investigated by (Ganesh et al., 2017). The maximum tensile strength of 549MPa was attained when the sample was treated at 130A using AISI 308 Filler Metal. For the sample, which is welded at 130A, the maximum hardness of RC 36 was found on the base metal SAE 2205 side, and an increase in the hardness values was attributed to the presence of higher chromium and sigma phase in the base metal SAE 2205. All the samples formed ultra-fine and refined grains at the HAZ zone. And the weldment, which is made of SS AISI 304, achieves the maximum Von Misses stress of 85MPa.

Subodh Kumar & Shahi (2011) investigated the effect of heat on the microstructure and mechanical properties of AISI 304 stainless metal joints welded with gasoline tungsten arc welding. Three heat input mixtures were chosen from the GTAW procedure's working window: low heat, medium heat, and excessive heat, and weld joints made with these combinations were subjected to microstructural and tensile testing to examine the impact of thermal arc strength on the microstructure and mechanical properties of these joints.

Halil İbrahim (2013) investigated the microstructure and mechanical properties of AISI 304 stainless steel sheets welded with 308-grade filler metal using GTAW welding. Microscopy was used to investigate the microstructures of base metal and how warmness influenced quarter and weld metal. This resulted in chromium carbide precipitation and dendritic structure in the weld metal.

Moslemi et al., (2015) used welding currents of 80, 90, 100, and 120 to investigate the effect of current on 316 Stainless Steel Welded Joint Characteristics, including Microstructure and Mechanical Properties (A). Tensile testing, Hardness (HV), and Metallographic inspection assessed the welding quality. As a result of the findings, it was discovered that.

- ✓ The maximum tensile strength, achieved from 100A, was 394.8MPa.
- ✓ The specimen with the highest hardness value among the specimens was 100A, indicating that 100A is the best TIG arc current for this material to achieve a satisfactory weld joint.
- ✓ The breadth and depth of the weld pool are increased as the welding current is increased.

Lakshminarayanan et al., (2009) investigated the effects of welding procedures such as shielded steel arc welding, gas metal arc welding, and gasoline tungsten arc welding on the tensile and impact properties of ferritic stainless steel according to the AISI 409M standard. Compared to shielded metallic arc and fuel steel arc welded joints, gas tungsten arc welded ferritic stainless metal joints have superior tensile and affect homes, primarily due to more refined grains in the fusion sector heat-affected quarter.

The experiment Optimization of 316 Stainless Steel Weld Joint Characteristics Using Taguchi Technique was carried out by **(**Bharath & Sridhar, 2014). Current, speed and root gaps have been found to influence the material's tensile and bending strength. According to the results of the analysis of variance (ANOVA), welding speed (46.51 percent contribution) has a more significant impact on bend strength, whereas current (96.75 percent) has the greatest impact on tensile strength. Furthermore, root gaps have influenced both tensile and bend strengths due to changes in weld materials and grain sizes formed during the welding process.

Jeng et al., (2007) used Inconel 52 and 82 (I-52 and I-82) as filler metals to determine the Microstructural Study of the Dissimilar Joints of Alloy 690 and SUS 304L Stainless Steel. The research utilized TIG welding with the following factors in mind: current speed, heat input, and microstructural inspection using SEM, TEM, EDXS, and EFTEM. The outcome demonstrates that.

- ✓ In the interdendritic region and along the grain boundary, both the I-52 and the I-82 fusion zones had a lot of sediments of varied sizes. In I-82, there were more interdendritic phases than in I-52.

✓ In the I-52 fusion zone, a small TiN with FCC lattice was discovered. Cr- carbides precipitated in future Welding passes due to the heat cycles of later Welding passes.

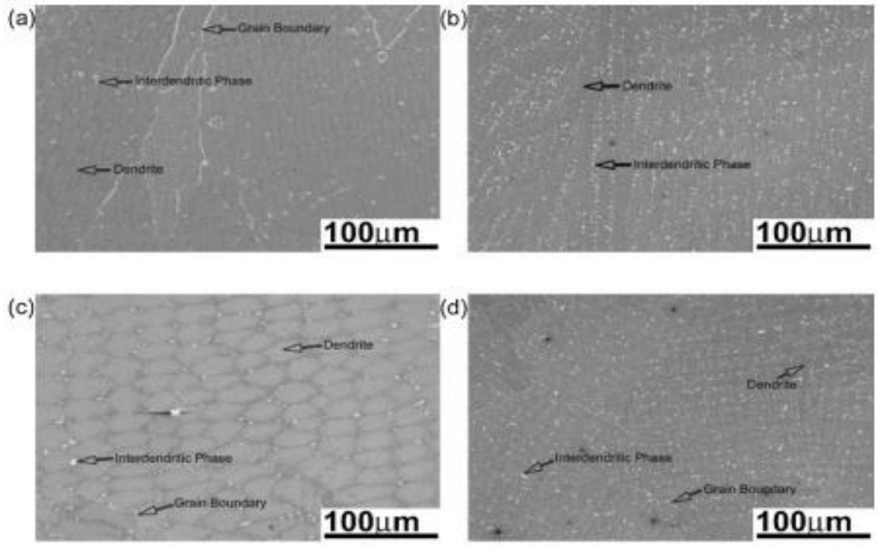

Figure 2.6 Interdendritic phases in the central area of fusion zone: (a) SEM micrographs of I-52 cap region, (b) SEM micrographs of I-82 cap region, (c) SEM micrographs of I-52 root region, (d) SEM micrographs of I-82 root region**,** (Jeng et al., 2007)

2.6. Optimization of Different TIG Welding Processes parameters

Process parameter optimization is important in the welding process because it helps to determine the best process parameters for a high-quality weld while also reducing the number of trials. As a result, choosing the right TIG welding process parameters and setting them at the right values is critical for getting the best mechanical characteristics and bead shape (Ayoola et al., 2019; Choudhary et al., 2019). Researchers are constantly developing statistical models to correctly optimize the welding process and produce higher-quality welds. Experimental Analysis and Optimization of any welding procedure is difficult due to the high cost, time commitment, and numerous interconnected aspects that must be considered (Ruggiero et al., 2011). Optimization is considered after several investigations on the parameter.

By selecting the influential parameters (welding current, welding speed, and filler diameter), (Natrayan et al., 2020) explored the optimization of process parameters in TIG welding of AISI 4140 stainless steel using the Taguchi technique. The material they chose was AISI 4140 stainless steel, which was welded using the TIG welding method, and the final weldment quality was confirmed using the tensile strength. The results show that welding speed was ranked first followed by welding current as a significant parameter according to S/N ratio depicted in figure 2.2. The welding current at level 1 (250A), weld speed at level 3 (5mm/sec), and filler diameter at level 3 (3.6mm) are the optimal process parameters for tensile strength.

Table 2.2: Signal to noise ratio for UTS (Larger is better) (Natrayan et al., 2020)

Level	Welding Current (A)	Weld Speed mm/sec	Filler Diameter (mm)
1	56.77	56.34	56.60
2	56.48	56.23	56.40
3	56.38	57.07	56.63
Delta	0.39	0.84	0.23
Rank	2	1	3

Pardeshi, (2020) used the DOE Taguchi technique to investigate the parametric study of the TIG welding parameter for SS317L steel. Welding current, voltage, and gas flow rate are process parameters, whereas Bending and Tensile tests are response variables. The welding current was shown to be the most influential parameter in tensile strength, followed by voltage and GFR. It can also be seen that voltage has the greatest impact on bending strength, followed by GFR and welding current as shown in ANOVA table 2.3 a, and b. The best input process parameters for tensile strength during TIG welding are 65A current, 25V voltage, and 16 lit/s gas flow rate, while the best input process parameters for bending strength are 60A current, 25V voltage, and 16 lit/s gas flow rate.

Table 2.3: ANOVA: a) Tensile strength, and b) Bending strength (Pardeshi & Dubey, 2020)

(a)

Source	DF	Adj SS	Adj MS	F-Value	P-Value
Current	2	1.61256	0.80628	20.66	0.046
Voltage	2	0.23152	0.11576	2.97	0.252
GFR	2	0.14711	0.07356	1.88	0.347
Error	2	0.07805	0.03903		
Total	8	2.06925			

(b)

Source	DF	Adj SS	Adj MS	F-Value	P-Value
Current	2	4.770	2.385	1.44	0.411
Voltage	2	9.804	4.902	2.95	0.253
GFR	2	8.507	4.253	2.56	0.281
Error	2	3.324	1.662		
Total	8	26.405			

Moi, et al., (2019) used three influential process parameters (welding current, gas flow rate (GFR), and welding speed) to perform experimental work on the Design Optimization of the TIG Welding Process for AISI 316L Stainless Steel. Under the work, they looked at Ultimate Tensile

Strength, Impact Toughness, and Weld Width as response variables. In addition, the weldment's microstructure is studied. That is demonstrated by the results of their experiment.

- ✓ The most important element impacting TS is gas flow rate, with welding current and welding speed coming in second and third place, respectively.
- ✓ In the case of weld width, welding speed is the most important component to consider.
- ✓ Welding speed and GFR both have an equal impact on impact strength.

The weld metals with moderate heat input exhibit very fine skeletal δ-ferrite and with low heat input exhibit dendritic lathy δ-ferrite structure in a simple austenitic matrix. The optimum welding combination for optimizing all the responses simultaneously obtained by desirability function approach is current =129.29 A, speed =16.85 cm/min and gas flow rate = 8.91 cm/min, and predicted UTS = 641.55 MPa, impact strength = 50.87J and weld width = 6.26 mm.

Moi, Rudrapati, et al., (2019) examined the Impact Behavior of TIG Weldments on SS316L using Hybrid RSM and CSO. Welding Current, Speed, and Gas Flow Rate are the process parameters for maximal impact strength. The most important element impacting impact strength, according to the findings, is welding speed. The gas flow rate and welding current are the next two important parameters to consider. Welding current = 126.62 A, welding speed = 15.39 cm/min, gas flow rate = 8.85 l/min, and matching impact strength = 51.62J were the optimal parametric settings predicted by the CSO algorithm.

By using gas flow rate, welding current, and welding speed as process factors**,** (Mohanavel et al., 2018) studied their findings on the optimization of tungsten inert gas welding parameters to achieve optimum impact strength in AA6061 alloy joints using Taguchi Technique. The welded joint's quality was tested using the maximum impact strength. The test results revealed that the gas flow rate is the most important factor affecting weld joint impact strength, followed by welding speed and welding current. Welding Current: 200 A, gas flow rate: 10 L/min, and welding speed: 58 mm/sec were found to be the best level combinations for optimum impact strength.

The Experimental Investigation and Optimization of TIG Welding Parameters on Aluminum 6061 Alloy Using Firefly Algorithm was studied by (R. Kumar et al., 2017). Welding Current, shielding gas flow rate, and Current polarity were chosen as parameters, with Ultimate tensile strength as the response parameter. At 175A welding current, 9 l/min gas flow rate, and current polarity, the maximum value of ultimate tensile strength is 137.104 MPa (0). And, according to the firefly algorithm, the optimal value of UTS is 98.896 MPa, which is a combination of welding current 150A, the gas flow rate of 10 l/min, and polarity of -1.

Wahule & Wasankar, (2018) used Grey Relational Analysis to perform an experimental study on Multi-response Optimization of Process Parameters of TIG Welding for Dissimilar Metals (SS-304 and Fe-410) and found that the optimum value for tensile strength was 120A of the current, 16L/min of gas flow rate, and 2mm of root gap, parametric set. ANOVA revealed that the largest contribution was 47.38 percent of current, with a gas flow rate of 37.95 percent and a root gap of 14.67 percent following. 120A of current, 16L/min of gas flow rate, and 1mm of root gap were found to be the best values for percentage elongation. The highest contribution, 62.88 percent, came from current, followed by gas flow rate, 24.08 percent, and root gap, 13.04 percent, according to ANOVA.

Moi et al., (2018) found that the determination of Tungsten Inert Gas Welding Input Parameters to Attain Maximum Tensile Strength Of 316l Austenitic Stainless Steel is affected not only by NTS but also by UTS, and that welding current and welding speed are important factors in this regard. The weld metal has a greater microhardness rating than the HAZ and base metal. Welded joints have been proven to have higher tensile strength than base metals.

Sanjay Kumar et al., (2017) used Taguchi's Analysis and Response Surface methodology to optimize TIG welding process parameters. They concluded that voltage is the most important factor in hardness and bending strength. The highest hardness was obtained with the (A2B3C1D1) parametric set at 70 A (2nd level of current), 50 V (3rd level of voltage), and 0.5mm (1st level of root gap), and 16 liter/min (1st level of gas flow rate). The largest bending strength, on the other hand, is found at the (A2B1C1D3) parametric configuration, which includes the 2nd level current, 1st level voltage, 1st level root gap, and 3rd level gas flow rate. According to the results of the ANOVA, voltage is the most influential factor in modifying the temperature.

Gupta, (2016) experimented with Optimizing Conditions for Performing GMAW (TIG) Welding on Ultra 904L Specimens and found that when the current was varied while the gas flow rate was kept constant, the welding joint was not produced below 50A and above 200A, and the specimen began to burn.

Patil & Waghmare, (2013) conducted an experimental study on MIG Welding Parameter Optimization for Improving Welded Joint Strength. They concluded that welding speed has a considerable impact on the tensile strength of welded connections. To improve welding settings, a Taguchi orthogonal array, the signal-to-noise (S/N) ratio, and analysis of variance (ANOVA) were used.

By selecting process parameters such as welding current, welding speed, and electrode distance, (Pasupathy & Ravisankar, 2013)investigated the Parametric Optimization of TIG Welding Parameters Using the Taguchi Method for Dissimilar Joint. Strength was used to test the weldment's final response. Finally, the results of the work demonstrate that the experimental value obtained from ideal welding conditions is 61.37 MPa, with an S/N ratio of 16.45.

2.7. Studies on mechanical properties

By considering advanced speed, welding amperage, and preheating temperature, (Salehpour-Oskouei et al., 2021) explored the Experimental Investigation of Tungsten Inert Gas Welding Input Parameters Effects on Mechanical Characteristics on SS316. The study's reaction output was distortion and tensile strength. The results reveal that increasing amperage reduces welding component strength due to plate edge burn defects, which can be mitigated by increasing welding speed and lowering the influence of intense heat on the edges. Finally, the optimal conditions of the adjustment parameters in butt-welding were gained among existing samples for welding 316 stainless steel by examining the effect of the input parameter on the output.

Maneiah et al., (2019) conducted an experimental investigation on TIG Welded Butt Joints of Aluminum Alloy 6061-T6 to Determine Tensile Strength at 0°, 30°, 45°, and 60°. The results revealed that the tensile specimens were tested in a variety of heat treatment techniques, including annealing, water quenching, and heat treatment without heat treatment. The highest strength, 109 MPa, and the highest percent elongation, 5.6 percent, exhibit better ductility upon annealing, welded at a 60°-degree angle. Without heat treatment, the strength reached 100 MPa when welded at an angle of 30° degrees. As a result, heat treatment techniques and weld angles have an impact on the weld joint's strength and tensile qualities.

Surjeet Singh et al., (2016) used TIG welding to test the tensile strength of AA6082 at various process parameters such as current, filler material, and shielding gas flow rate. To produce a

Tensile strength response, AA 4043 and AA 4047 were employed as filler materials. When the current is increased from 80 Amp to 120 Amp, the tensile strength increases by 4.5 percent on average. When compared to AA 4047, AA 4043 produces better results.

Anand Rao & Deivanathan, (2014) used TIG process parameters such as current, filler materials, and welding speed to conduct an Experimental Investigation for Welding Aspects of Stainless Steel 310 for TIG welding. The quality of a weld is determined by its mechanical and microstructural qualities. Welding current 120A and electrode 309L achieved tensile strength of 454.6MPa, according to the results. A welding current of 80 A with an electrode of 316L, on the other hand, resulted in a specimen with a minimum tensile strength of 51.79 MPa. The welding current of 120A with electrode 316L produced a maximum bending strength of 646.55MPa in the bend test, while the same welding current with electrode 347 produced a minimum bending strength of 211.37MPa for the specimen studied. The tensile and bending strength of the 309L filler material has improved. Microstructure images show that 309L has prominent second phase formation because of varying chromium percentage retarded transformation and uncontrolled heat input.

Experimental Research on Gas Tungsten Arc Welding of Stainless Steel-An Overview was conducted by (Devakumar & Jabaraj, 2014). Low heat input is recommended when welding AISI 304 stainless sheets of steel using the GTAW process to ensure good tensile strength and elasticity. In comparison to the weld metal and base metal regions, the heat-affected zone and grain coarsening obtained in the weld joint are less, and the hardness is less in the HAZ region. The GTAW technique achieves an enhanced strength value of roughly 10% for SMAW joints and 20% for GMAW joints. In addition, as the current is increased, the Bowing distortion increases.

2.8. Some studies on Weld geometry

Welding process factors have a big impact on weld bead geometry variables, and they're also important for determining welding mechanical qualities including tensile, hardness, and bending. Using process parameters such as welding speed, welding current, and gap-width, (Ondieki, L. N. A. M. C., & Odhong, 2021) investigated an Experimental Investigation of TIG Welding Parameters in Butt- Joint Configuration of Mild Steel by DOE technique. Penetration depth, bead width, heat-affected zone, and ultimate tensile strength were used to evaluate weld quality. The

Welding Current was discovered to be an important factor in the heat energy input equation that determines the weld joint quality parameters. Low welding currents reduce heat-affected zones, but they impair weld penetration depth and weaken the tensile strength of the joint. Increases in welding current result in an average or complete depth of penetration, which has a favorable effect on the joint's tensile strength. Metal spatter, porosity and severe weld penetration are all problems caused by excessive welding currents. TIG weld creation with good or excellent quality requires a current of 100Amps-140Amps.

Panwar & Kakirde, (2021) used relevant characteristics such as welding current, voltage, and welding speed to perform an Experimental Investigation of the Tungsten Inert Gas Arc Welding Process Parameter of Mild Steel. Weld width, weld penetration, HAZ breadth, depth of HAZ, cross-sectional weld area, and arc spread are all used to assess weld quality. According to the findings, increasing the welding current from 50 A to 90 A increases the bead width, and increasing the welding current from 50 A to 90 A also increases penetration.
It has been noticed that as the welding speed is increased from 14 mm/min to 44 mm/min, the bead width begins to drop. The penetration in the weld joint is greater at a lower speed, such as 14 mm/min, and it is lower at a higher speed, such as 44 mm/min.

S. S. Kumar et al., (2021) conducted an experimental examination on Inconel 625 pulsed TIG welding utilizing several fluxes, including Al2O3, TiO2, and V205. Penetration depth, bead width, and ultimate tensile strength were used to evaluate the joint's quality. Full penetration was not obtained in any welding trials, according to the results. Maximum penetration was achieved using the V205 flux. When V205 was utilized as a flux, the depth of penetration increased by 0.3 mm. When Al203 was employed as the flux material, the ultimate tensile strength was achieved. When Al203 was employed as the flux material, the tensile test was raised by 12%.

Using Groove Angle (Degree), Root Face (mm), and Root Gap (mm) as process parameters, (Kailas A. Gite & Ramkisan S. Pawar, 2016) calculate the Effect of Welding Geometry Parameter on Hardness for AISI304 TIG. The test's response parameters were tensile strength and microhardness, which they obtained from the results.

- ✓ It has been noticed that as the groove angle increases, so does the hardness.
- ✓ Microhardness is also reported to decrease when the root faces approach 1.5 mm. After then, the microhardness rises to 1.5 mm to 2 mm.

- ✓ As the root gap widens, so does the hardness of the soil.
- ✓ TIG welding gave a higher microhardness of 236 Hv at 60 groove angle, 1 mm rib thickness, and 1.5 root gap.

P. Singh & Singh, (2014) used the TAGUCHI technique to choose the parameters, current, gas flow rate, and several passes for an Experimental Investigation of the Deposition Rate of TIG Welding of Grade 316 Stainless Steel. Responses such as metal deposition rate and weld bead hardness tests were used to assess weld quality. According to the findings, the number of passes is the most important factor in Stainless Steel (SS316) welding, followed by current and gas flow rate, for deposition rate, and gas flow rate is the most important factor, followed by no of passes and current, for hardness as the reaction.

2.9. Weld quality by considering thermal aspects

Differences in melt temperature, coefficient of thermal expansion, and thermal conductivity are all important factors to consider when welding metals. One of the governing criteria is heat input during welding similar or dissimilar materials, and the microstructure of parental materials is dependent on heat input during welding.

2.9.1. Thermal Conductivity

When welding metals with significantly different thermal conductivity, the heat source must provide a thermal differential for proper thermal equilibrium. The heat conduction rapidly from the molten weld pool to the base metal, base metal with higher thermal conductivity takes away the thermal energy and affects the energy input required to melt the base metal locally. Thus, the heat source is always directed towards the metal with higher thermal conductivity to balance the heat. Preheating the base metal with a higher thermal conductivity can control heat loss to the base metal and reduce the cooling rate of the weld metal and the heat-affected zone (HAZ) (Chaudhari et al., 2020; Kah & Jukka Martikainen, 2013).

2.9.2. Coefficient of Thermal Expansion

During cooling, the difference in thermal expansion coefficients between the base metals creates tensile stress in one and compressive stress in the other. The metal deposited under tensile stress may experience hot cracking during welding or cold cracking during service if the stress is not released. This is critical in recirculation applications where the seal must operate at high temperatures (Chaudhari et al., 2020; Kah & Jukka Martikainen, 2013).

Balram et al., (2019) used Infra-Red (IR) thermography pictures to examine the thermal stress analysis of AISI 316 stainless steel weldments in TIG and pulse TIG welding processes. IR pictures were taken at 12 s, 25 s, and 4 s during each welding pass. Because of the pulse effect during the pulse TIG welding process, changes in peak temperatures and their distribution to base metals were found in both welding methods; nevertheless, the solidification time and distribution were negligible when compared to the TIG welding process.
The nature of maximal tensile strength The TIG welding technique showed a residual stress value, which might be explained by the accumulation of additional heat in the weld zone due to heat resistance during the solidification process. By keeping the pulse arc mode and low frequency, the produced stresses were kept to a minimum (4 Hz).

Using ANSYS, (Sagar et al., 2018) conducted an experimental study on Thermal Analysis of TIG-welded Ti-6AI-4V plates. The heat-affected zone is more at the lower speed of welding (3mm/sec) specimen and much less at the higher speed (6mm/sec) of high heat concentration at the low speed, according to the ANSYS temperature profile. And, as shown in the graph, the temperature drops as welding progresses.

Krishna et al., (2016) investigated the effect of welding parameters in TIG welding for INCONEL 625 alloy using Numerical Analysis. SOLIDWORKS is used to construct and assemble the 50mmx50mmx3mm plates for the v butt joint, and then this model is loaded into the FEA software (ANSYS) to perform the transient temperature analysis. Different welding parameters such as voltage, current, velocity, speed, and melting efficiency are used in the analysis. He also highlighted how the length of the heat impacted zone varies depending on the welding conditions.

Thermo-mechanical Analysis in TIG welding of SS 304 was investigated experimentally by (Gohel et al., 2016). They discovered that the modeling and experimental temperature profiles were very similar. The temperature created during welding can be measured using a variety of experimental approaches. They are, however, expensive, and time-consuming. When welding applications deal with complex goods, FEM is employed to produce better results with the least amount of volatility in experimental data.

Jebaraj & Ajaykumar, (2013) investigated the impact of microstructural modifications on weldment toughness and base steel toughness of duplex stainless metal AISI 2205 for low-temperature applications. DSS weld connections were created using a gas tungsten arc welding method with carefully controlled welding conditions. Quantitative metallographic photo analysis was used to determine the ferrite austenite ratio in the weld zone, heat-affected sector, and base steel. The influence examines the effects of the cracked floor and the microscope used to examine the examined specimen.

2.10. Literature summary

From the above literature review, it observed that most of the researchers had taken input parameters such as welding current, welding speed, voltage, gas flow rate groove angle and root geometry, while some have taken, electrode diameter, base metal thickness, electrode angle, gap between workpiece and electrode tip, and so on to find out their impact on performance parameters including mechanical properties, microstructural properties, and joint geometries. Most researchers conclude that parameters that have a significant effect on the tensile strength was welding current followed by gas flow rate. Other authors observed that the welding speed was the significant factor followed by voltage. Also, the microstructure of the metal was much protected by controlling the welding current and welding speed. The literature review reveals that researchers have focused on various investigate of the effects of welding parameters on the resulting mechanical properties to determine optimal welding conditions. The various authors have used the Taguchi method, RSM, genetic algorithm, firely algorithm, and so on. as optimization techniques. Table 2.4 below shows some recent literatures by considering the base metals, predictive and optimization method used to overview which process parameters much affect the welding of steels.

Table 2.4: Summary of literature review

S.N	Title	Author names	Material	TIG Parameters	Method and Types of Tests	Summary of findings
1	Experimental investigation on the effect of welding parameters of TIG welded joints using ANOVA	Kumar et al. (2020)	AISI 304	Voltage, Current, Gas flow and root gap.	Taguchi Method tensile strength test	Current is the most influential parameters in case of tensile strength as indicated by response value graph.
2	Optimization of process parameters in TIG welding of	Natrayan et al	AISI 4140 stainless	welding current, welding	Taguchi Method	Anova results indicate that the welding speed is the more significant parameters

	AISI 4140 stainless steel using Taguchi technique	(2020)	steel	speed and filler diameter	tensile strength	than the welding current and filler diameter.
3	Experimental investigation of TIG welding on AA 6082 and AA 8011	Hazari et al. (2019)	AA 6082 and AA 8011	Welding current, filler rod diameter, and gas flow rate	UTS Hardness	So, from the result it is observed that current is the most affecting parameters for UTS and Hardness and GFR is followed it.
4	Design Optimization of TIG Welding Process for AISI 316L Stainless Steel	Moi et al. (2019)	AISI 316L Stainless Steel	welding current, gas flow rate (GFR) and welding speed	**RSM** UTS, IS microstructure	The most significant factor affecting UTS is gas flow rate. welding speed is the most Significant factor affecting weld width. Welding speed and GFR have equal contribution affecting impact strength.
6	Investigation of filler material influence on hardness of TIG welded joints	Anbarasu et al (2019)	mild steel (IS 2062)	current, weld speed and gas flow rate	**Taguchi Method** Microhardness and microstructure	Higher the welding current better will be hardness and microstructure.
7	Optimization of tungsten inert gas welding parameters to attain maximum impact strength in AA6061 alloy joints using Taguchi Technique	Mohanavel et al. (2018)	AA6061 alloy	gas flow rate, welding current and welding speed	Taguchi Method maximum impact strength	Gas flow rate is the significant parameter on impact strength of weld joints, followed by welding speed and welding current.
8	Experimental investigation of the effect of welding current, voltage, and gas flow rate on welding characteristics of TIG welded S31603 material	Jeevahan et al. (2016)	316L stainless steel	welding current, welding voltage and gas flow rate	**Taguchi method** Tensile test, hardness test and impact test	The effect of changing welding current, welding voltage and gas flow rate improve the welding characteristics.

9	Effect of Current on Characteristic for 316 Stainless Steel Welded Joint Including Microstructure and Mechanical Properties	Moslemi et al. (2015)	for 316 Stainless Steel	Welding current 80, 90, 100 and 120 (A)	Metallographic examination	At a constant welding speed, the overheating degree of metal in the welding pool increases with the increment of the welding current .
10	Effect Of Welding Geometry Parameter on Hardness for AISI304 TIG	Gite et al. (2015)	AISI304 stainless steel	Groove Angle (Degree), Root Face (mm) and Root Gap (mm)	Taguchi Method tensile strength and micro hardness	Root gap goes on increasing so hardness also goes on increasing. Higher micro hardness 236 Hv produced at 60 groove angle, 1 mm rib thickness and 1.5 root gap in TIG welding.

2.11. Research Gap

So, by observing the past work-done austenitic stainless steel has been the subject of various investigations. Some research focused on application, different grades of material, and single response welding parameter optimization. However, no attention was paid to SS316 and mild steel AISI 1020 (dissimilar metals) in terms of the effect of filler metal type and Root Gap during TIG welding, as well as composite response optimization of similar and dissimilar welded metals. And no one focused to protect the backside or inner side of the weld zone using purging gas as front or torch side from oxidation. So, in the present work, using purging gas in both side of the weld zone (torch side and backside) and considering the parameters such as welding current, Root Gap, Gas flow rate, and type of filler metals during a similar and dissimilar welding to know the influence of the parameters and backside gas protection on weld quality.

CHAPTER - 3

MATERIAL AND METHOD

3.1. Introduction

After surveying the literature, some advice and expertise on the correct workpiece and filler material selection, managing process parameters, research methodology, electrode, and welding conditions are now available. Using a manual TIG welding machine, an experiment was carried out using a proper selection of orthogonal arrays for an experimental plan, considering TIG welding process parameters such as welding current, gas flow rate, type of filler, and root gap for similar between (SS316) and dissimilar (SS316 and MS 1020).

3.2. Experimental Procedure (Methodology)

To meet the research goal outlined in Chapter 1. The schematic diagram of the framework of the applied techniques is shown in Figure 3.1.

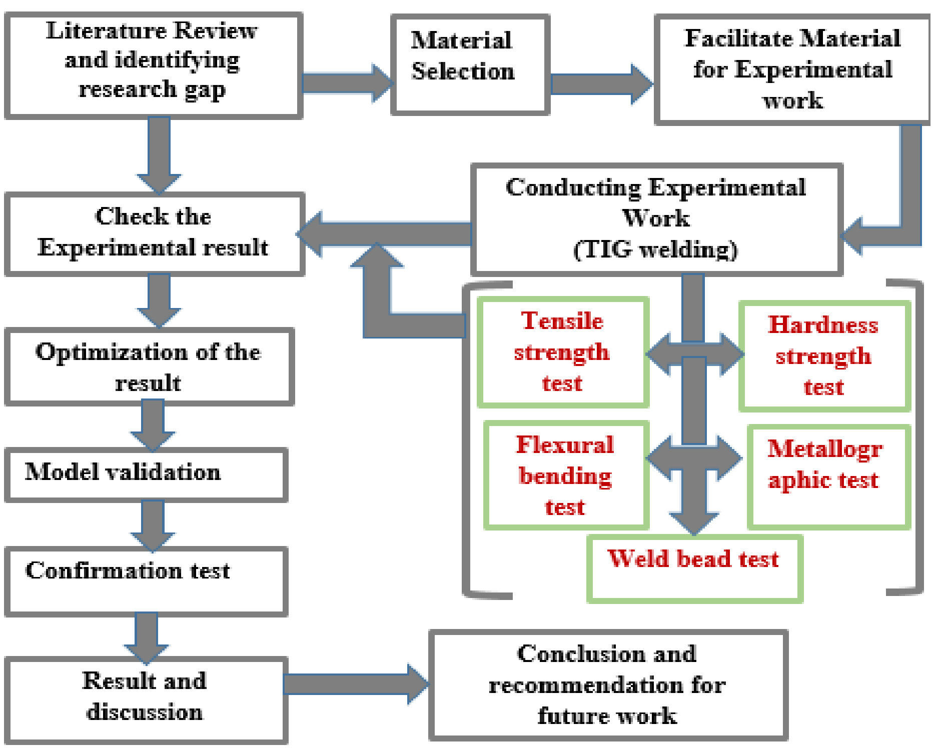

Figure 3.1 Flow chart for experimental work (research methodology)

3.1. Material Selection

The workpiece material employed in this experiment were stainless steel (SS316) and mild steel (AISI 1020).

3.1.1. Base material

3.1.1.1. AISI 316 Stainless steel

Type SS316 is an austenitic chromium-nickel stainless steel with a molybdenum concentration of 2% to 3%. The inclusion of molybdenum improves general corrosion resistance as well as strength at high temperatures. This material has the same properties as Type 304, except it is stronger at higher temperatures. furnace components, heat exchangers, jet engine parts, pharmaceutical and photographic equipment, valve and pump trim, chemical equipment, digesters, tanks, evaporators, pulp, paper, and textile processing equipment parts are some examples of typical applications (MakeItFrom.com, n.d.).

3.1.1.2. AISI 1020 Low Carbon

AISI 1020 is low carbon steel with a Brinell hardness range of 119 to 235 and a tensile strength range of 410 to 790 MPa. Machinability, strength, ductility, and weldability are all excellent. It resists induction hardening and flame hardening due to its low carbon concentration (eFunda, 2012). AISI 1020 steel can be used in a wide range of industrial applications to improve weldability and machinability. It is employed in a range of applications including general engineering parts and components, machinery parts, shafts, camshafts, and others.

3.1.1.3. Weldability of both materials

The austenitic class of stainless steel is thought to be weldable using standard fusion and resistance procedures. Avoiding hot cracking requires special consideration, such as ensuring the production of ferrite in the weld deposit. Due to the structure of the weld metal, a higher alloyed filler metal may be required. This steel does not require any preheating. The heat conductivity of austenitic steels is only 30% that of non-alloyed steels. Due to their lower fusion point than non-alloyed steels, austenitic steels must be welded with lower heat input than non-alloyed steels. (MakeItFrom.com, n.d.). Welding AISI 1020 can be done with the most common welding processes. Cold-drawn or turned and polished steel is more weldable. When the metal has been heat-treated or carburized, it is recommended that the welding technique be avoided (eFunda, 2012).

3.1.1.4. Chemical composition of base and weld metals

The steel's composition will always be a compromise. It can be costly to obtain desirable weldability and hardness, although a small compromise in those aspects can lower the price (Hannerz, 2002). The elements and their effects on weldability and other properties of the metal are listed below.

Carbon (C): Carbon is required for steel to build strength, yet it is inexpensive. Carbon concentration increases tensile strength and hardness while decreasing ductility and weldability. (Hannerz, 2002).

Nickel (Ni): Corrosion and heat resistant austenitic steels are made with nickel over 8% wt. coupled with high chromium content. It enhances the strength of steel (Maalekian, 2007).

Chromium (Cr): Increased chromium content can have a deleterious effect on reheat cracking up to 1.5 percent wt., but after that, the danger of reheating cracking reduces as chromium content increases (Maalekian, 2007).

Molybdenum (Mo): Molybdenum increases pitting corrosion resistance in austenitic steels and strengthens and hardens low alloy steels at high temperatures (Maalekian, 2007)

Manganese (Mn): Steel manganese content is proportional to carbon content; lower carbon content necessitates higher manganese content, and vice versa (Hannerz, 2002; Leonghuat, 2015). Steel can become brittle if carbon and manganese levels are too high. Manganese should be 0.30 percent wt. to 0.80 percent wt. to promote weldability.

Silicon (Si): Low carbon and silicon can harm welding surface quality, and high carbon and silicon together can exacerbate cracks. Silicon also affects steel toughness and can help prevent pores and cavities in welds (Leonghuat, 2015).

Phosphorus (P): It improves toughness and ductility while decreasing strength and hardness. Although phosphorus can improve machinability in some steels, concentrations greater than 0.04 percent wt. can increase the likelihood of cracking and render welds brittle (Leonghuat, 2015; Maalekian, 2007).

Sulfur (S): Sulphur reduces ductility while increasing machinability. Weldability is reduced when the sulfur level rises (Leonghuat, 2015).

The chemical composition of the base and weld metals were performed at Ethiopian Technical Institute using ARC-MET8000 spectrometer which is an analysis of metal using air and argon. Tables 3.1 illustrate the chemical composition and mechanical properties of SS316 and AISI

1020 mild steel. ARC-MET8000 has been designed to identify all the key elements in metals, including carbon and other light elements as shown in Figures 3.3 and 3.4 below. Recognizing that carbon identification is of primary concern in all material verification functions, especially welding, ARC-MET8000 has the unique capability of measuring carbon in both air and argon modes (Oxford instruments, 2007).

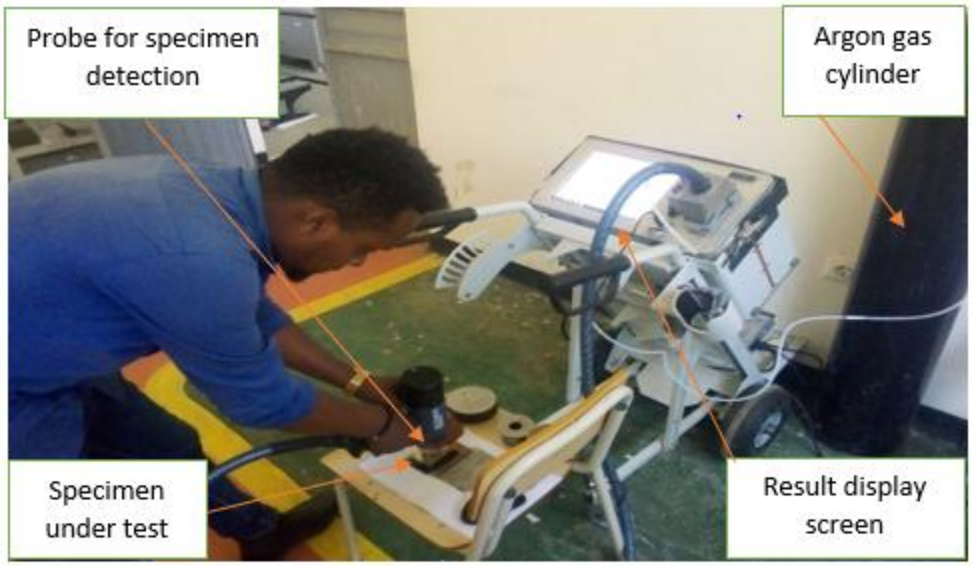

Figure 3.2 chemical composition test ARC-MET8000 portable spectrometer (at Ethiopian Technical university)

Figure 3.3 specimen for chemical composition after testing

Table 3.1: Chemical composition of SS316 and AISI 1020

Materials (AISI designation)		Chemical composition (wt.%)									
		C	Mn	P	S	Si	Cr	Ni	Mo	N	Fe
Base metals	AISI 316	0.08	1.95	0.045	0.03	0.70	16.50	12.06	2.40	0.10	65.180
	AISI1020	0.20	0.40	0.042	0.03	-	-	-	-	-	99.328

Table 3.2: Chemical composition of weld metal

Weld metals		Chemical composition (wt.%)										
Weld	Filler used	C	Mn	P	S	Si	Cr	Ni	Mo	N	Cu	Fe
Similar metal welding	ER-316	0.045	1.63	0.044	0.03	0.50	17.36	11.35	2.27	0.093	-	65.48
	ER-309	0.045	1.99	0.042	0.03	0.77	21.63	12.83	1.25	0.015	0.52	60.88
	ER-312	0.101	1.95	0.035	0.03	0.56	20.25	10.62	1.25	0.015	0.52	64.67
	ER-70S-3	0.094	1.27	0.028	0.03	0.53	5.588	3.701	0.36	0.015	0.25	88.13
Dissimilar metal welding	ER-316	0.063	1.70	0.043	0.03	0.40	14.61	10.74	1.90	0.078	-	70.44
	ER-309	0.063	1.75	0.041	0.03	0.67	17.99	9.81	0.89	0.015	0.52	68.22
	ER-312	0.119	1.72	0.034	0.03	0.46	20.25	11.05	0.89	0.015	0.52	64.91
	ER-70S-3	0.112	1.03	0.027	0.03	0.42	2.843	1.89	0.36	0.015	0.25	93.03

Table 3.3: mechanical properties SS316 and AISI 1020 (MakeItFrom.com, n.d.; eFunda, 2012)

Mechanical properties	Value	Value
	SS 316	**AISI1020**
Ultimate tensile strength	579MPa	394.72 MPa
Yield strength	290MPa	294.74 MPa
Percentage elongation(in 50mm)	50%	36.5 %
Rockwell hardness B	79HRB	64 HRB
Mean Coefficient of thermal expansion (0-649°C)	(18.5)µm/m*K	14.8 µm/m*K

3.3.2. The material used for filler

ER316, ER309 stainless steel, ER70S-3 mild steel, and ER312 stainless steel filler material with a diameter of 2mm were employed as filler metals.

ER-316L: Welding low carbon molybdenum-bearing austenitic alloys with ER316L is the most common use. This filler metal has the same chemical composition as ER316, with the exception that the carbon concentration is limited to 0.03 percent to prevent intergranular carbide precipitation. At high temperatures, this low carbon alloy is not as robust as ER316H (Inweld.com, n.d.-c).

ER-309L: 309L is austenitic stainless steel that can be used to weld 309, 309L, 304, 316, and other 300 series stainless sheets of steel. Excellent for welding austenitic clad stainless steel to mild or carbon steels, buttered passes on steel overlay work, and attaching stainless steel to mild or carbon steels. Because of the lower carbon concentration (L), the weld deposit is more resistant to inter-granular corrosion produced by carbide precipitation, which may occur if employing straight 309 grade (Inweld.com, n.d.a).

ER-312: The ER312 stainless-steel electrode is the most versatile of the All-Position electrodes. On difficult-to-weld steels including low, medium, and high carbon steels, this is an excellent choice. When the base metal is an unknown grade of steel, this electrode is ideal. Manganese-hardening steel, Armor steel, rail steel, nickel-clad steel, tool and die steel, and aircraft steel are all suitable for a variety of uses. In hard-facing applications, it's commonly utilized as a wear-resistant build-up and "buffer" layer. Work hardens to a Brinell hardness of 200. The weld deposit has a microstructure of 29 percent chrome, 9 percent nickel, and 30% ferrite in an austenitic matrix (Inweld.com, n.d. b).

ER-70S-3: The silicon and manganese levels in ER70S-3 are adequate for general-purpose welding over clean to light levels of rust and mill scale. The ER70S-3 can deliver trouble-free performance in a wide range of applications, from heavy-duty, high-speed spray or pulse applications to lighter-duty, lower-speed short-arc applications. ER70S-3 produces a clean, stable arc with minimum spatter even in the most demanding situations, resulting in a weld a bead that ties in evenly with the sides and has a smooth completed appearance. (Unibraze corporation, 2000).

Table 3.4: chemical composition of commercial filler metals

Materials (AWS designation)		Chemical composition (wt.%)										
		C	Mn	P	S	Si	Cr	Ni	Mo	N	Cu	Fe
Filler metals	ER-316L	0.03	1.92	0.043	0.03	0.42	16.98	12.05	2.21	0.09	-	Bal.
	ER-309L	0.03	2.00	0.04	0.03	0.80	23.06	13.20	0.75	-	0.74	Bal.
	ER-312	0.11	1.95	0.03	0.03	0.50	25.00	10.00	0.75	-	0.74	Bal.
	ER-70S-3	0.10	0.98	0.021	0.03	0.46	0.14	0.12	-	-	0.35	Bal.

- **Shielding gas used**: Pure Argon
- **Electrode used**: non-consumable tungsten with 2% thorium electrode having 2.4mm diameter.
- **Metal thickness**: 3mm.
- **Filler metal diameter**: 2mm.

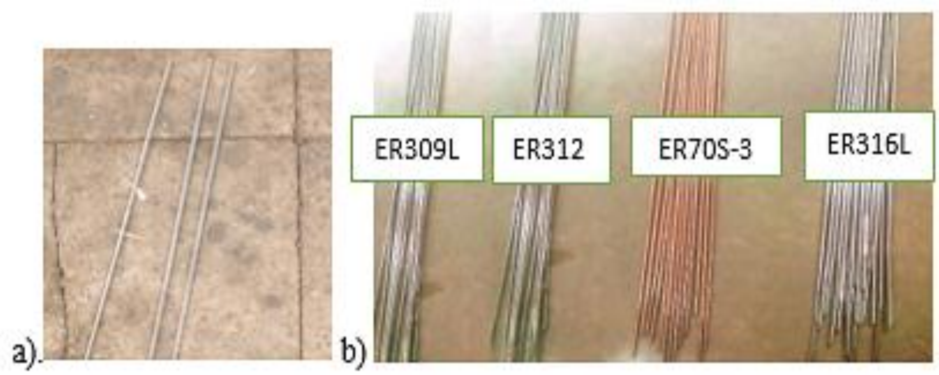

Figure 3.4 material used: a) Tungsten (98%) with (2%) thorium oxide electrode, b) filler metals

3.4. Experimental Work

Experiments are conducted at the Centre of Excellence for Engineering (welding training center) workshop on TELWIN Superior 322 TIG welding machine as per DOE Taguchi by considering process parameters like welding current, Root Gap, Gas Flow Rate, and type of filler metals at 4 levels which gives L16 Orthogonal array and analyze the output results based on ANOVA. Table 3.5 shows process parameters and their levels.

Table 3.5: selected process parameters and their levels

S. No	Process parameter	Units	Levels			
			1	**2**	**3**	**4**
1	Welding current	Amp (A)	70	90	110	130
2	Root Gap	Mm	1	1.5	2	2.5
3	Gas flow rate	L/Min	7	10	13	16
4	Type of filler metals	Type	ER316	ER309	ER70S-3	ER312

3.4.1. Sample Preparation and welding condition

As illustrated in the figure 3.7, stainless and mild steel stock sheets with dimensions of 100mmx75mmx3mm are sectioned. The E21S ESTUN shear cutting machine shown in figure 3.8 is subsequently used to cut the produced stock sheet into plates. To make the weld joint, the edge preparations will be arranged. Finally, 100mm x 75mm x 3mm specimens are manufactured, and butt joints are formed using these specimens. The edges of the work components will be adequately prepared before welding. Using a wire brush, dust will be removed from the edges and the space surrounding them.

a) b) c)

Figure 3.5 specimen preparation: a) stainless steel, b) mild steel, c) after shear cutting

Figure 3.6 shear cutting machine (@ CEE)

3.4.1.1. Back purging tool preparation

The welding torch is designed to spray shielding gas to protect the front of the weld during the welding process (Soul performance Products, 2019). The back purging tool is made to fit the type and dimensions of the welded joint. The purging gas tool is used in this study to protect the weld from lack of penetration and sugaring (oxidation). The designed and prepared back purging tool for gas extraction was shown in figure 3.9.

Figure 3.7 Back purging tool a) 2D with dimension b) 3D model c) on device preparation d) finished device

3.4.2. Experimental setup

The welding setup has the following parts as shown in figure 3.10.

- **TIG welding machine**: Direct current with a negative electrode was used. During welding, current and voltage are delivered. Depending on the current setting, a current range of 10-180 amps and a voltage of up to 230 V will be used but here current (70-130) and voltage (13) were used.

- **Cylinder for front and back purging gas**: TIG welding uses argon gas, which is fed into the welding flame at a specific flow rate (7-16 l/min) to provide an inert atmosphere and a steady arc.
- **Work holding table:** A surface plate (made of cast iron) is used to hold the back purging tool, on which a workpiece is secured so that the welding gap between the tungsten electrode and the workpiece can be manually maintained between 1 to 3mm. The work parts to be welded are then positioned concerning one another, and the welding process is carried out at a constant voltage with the wire diameter in a flat (down hand) position. However, according to 16 combinations of data from the L16 orthogonal array shown in table 3.6, the welding current, Root Gap, Gas Flow Rate, and type of filler metals vary for each test.

Figure 3.8 Equipment used for TIG welding setup (@ CEE)

Table 3.6: Experimental plan for similar and dissimilar welding (L16) OA

S. No	*Welding Current (A)*	*Gas Flow Rate (L/min)*	*Root Gap (mm)*	*Filler metal Type*
S1	70	7	1	ER70S-3
S2	70	10	1.5	ER316
S3	70	13	2	ER309
S4	70	16	2.5	ER312
S5	90	7	1.5	ER309
S6	90	10	1	ER312
S7	90	13	2.5	ER70S-3
S8	90	16	2	ER316
S9	110	7	2	ER312
S10	110	10	2.5	ER309
S11	110	13	1	ER316
S12	110	16	1.5	ER70S-3
S13	130	7	2.5	ER316
S14	130	10	2	ER70S-3
S15	130	13	1.5	ER312
S16	130	16	1	ER309

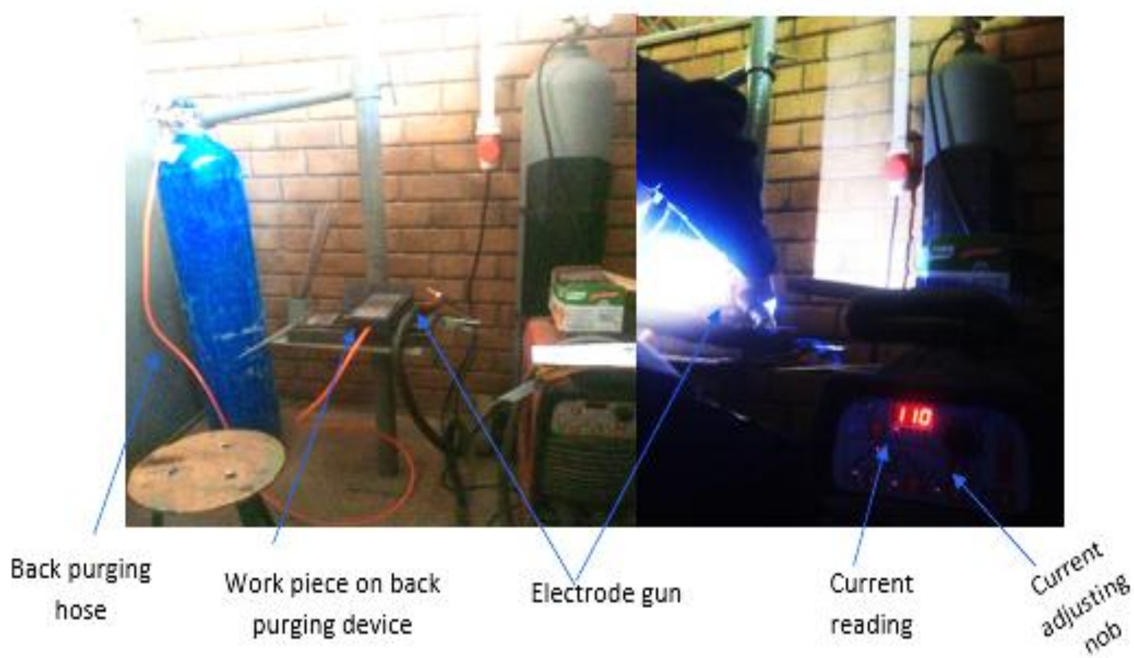

Figure 3.9 GTAW experimental setup (at Centre of Excellence for Engineering, Addis Ababa, Ethiopia)

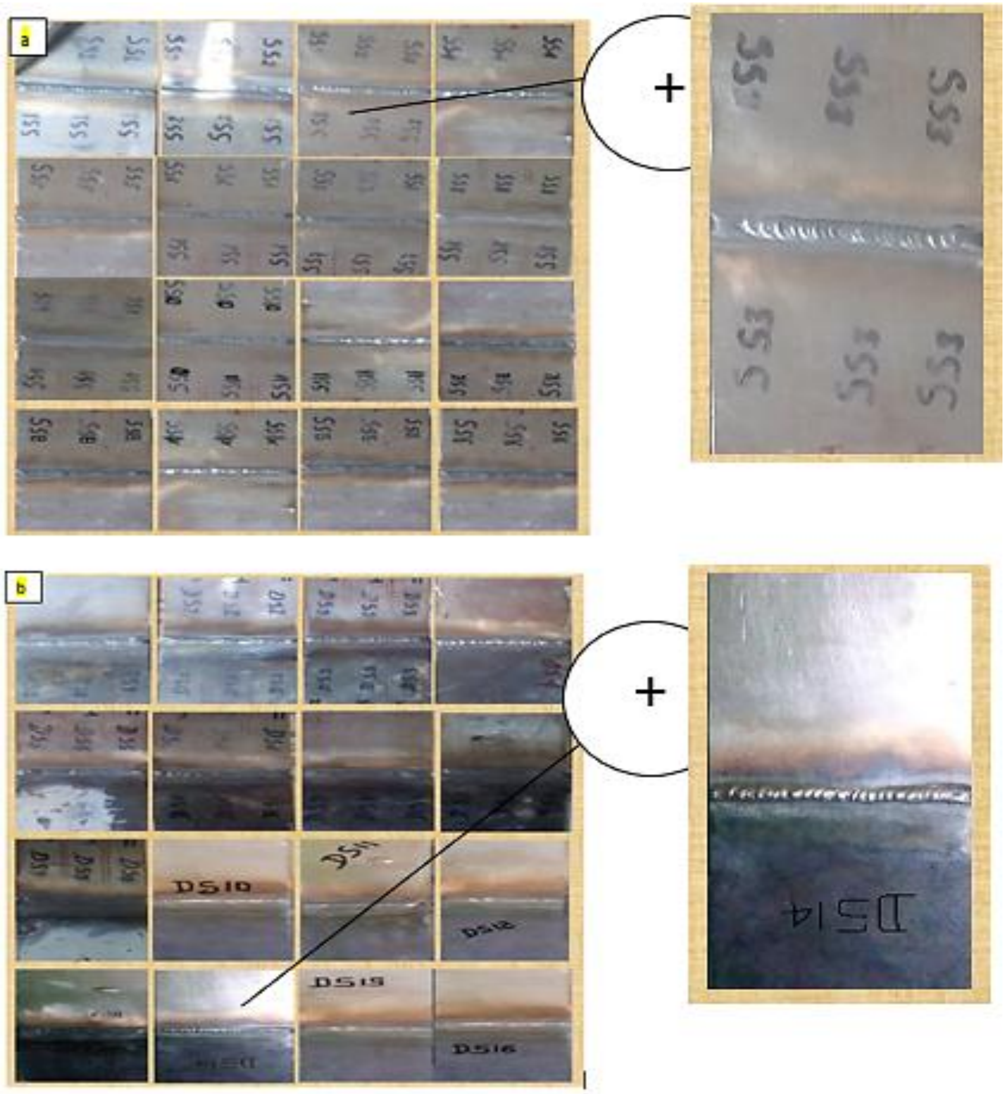

Figure 3.10 welded samples before polishing, a) similar samples, b) dissimilar samples

3.5. Weld Bead Geometry Testing

TIG welding (tungsten inert gas) is a multi-objective, multi-parameter metal manufacturing process. Several process parameters interact in a complicated way, having direct or indirect effects on weld bead geometry, mechanical properties, metallurgical aspects of the weldment, and weld chemistry. TIG weld quality is mostly determined by the geometry of the weld bead. Welding process parameters such as welding speed, welding current, shielding gas flow rate, and gap distance greatly influence bead geometry variables such as heat-affected zone, bead width, bead height, penetration, and area of penetration, and it also plays an important role in determining the mechanical properties of the weld such as tensile strength, hardness, and bending strength of the weld (Esme et al., 2009).

3.5.1. Bead width geometry of the weld

The width of each welded sample was measured with 0.01 mm least count vernier calipers to determine the weld bead width. Because the width of each welded sample varies depending on the parameter utilized, the weld with the smallest bead width is considered a good weld. Figure 3.13 shows the weld bead that has been measured for bead width of similar and dissimilar welded metals.

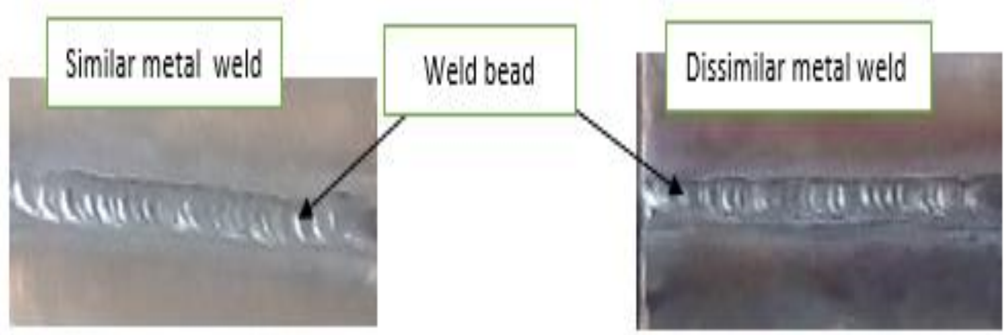

Figure 3.11 weld bead of simar and dissimilar welded samples

3.6. Welding Defects Using Non-Destructive Testing (NDT)

A faulty weld fails to meet any or all the standards of a certain specification or code. It's impossible to evaluate a faulty weld. Without a reference to a specific standard or criteria about the weld's intended purpose (AWS committee, 2000).

3.6.1. Liquid penetrant test (PT)

Liquid or dye penetrant testing (PT) is a non-destructive material testing method that employs capillary forces to locate and see surface cracks or holes. It can identify faults on the surface, like as fractures, laps, and porosity. The penetration of liquid penetrant through open surface discontinuities is the basis of PT. Surface flaws such as surface cracks, porosity, absence of fusion, and intergranular corrosion is detected using the dye penetrant method. Welds and parent material are subjected to dye penetrant testing. PT testing can be used on any non-porous, clean material, whether metallic or non-metallic, however, it is not recommended for extremely rough surfaces. Surface cleaning is an important aspect of penetrant testing.

3.6.2. Experimental Procedure

The initial surface area of a test piece is evaluated. Then, using a multi-purpose cleaner, pre-clean the area to remove any superfluous material such as scale, slag, grease, oil, paint, water, and the like. Cleaning with chlorinated hydrocarbons, volatile petroleum distillates, or acetone. Some dwell time should be allowed for the evaporation of the volatile cleaner from discontinuities before the penetrant is applied. Then the penetrant is applied to the surface area of the test samples by spraying. After the penetrant is applied some dwell time was allowed until the capillary action allows this to permeate small fractures or pores. After carefully removing the remaining test media from the surface, a developer is used to draw the dye penetrant out of the pores and cracks, sufficient time should be allowed after the developer has been applied to permit it to draw or blot out the penetrant from any discontinuities which Resulting in indications that may be analyzed as a defect. Finally, the test specimens were cleaned with solvents following the completion of the examination as shown in figure 3.14.

Figure 3.12 PT Processes: a) pre-cleaning samples by using general-purpose cleaner, b) penetrant for segregation c) developer d) Application of a penetrant liquid, e) Application of developer f) Inspection of the test surface, g) post-inspection cleaning (anti-corrosion solutions)

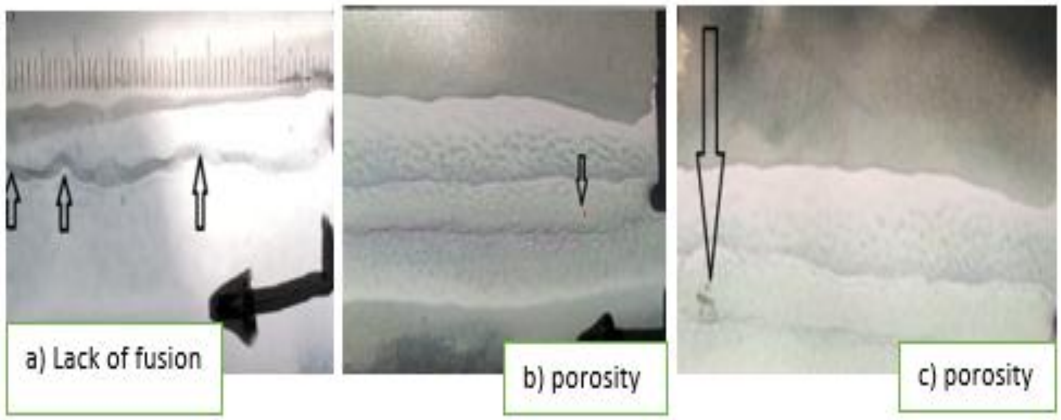

Figure 3.13 defects on similar weld metal: a) sample no.1, b) sample no.2, and c) sample no.9

Figure 3.14 defects on dissimilar weld metal: a) sample no.1, b) sample no.2, and c) sample no.13

3.7. Mechanical Property Testing

For various testing, TIG-welded experimental specimens were created from welded SS316 and AISI1020 MS metals and machined using ASTM to determine the necessary dimensions for studying their properties.

3.7.1. Tensile Strength Testing

Tensile testing is a fundamental material science and engineering test in which a sample is subjected to a controlled tension until failure. Properties that are directly-measured via a tensile test are ultimate tensile strength, breaking strength, maximum elongation, and reduction in area (Davis, 2004). Uniaxial tensile testing is the most used for obtaining the mechanical characteristics of isotropic materials. Some materials use biaxial tensile testing. The main difference between these testing machines is how the load is applied to the materials (Davis, 2004). The tensile properties for any base material are also applied as the same procedure and specimen preparation it is important that the tensile properties of the base metal, the weld metal, the bond between the base metal and weld metal, and the HAZ conform to the design considerations of the weldment. Where butt joints are used, the weld metal should usually develop the minimum tensile properties of the base metal (AWS committee, 2000).

3.7.1.1. Specimen preparation and test procedures

The preparation of test specimens depends on the purposes of testing and the governing test method or specification. A tensile specimen usually has a standardized sample cross-section. As shown in table 3.7 and figure 3.17. It has two shoulders and a gauge (section) in between. The shoulders and grip section are generally larger than the gauge section by 33% so they can be easily gripped (Davis, 2004). The specimens prepared for testing were shown in figure 3.18 according to ASTM E8M (D370).

Table 3.7: ASTM E8 standard for tensile test specimen (Davis, 2004)

All values in inches (1 in = 25mm)	Plate type (1.5 in. wide)	Sheet type (0.5 in. wide)	Sub-size specimen (0.25 in. wide)
Gauge length	8.00 ± 0.01	2.00 ± 0.005	1.000 ± 0.003
Width	1.5 + 0.125– 0.25	0.500 ± 0.010	0.250 ± 0.005
Thickness	0.188 ≤ T	0.005 ≤ T ≤ 0.75	0.005 ≤ T ≤ 0.25
Fillet radius (min.)	1	0.25	0.25
Overall length (min.)	18	8	4
Length of reduced section (min.)	9	2.25	1.25
Length of grip section (min.)	3	2	1.25
Width of grip section (approx.)	2	0.75	3⁄8

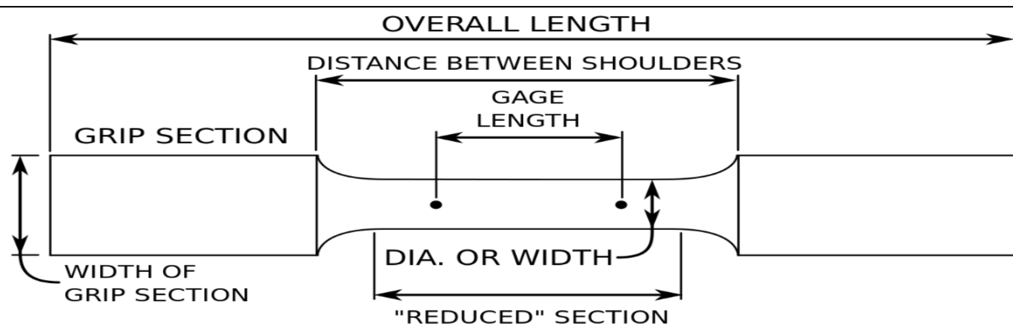

Figure 3.15 tensile test specimen standard dimension (Davis, 2004)

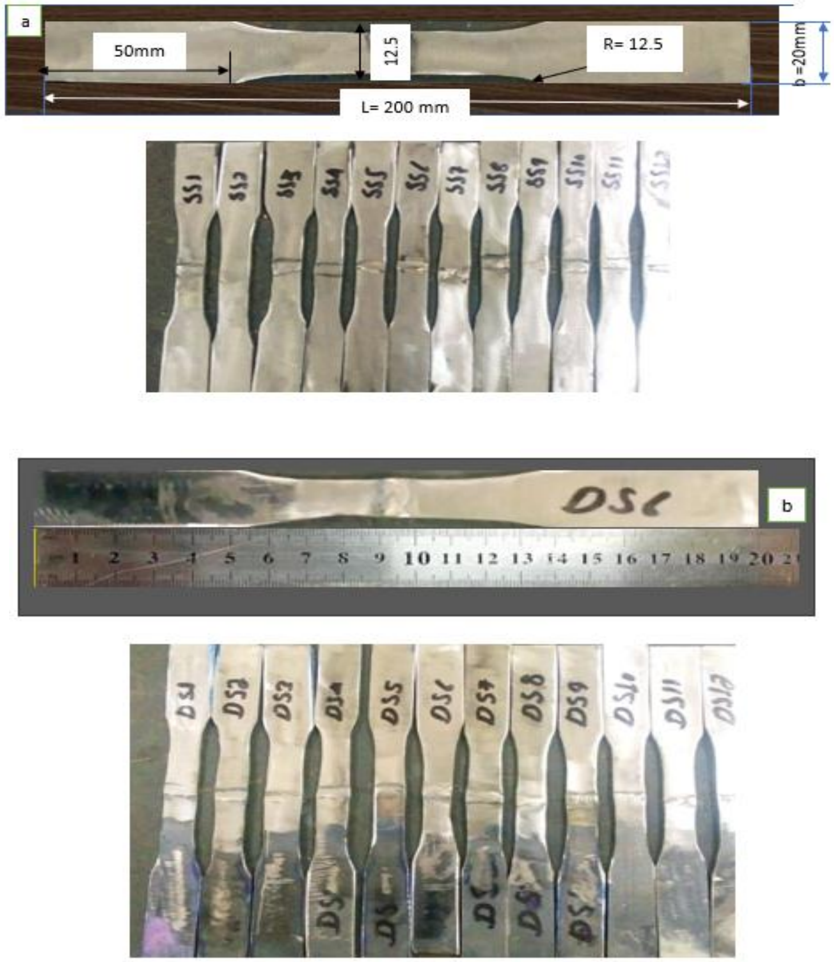

Figure 3.16 sample of specimen prepared for tensile strength: a) for similar, b) for dissimilar

The experimental procedure was carried out at Ethiopian Technical Institute using a HUT 600 servo-hydraulic Universal testing machine with a piston speed (strain rate) of 8mm/min as illustrated in figure 3.19. After specimens were prepared and the UTM machine was set up properly the test process was performed by placing the test specimen in the testing machine and slowly extending it until it fractures as shown in figure 3.20. During this process, the elongation of the gauge section is recorded against the applied force. The data is manipulated so that it is not specific to the geometry of the test sample. The elongation measurement is used to calculate the engineering strain, ε, using the following equation (Davis, 2004).

$$\varepsilon = \frac{\Delta L}{L} \tag{3.1}$$

where ΔL is the change in gauge length, L_0 is the initial gauge length, and L is the final length. The force measurement is used to calculate the *engineering stress*, σ, using the following equation:[5]

$$\sigma = \frac{F}{A} \tag{3.2}$$

$$A = b * t \tag{3.3}$$

where F is the tensile force, A is the nominal cross-section of the specimen, b is the width of the specimen and t is the thickness of the specimens. The machine does these calculations as the force increases so that the data points can be graphed into a stress-strain curve.

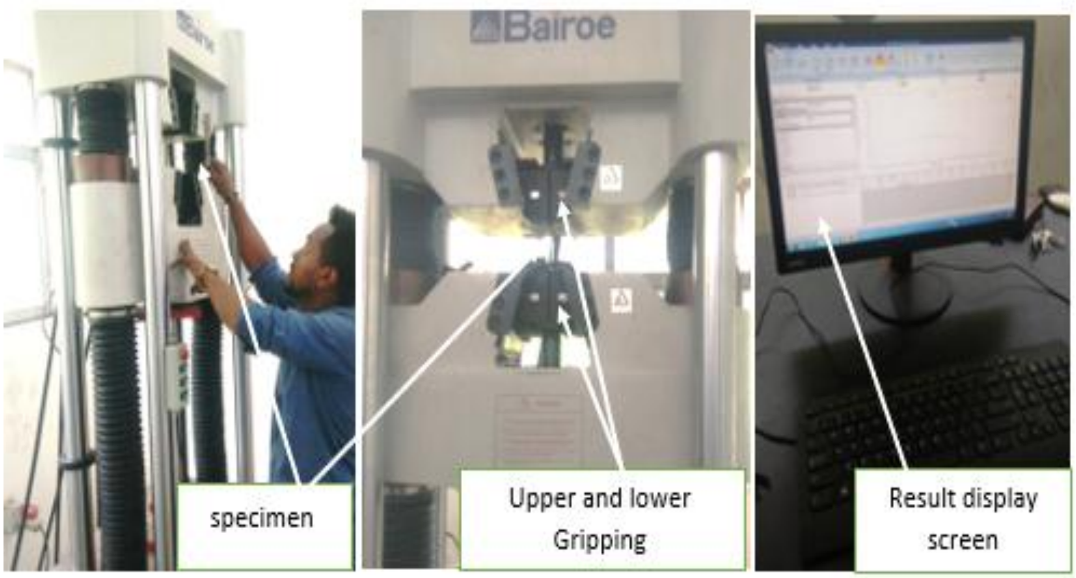

Figure 3.17 tensile test experimental set-up (at Ethiopian Technical Institute)

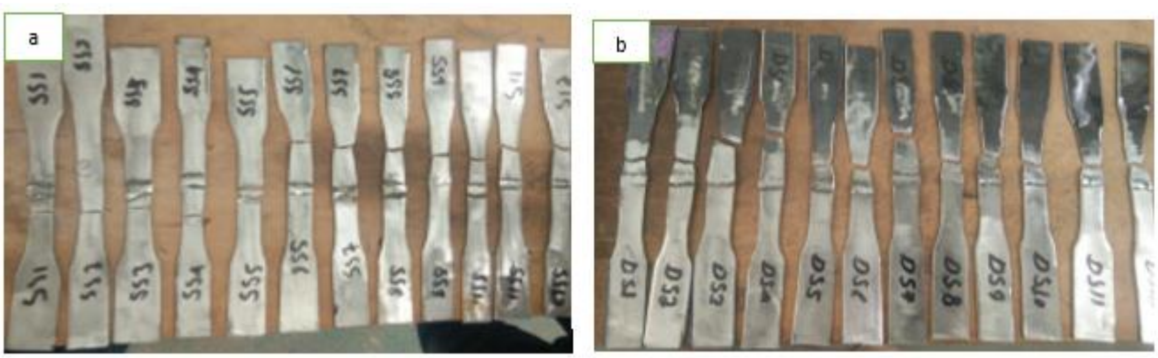

Figure 3.18 some of specimens after the tensile test: a) similar specimen, b) dissimilar specimen

3.7.2. Hardness Testing

Hardness refers to a material's ability to resist deformation, which is determined by a standard test that measures surface resistance to indentation. In a calibrated hardness testing equipment, the hardness of a weldment or welded specimen is assessed by pushing a hardened steel ball or diamond point into a flat surface on the weldment or welded specimen with a prescribed load and measuring the size of the resulting indentation (AWS committee, 2000). Vickers's test, Brinell test, and Rockwell test are the three most used hardness testing equipment. The Rockwell test method can be used on any metals unless the indentations are too large for the specimens, or the shape of the specimen prevents it from being used. The Rockwell hardness test is very easy to perform. However, some precautions must be taken, such as a good surface finish on the specimens for more accurate and repeatable results, the bottom side of the specimens must securely contact the anvil without interference from debris or other loose material, and the specimens must be held stably throughout the test unless the specimen can affect the result. In most cases, a steel ball or a diamond indenter is used in the Rockwell hardness test. Rockwell hardness values are represented by a combination of a hardness number and a scale symbol that symbolizes the indenter as well as the major and minor loads.

3.7.2.1. Experimental procedure

The experimental work took place at the Metal Industry Development Institute (MIDI). Polished specimens were evaluated using ASTM E-18 (30x20x3 mm3), and the hardness strength of the welded samples was examined using a BROOKS Rockwell hardness testing equipment with ball shape indenter at a force of 100kg for 10 seconds as depicted in figure 3.21. The test was performed on the welded specimens at three distinct places, and the average result for the BM zone, HAZ, and weld zone was recorded as the hardness of the weld joint. Two methods of testing were used in each testing session. The HRB hardness of the weld is first determined using a conventional Rockwell hardness test machine with a ball shape indenter, and then the hardness of the material is determined using an EQUOTIP2 Digital hardness testing machine that reads in HRB. In Rockwell hardness testing, a modest load is applied to the welded specimen with 10Kg as reference (minor load). Following that, the main load of 100Kg is imposed. Finally, the Rockwell hardness test value is calculated using the increased depth of penetration caused by the major load, and the result is displayed on the machine's dial display.

Figure 3.19 Conventional Rockwell hardness testing machine @ MIDI, Addis Ababa

An impact body with a hard metal test tip is driven against the surface of the test piece by spring force in a portable digital hardness tester. When the impact body collides with the test surface, surface deformation occurs, resulting in kinetic energy loss. This energy loss is determined by comparing velocities vi and vr for both the impact and rebound phases of the test when the impact body is at a specific distance from the surface. A permanent magnet in the impact body provides an induction voltage in the coil, which is properly positioned in the impact device, which is used to measure velocity. The voltage observed is proportional to the impact body's velocity. Following that, signal processing provides the hardness reading.

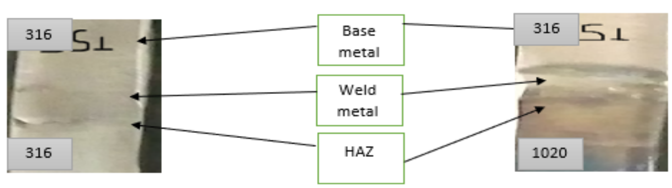

Figure 3.20 specimen prepared for hardness test

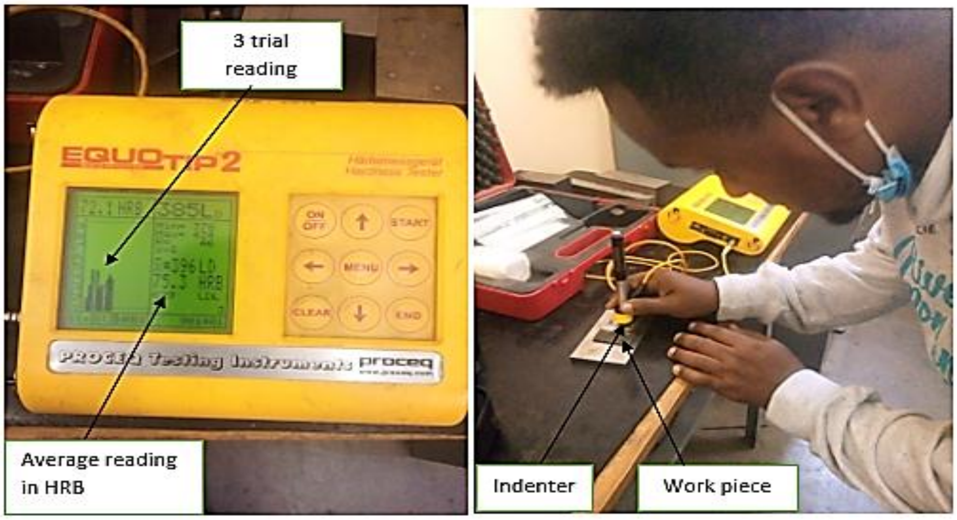

Figure 3.21 Portable digital hardness testing machine @ MIDI, Addis Ababa

3.7.3. Flexural Strength Testing

The amount of force an object can withstand without breaking or permanently deforming is known as flexural strength (or modulus of rupture). Flexural strength is the maximum pushing force the wood can withstand before breaking. Flexural strength describes the material's maximal stress tolerance and is expressed as a force (in newtons or pounds-force) per unit area (Johnson, 2022).

In a three-point flexure bending strength test, In the center of the sample, a steadily increasing load is applied until the material breaks or bends permanently. A flexural test machine can apply increasing levels of force while simultaneously recording the force at the point of failure. A rectangular cross-section specimen is put on two parallel supporting pins in the test. By using a loading pin, the loading force is applied in the center. This arrangement ensures that the specimen is loaded evenly and that there is no friction between the specimen and the supporting pins (Dr. Dmitri, 2021).

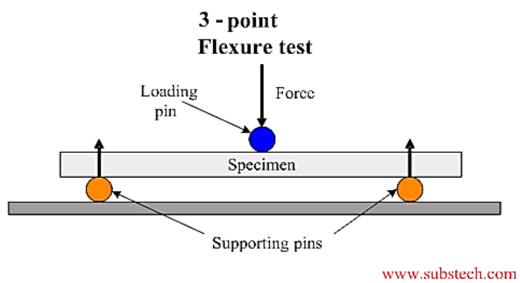

Figure 3.22 3-point bending fixture (Dr. Dmitri, 2021)

3.7.3.1.Flexural strength calculation

The specimen bends as a result of the loading, creating tension on the convex side and compression stress on the concave side. In a flexural test, the crosshead speed is usually between 0.1 and 10 mm/min. In most testing, speeds of 1 mm/min and 2.54 mm/min are used. For each load value, the maximum stress and related maximum strain are determined. The stress-strain diagram is then used to plot the results. The stress of a specimen's extreme fiber at failure in the Flexure Test is known as the Modulus of Rupture (Flexural Strength) (Dr. Dmitri, 2021). The formula for calculating the flexural strength of a rectangular specimen in a 3-point test (AWS Committee, 2000) is:

$$\boldsymbol{\sigma} = 3LF/(2bd^2) \qquad (3.4)$$

where L - specimen length.

F - total force was applied to the specimen by two loading pins.

b - specimen width.

d - specimen thickness

3.7.3.2.Preparation of 3-point flexural bending fixtures

The flexural bending fixture was prepared at the center of excellence for engineering in the welding workshop. The sample rests on supports or the bottom block and is not clamped during the test. The distance between supports is selected to force the specimen to conform to the mandrel radius without excessive interference. This clearance is often the mandrel diameter, *d*, plus three times the specimen thickness, *t* as shown in figure 3.25. Bending force is applied at the center of the specimen (ASM Handbook Committee, 2000).

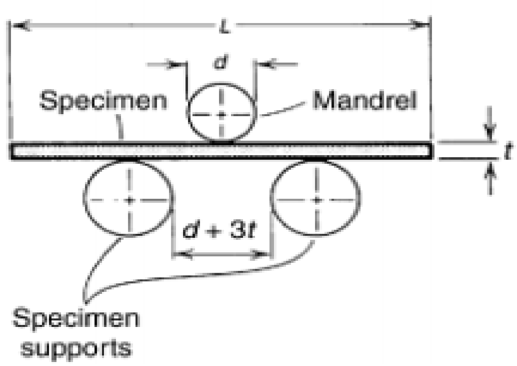

Figure 3.23 dimension for 3-point bending fixtures (ASM Handbook Committee, 2000)

Figure 3.24 3-point flexural bending fixture after preparation

The span length of the prepared fixtures was 29mm since the diameter of the mandrel is 20mm and the thickness of the base metal is 3mm. figure 3.26 show the manufactured 3-point fixtures.

3.7.3.3. Specimen preparation and test procedure

Sheet and plate specimens normally are full thickness and are prepared by shearing or sawing. Narrow strips and bar sections can be tested with specimens cut to length. So, the specimen under this test is sectioned by using a power hacksaw that has a cooling fluid to keep the material properties, at the Center of excellence for the engineering workshop shown in figure 3.27.

The flexural test, which combines tensile and compressive testing to evaluate a material's flexural strength, is one of the most fundamental bending tests. The capacity of a material to resist bending stresses applied perpendicular to its longitudinal axis, or the maximum force it can withstand before breaking or yielding, is referred to as flexural strength. The material test specimens for the 3-point bending test were manufactured following ASTM E290. The dimensions of each specimen were 200x20x3mm in length, width, and thickness, according to this standard as shown in figure 3.28. A flexural test was performed at Ethiopian Conformity Assessment Enterprise (ECAE) utilizing an EN 10002-1; DIN 50.125 and UNE 7184 Servo-hydraulic universal testing machine with a crosshead velocity of 10mm/min at room temperature as shown in figure 3.29. Figure 3.30 (a), (b), (c), and (d) illustrates the experimental apparatus and welded specimens for the 3-point bending test. Two specimens are taken for each test to demonstrate the reproducibility of the results, hence reducing experimental mistakes. In this machine, 32 specimens were tested for a single objective.

Figure 3.25 gazelle power hacksaw for specimen sectioning (at CEE)

Figure 3.26 some of specimen after sectioned for flexural strength testing

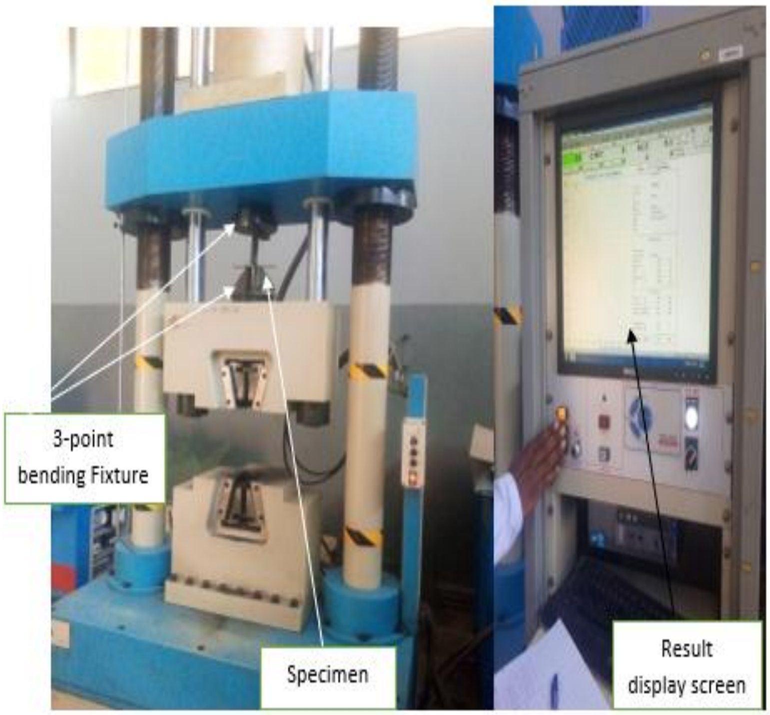

Figure 3.27 flexural testing set up (@ Ethiopian Conformity Assessment Enterprise)

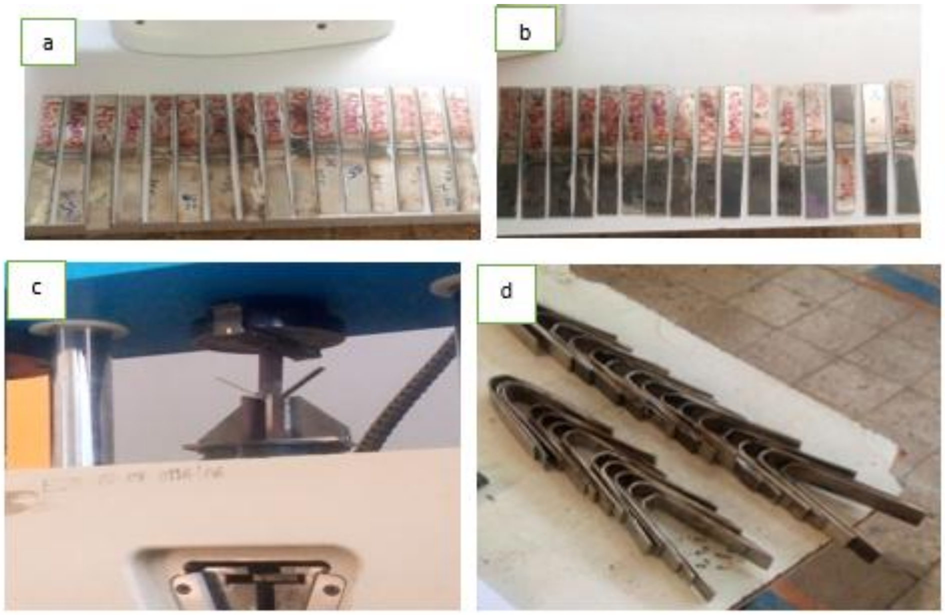

Figure 3.28 specimens: a) similar before testing, b) dissimilar before testing, c) specimen under 3-point flexural testing, and d) specimens after testing

3.8. Micro-structure and micro-hardness testing

The microstructure and micro-hardness of this study were computed at Adama science and technology university (ASTU) using the optical microscopy Model: HUVITZ HR-300 series at the material science engineering laboratory. Scanning electron microscopy (SEM) (JCM-6000Plus scanning electron microscope*)* for microstructure, morphological, and fractural mechanisms testing of the weld zone was used at the biology laboratory. Micro-hardness testing using Vicker's hardness testing machine at the material engineering laboratory. For each test, a very small diamond indenter having pyramidal geometry is forced into the surface of the specimen. The resulting impression is observed under a microscope and measured; this measurement is then converted into a hardness number (William D. Callister, 2007).

For microstructural and micro-hardness testing the samples were sectioned using an abrasive cutter that has a coolant to protect the properties of the metal for testing. Then the material was going for hot mounting. After mounting the sample then the specimens were ground using silicon carbide grit papers having #220-600-800-1200-2000 respectively. Furthermore, the samples were polished using a diamond Suspension polishing agent using the electro-polishing machine as shown in figure 3.31. Finally, the specimens were etched with the etchant solution consisting of

70% nitric acid (HNO3) for 15 seconds. Then the metallographic test was performed. The hardness testing machine is as shown in Fig. 3.32

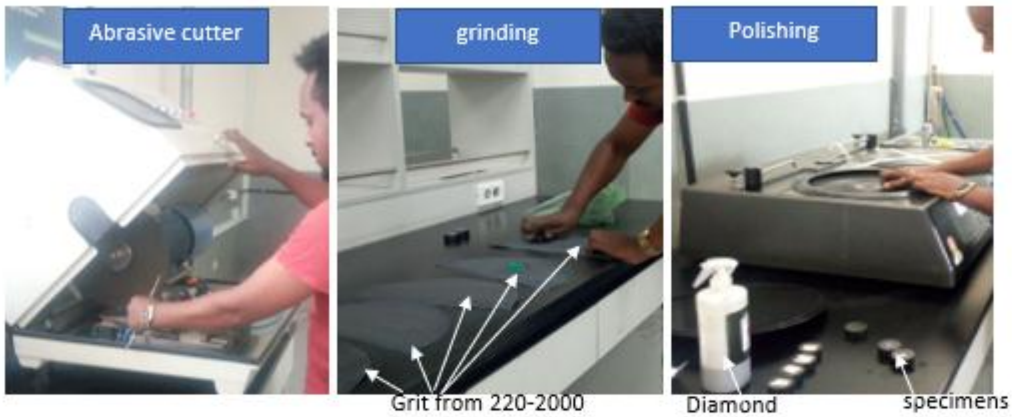

Figure 3.29 preparing a specimen for metallographic analysis

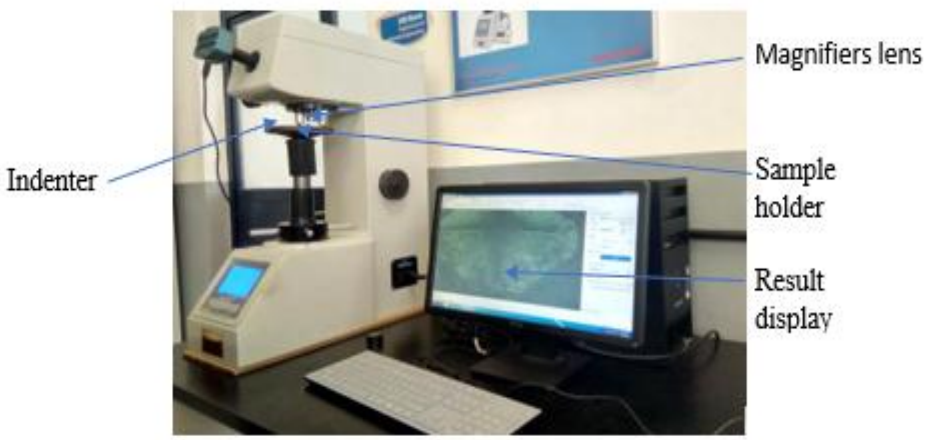

Figure 3.30 Vicker's HVS50 hardness testing machine (ASTU material laboratory)

The microstructure observation was conducted using scanning electron microscopy in the Biology laboratory, using JCM-6000Plus scanning electron microscopy. The specimen preparation considers the sample's size, shape, state, and conductive properties before sample preparation. The samples were prepared with a 30mm x 20mm x 3mm cross-section. The samples were cleaned very well. Then the samples were mounted and observed. Optical and SEM microscopy is shown in Fig. 3.33 a and b.

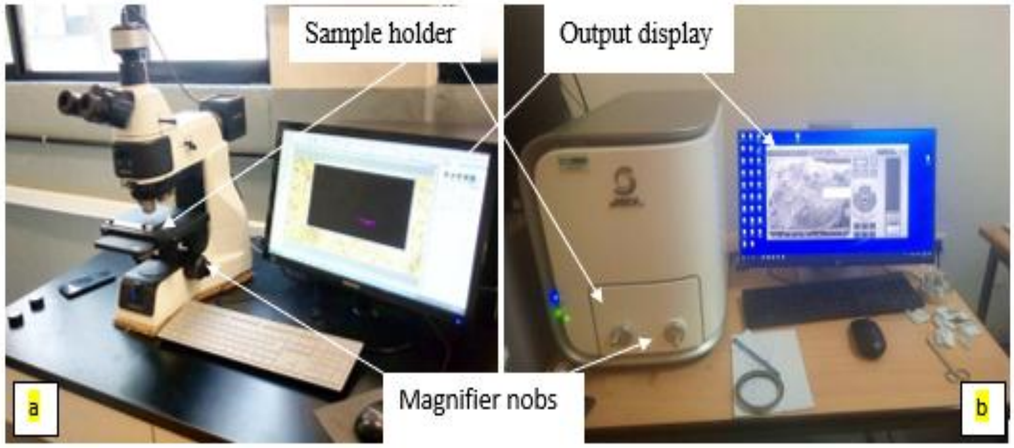

Figure 3.31 optical and scanning electron microscope (at ASTU material engineering and biology laboratory)

3.9. Taguchi Method

Taguchi's, which is one of the Designs of Experiment (DOE) applications, is used to investigate the effect of a variety of parameters and their behavior by conducting a small number of experiments and evaluating their impact on certain behavior. It can determine the best conditions for the experiment at the same time, resulting in a superior outcome. According to Taguchi, there are three primary phases: planning, conducting, and analysis (Krishnaiah & Shahabudeen, 2012). Four parameters were evaluated in this process: welding current, gas flow rate, root gap, and filler wire type. The use of an orthogonal array is determined by the total degrees of freedom of the process parameters in the Taguchi DOE concept. The number of comparisons required to optimize each parameter (factor) with the selected levels is accounted for or defined as the degree of freedom. With four components and four levels of the experiment, Minitab 19 statistical software is used to develop the experimental design of process parameters and numerical analysis.

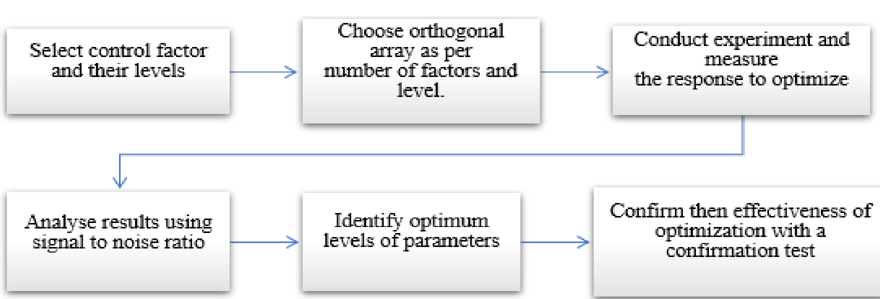

Figure 3.32 Design procedure of Taguchi methods

During TIG welding of comparable 316 stainless steel and dissimilar 316 stainless steel with AISI 1020 mild steel, the influence of welding parameters on tensile strength, hardness, flexural strength, and weld bead width was investigated at four levels of study. These TIG welding settings were chosen based on the information gathered from the literature, the guidelines of the American Welding Society (AWS), and the advice of experienced and certified people at the welding training center, Centre of Excellence for Engineering (CEE) (Addis Ababa, Ethiopia).

3.9.1. Orthogonal Array:

Before choosing the orthogonal array, estimate the minimum number of experiments to execute based on the total number of degrees of freedom. The total degrees of freedom provided must be more than the number of experiments required to study the factors (Krishnaiah & Shahabudeen, 2012). In this study, the number of layers of various factors was used to identify which orthogonal array to use. Four factors were chosen for the experiments, each having four levels.

$$DOF=P^{*}(L-1) \tag{3.5}$$

Where, DOF= degree of freedom,

P = number of factors and,

L = number of levels

DOF= 4(4– 1) = **12** (OA≥ DOF, So OA has **16** experimental runs)

After calculating the Degree of Freedom (DOF), the number of experimental runs was chosen from an orthogonal array. The total number of orthogonal array (OA) experiments should be larger than or equal to the computed value, hence the L16 orthogonal array was chosen for the experiment design.

3.9.2. Signal to noise ratio (S/N ratio)

The Taguchi technique emphasizes the value of evaluating response variation using the signal-to-noise ratio, which reduces the effect of uncontrollable parameter variation on quality characteristics. The desired value (mean) for the output characteristic is referred to as signal, while the undesired value (deviation, SD) is referred to as noise in the Taguchi method. As a result, the S / N ratio equals the average to SD ratio. Taguchi used the S / N ratio to assess the quality attribute that deviates from the desired value. There are numerous S / N ratios available depending on the type of characteristic; smaller is better, nominal is best, and larger is best (Karna & Sahai, 2012; Ross, 1996).

A. Larger the better (Maximization)
B. Smaller the better (Minimization)
C. Nominal the best

Standard S/N ratio formula:

$$\frac{S}{N}\,\text{ratio} = -10\log\left[\frac{1}{n}\sum_{j=1}^{n}\frac{1}{Yij^2}\right] \tag{3.6}$$

Where 'i' is the number of a trial; 'Yi' is the measured value of quality characteristic for the i^{th} trial and j^{th}experiment, 'n' is the number of repetitions for the experimental combination.

3.10. Multi-response optimization

Optimization of the multi-response problem is a challenge to optimizing output responses altogether. Among the simultaneous optimization methods, most of the authors used approaches that combine all the different response requirements into one composite requirement. Hence, the compromise solution is obtained in a much simpler way (S. Raissi and R- Eslami Farsani, 2009).

3.10.1.Desirability Function Analysis

Harrington invented the desirability function to simultaneously optimize many responses, and Desirability function analysis is a widely used technique in academics and industry for simultaneous optimization of several responses (Harrington, Edwin, 1965). Derringer and Suich were eventually modified to increase their usefulness, and they became quite popular (Derringer & Suich, 1980). The desirability function approach is one of the most widely utilized multi-response optimization strategies in practice. The desirability scale ranges from 0 to 1, and it measures how near an answer is to its ideal value. The desirability of response is 0 if it falls within the unacceptable intervals, and 1 if it falls within the ideal intervals or the response reaches its ideal value. Meanwhile, the desirability ranges from 0 to 1 when a response falls within the tolerance intervals but not the ideal interval, or when it fails to reach its ideal value. The closer the response comes to the ideal intervals or ideal values, the more desirable it becomes. According to the objective features of a desirability function, the nominal-the-best (NB) answer, the larger-the-better (LB) response, and the smaller-the-better (SB) response can be classified. The proposed desirability function converts each response into a desirability rating ranging from 0 to 1. A composite desirability function can be created by combining all the desirability functions to turn a multi-response problem into a single-response problem.

3.10.1.1. Steps in desirability function analysis

For the proposed methodology, the following stages must be followed:

- **I.** Identification of the goals and their characteristics, as well as the creation of a decision matrix to reflect performance characteristics concerning various variables.
- **II.** For each response, the desirability index (di) value is calculated. The nature of the corresponding output determines the di value.

When the output response is "Larger-is-better" :

The bigger the value of ŷ is predicted to be, the better. The desirability value equals 1 when the surpasses a specific criteria value, which can be considered a requirement; if the is less than a specific criteria value, which is unacceptable, the desirability value equals 0.

$$di = \begin{matrix} 0, & \hat{y} \leq \widehat{ymin} \\ \left(\frac{\hat{y}-ymin}{ymax-ymin}\right)^r, & ymin \leq \hat{y} \leq ymax, r \geq 0; \\ 1, & \hat{y} \geq ymax \end{matrix} \tag{3.7}$$

When the output response is "target value":

The value of ŷ is required to get a particular target T. When equals T, the desirability value is 1; if ŷ exceeds a certain range from the target, the desirability value is 0, and this is the worst-case scenario.

$$di = \begin{cases} \left(\frac{\hat{y}-ymin}{T-ymin}\right)^s, ymin \leq \hat{y} \leq T, s \geq 0 \\ \left(\frac{\hat{y}-ymax}{T-ymax}\right)^t, T \leq \hat{y} \leq ymax, t \geq 0 \\ 0 \end{cases} \tag{3.8}$$

When output response is "smaller the better":

The value of ŷ is expected to be the smaller the better. When the ŷ is less than a particular criteria value, the desirability value equals 1; if the ŷ exceeds a particular criteria value, the desirability value equals 0.

$$di = \begin{cases} 1, & \hat{y} \leq ymin \\ \left(\frac{\hat{y} - ymax}{ymin - ymax}\right)^r, & ymin \leq \hat{y} \leq ymax, r \geq 0; \\ 0, & \hat{y} \geq ymax \end{cases} \tag{3.9}$$

Where the $ymin$ represents the lower tolerance limit of ŷ, the $ymax$ represents the upper tolerance limit of ŷ and r represents the weight. The weights s, t, and r in the above Equations are defined according to the user's requirements. The weight can be set to a larger value if the corresponding response is expected to be closer to the target; otherwise, the weight can be set to a smaller value.

III. Compute the Composite desirability index: To calculate the total desirability, the individual desirability values were added together.

$$Dg = \sqrt[w]{d1^{w1} * d2^{w2} * \ldots * di^{wi}} \tag{3.10}$$

Where Di and *Wi* are the individual desirability and weight of the response Yi. W is the sum of the individual weights and Dg is the Composite Desirability or overall desirability.

IV. Determine the optimal parameter and its level combination. The higher composite desirability value implies better product quality.

V. The most significant parameter is subjected to an analysis of variance (ANOVA). ANOVA determines the relative importance of variables.

VI. Finally, using the ideal level of design parameters, predict and validate the quality features.

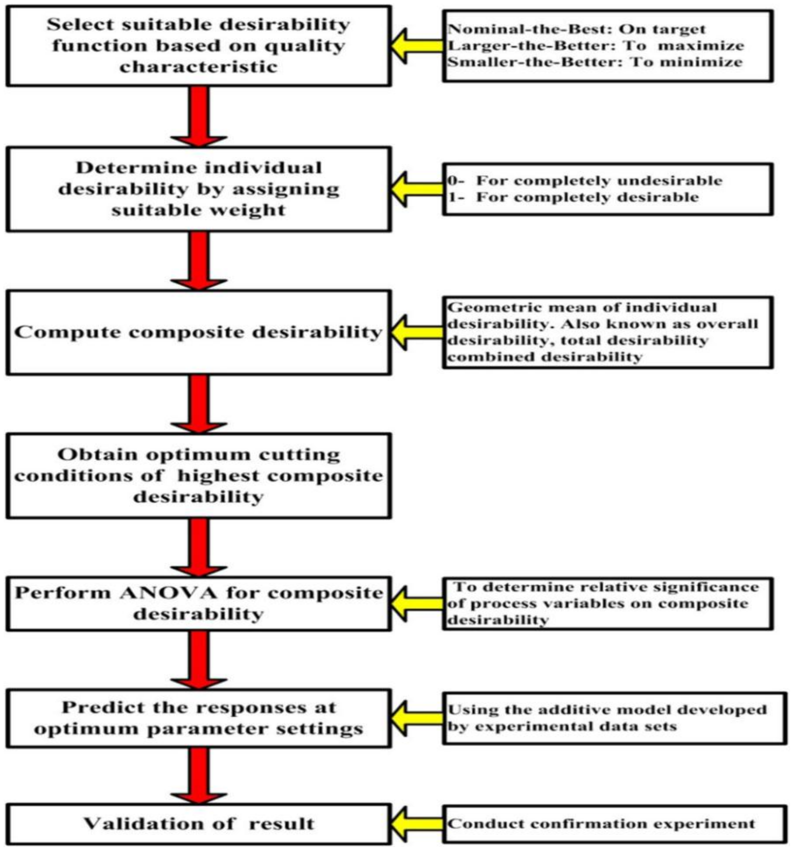

Figure 3.33 DFA optimization flowchart (Derringer & Suich, 1980)

3.10.2. Analysis of variance (ANOVA)

Minitab19 statistical software is used to calculate analysis of variance for the inquiry, as well as analysis of a response parameter for several experimental responses. The statistical approach of ANOVA is used to determine the influence of all control values. The percentage contributions of each control factor were utilized to measure the associated impacts on the performance characteristics in the analysis of variance. The significance level was set at 5%, which corresponded to a 95% level of confidence. The following formula was used to obtain the percentage contribution of each influential parameter from the analysis of variance (Krishnaiah & Shahabudeen, 2012).

$$P(\%) = \frac{SSTR}{SST} * 100 \quad (3.11)$$

Where P is the percentage contribution of individual factors, SSTR is the sum of squares or treatment sum of squares, and SST total sum of squares.

CHAPTER - 4

RESULT AND DISCUSSION

4.1. Introduction

During the TIG welding process, the influence of welding parameters on mechanical properties, welding joint shape, and microstructural properties of similarly welded SS316 stainless steel and dissimilarly welded SS316 and AISI 1020 mild steel was investigated. After the welding process was completed, the welded samples were visually inspected for welding defects by liquid penetrant. After performing non-destructive testing, destructive testing was carried out, and the reaction parameters were measured. The outcome results for each experiment were discussed in this chapter in detail. The response results from an orthogonal array of experimental investigations were analyzed using Taguchi methods to identify the initial optimum TIG welding parameters, and the most influential welding parameters on tensile strength, flexural strength, hardness, and welding joint geometry for both similar and dissimilar welding were identified by analysis of variance (ANOVA). The initial optimum parametric setting from Taguchi methods was used for multi-response optimization using desirability function analysis.

4.2. Welding Defects of Similar and Dissimilar Welded Metals

4.2.1. Liquid Penetrant and visual Defect Testing

Liquid or dye penetrant testing (PT) is a non-destructive material testing technique that uses capillary forces to detect and locate surface fractures or holes. PT work was based on the penetration of liquid penetrant via concave surface discontinuities. It can detect surface flaws, including fractures, laps, and porosity. Table 4.1 below shows the PT test results for similar and dissimilar specimens.

4.2.1.1. Visual inspection analysis

While the welding was being done, all the samples were visually inspected. A few welding faults, such as a bit of undercut at the end, excessive reinforcement height, lack of fusion, root crack, and lack of penetration, have been detected in similar and dissimilar welded samples. These samples are for similar samples nos. 1, 2, and 3. Under the specific parametric condition, other all samples have nearly no flaws, while dissimilar sample numbers 1, 2, and 5 have problems, but the rest of the samples are defect-free.

4.2.1.2. Liquid penetrant testing result analysis

Lack of fusion: There was a lack of fusion in dissimilar samples number 2 and 5 and similar samples number 1. This defect occurred due to minimum current input, arc length, electrode angle, electrode manipulation, and improper welding parameter settings, which contributed to the fusion failure (AWS committee, 2000).

Porosity: Porosity was observed on similar sample numbers 2 and 9 and a dissimilar sample number 13. This defect was caused by leaks in the gas line, too high a gas flow rate, draughts, and excessive turbulence in the weld pool. For example, porosity happens when contaminants or moisture enter the weld puddle. Contaminants can be found in several locations, including the base. On the metal surface and the filler metal surface, welding fluxes, welding gases, and welding equipment are all employed (AWS committee, 2000).

Undercut: An undercut defect was observed on similar sample number 3 and dissimilar sample number 1. This defect, caused by inappropriate joint geometry in some samples, can also result from an immoderate welding current (AWS committee, 2000).

Table 4.1: liquid penetrant testing result for similar and dissimilar TIG-welded samples

Sample No	**Non- Destructive test result**	
	Dissimilar	**Similar**
Sample 1	Undercut	Lack of fusion
Sample 2	Lack of fusion	porosity
Sample 3	Defect-free	Undercut
Sample 4	Defect-free	Defect-free
Sample 5	Lack of fusion	Defect-free
Sample 6	Defect-free	Defect-free
Sample 7	Defect-free	Defect-free
Sample 8	Defect-free	Defect-free
Sample 9	Defect-free	Porosity
Sample 10	Defect-free	Defect-free
Sample 11	Defect-free	Defect-free
Sample 12	Defect-free	Defect-free
Sample 13	porosity	Defect-free
Sample 14	Defect-free	Defect-free
Sample 15	Defect-free	Defect-free
Sample 16	Defect-free	Defect-free

4.3. Microstructural analysis of similar and dissimilar welded metals

An optical microscope (Model: HUVITZ HR-300 series) was used to examine the microstructure of all TIG welded samples, both similar and dissimilar, as well as the base material. However, only two specimens were supplied with base materials: sample number 8 and sample number 15 for similar welded samples and sample number 10 and sample number 1 for different welded samples. These samples were chosen for microstructural investigation based on their tensile test result. Sample numbers 8 and 10 indicate maximum UTS joint strength for similar and dissimilar welds, respectively, whereas sample numbers 15 and 1 show minimum UTS joint strength for similar and dissimilar welds, respectively.

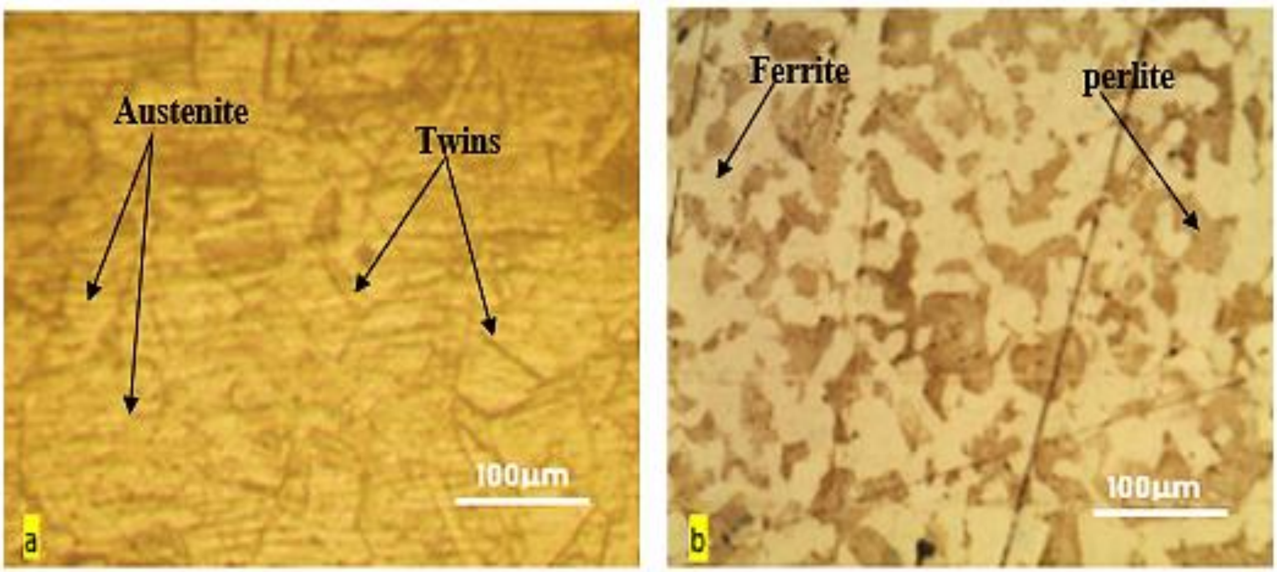

Figure 4.1 Microstructure of base metals; a) 316 stainless steel, b) AISI 1020 low carbon steel

Figure 4.1, a, and b, shows a typical optical micrograph of the base metal. In the microstructure of 316 stainless steel, there is a fully austenitic structure with little annealing twins. Similar results were also reported for stainless steel 316 (Moi et al., 2019). The structure of the low carbon steel AISI 1020, on the other hand, shows a mixture of pearlite and a dominant ferritic phase. Figures 4.2 and 4.3 show the optical microstructures of TIG-welded joints and weld metal from the selected samples. On all sample micrograph pictures, the base metal (BM), heat affected zone (HAZ), and weld metal (WM) can be easily differentiated. Sample number 8 was welded with AWS-ER316L filler wires, resulting in a microstructure of ferrite and austenite (i.e. -ferrite structure) that could be explained by principal solidification modes of weld metals. The

Creq/Nieq ratio explains the weld metal solidification mode. The Schaeffler formula is used to calculate the Creq/Nieq ratio (AWS committee, 2000).

$$Cr_{eq}/Ni_{eq}\text{ ratio } = \frac{Cr_{eq\text{ of weld metal}}}{Ni_{eq\text{ of weld metal}}} \quad (4.1)$$

Sample 8- $Creq/Nieq$ ratio $= {}^{17.36}/_{11.35}$ =**1.53**

Sample 15- $Creq/Nieq$ ratio $= {}^{20.25}/_{10.62}$ =**1.91**

Sample 10- $Creq/Nieq$ ratio $= {}^{17.99}/_{9.81}$ =**1.83**

Sample 1- $Creq/Nieq$ ratio $= {}^{2.84}/_{1.89}$ =**1.50**

Therefore, the solidification mode is a ferritic-austenitic mode for all samples as:

$$FA = 1.48 \leq Creq/Nieq \leq 1.95 \quad (4.2)$$

(Chemical composition of weld metal with a type of filler wire used was listed in Table 3.2).

Sample number 10 was welded using AWS ER-309L filler wire and the microstructure of this weld also consists of ferrite and austenite. And the $Creq/Nieq$ ratio of these samples was 1.83.

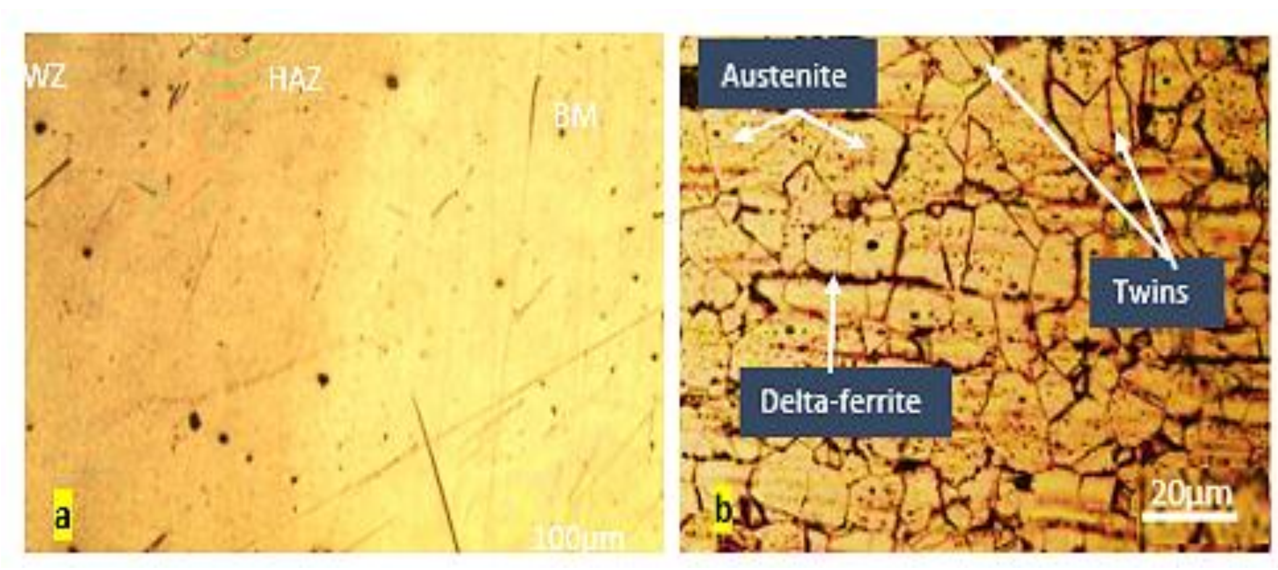

Figure 4.2 microstructure of similar welded joint of SS316 (sample 8): a) welded joint, b) weld metal

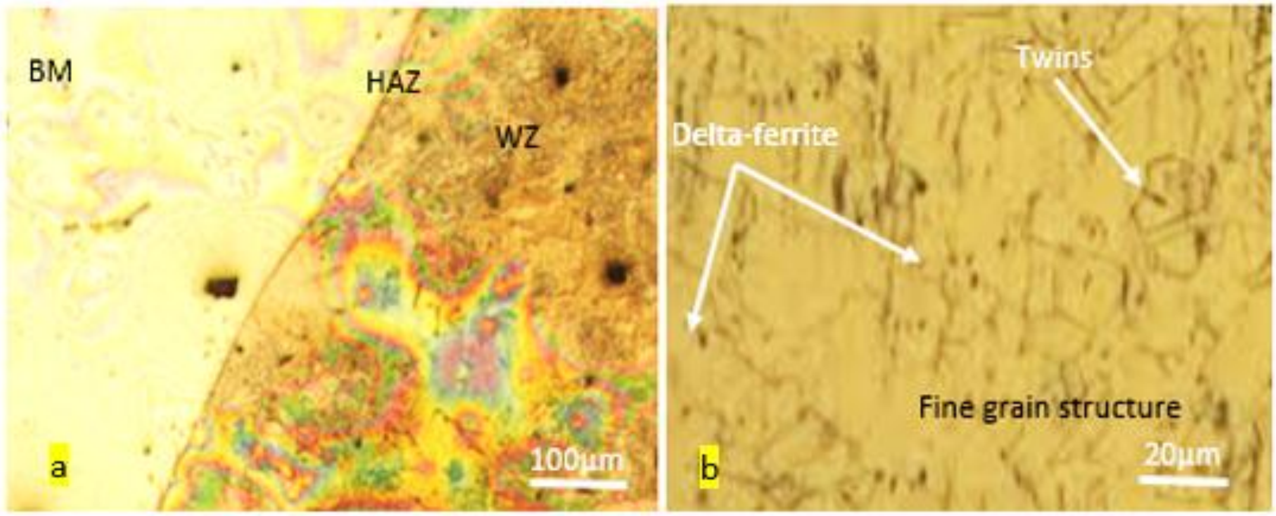

Figure 4.3 Microstructure of dissimilar welded joint of SS 316 and AISI 1020 (sample 10): a) welded joint, b) weld metal

Due to moderate heat input and moderate cooling rate, the weld zone of sample numbers 8 and 10 for similar and dissimilar welding types reveals a very fine skeletal-ferrite together with grain, sub-grain, and migrating boundaries in a plain austenitic matrix (Hedhibi et al., 2021) also reported the same result. In the TIG weld zone, the delta ferrite (δ) is finer, as shown in Figures 4.2 and 4.3, respectively. The heat provided by the welding process, which was modest (90A and 110A for comparable and different welded samples, respectively), is related to the delta ferrite (δ) size. When heat input is modulated, a modulated cooling rate occurs, and a finer skeletal ferrite is generated as a result. Distinct cooling rates in multi-pass welding have resulted in different forms of ferrite transformation, resulting in a change in ferrite within the weld. A skeleton δ-ferrite had formed where cooling rates were moderate. This occurs as austenite consumes the ferrite until it is sufficiently enriched in ferrite-transforming elements, such as chromium, and deficient in austenite-transforming elements, such as nickel, to be stable at lower temperatures where diffusion is limited. A lathy δ-ferrite has produced when the cooling rates were high. Restricted diffusion during the ferrite–austenite reaction created the lathy structure. Diffusion distances are reduced, which increases the efficiency of the transformation and hence reduces the number of spaced laths (Lippold & Kotecki, 2005). Due to very low welding heat inputs, i.e., high cooling rates, sample number 1 for dissimilar weld metals includes δ -ferrite in the form of dendritic lathy-ferrite. The delta ferrite (δ) in the TIG weld zone of sample number 15 is coarser. The heat input was increased to 130A on this sample. High heat input caused a slow cooling rate and a transition from the ferrite to the austenite phases. In the case of TIG welding, on the other hand, the high heat input causes coarse substructure during solidification, resulting in a more widely distributed ferrite network. High cooling rates don't allow enough time for the phase transition to finish. As a result of the faster cooling rates, more d-ferrite is retained in the weld zone. To minimize solidification and hot cracking, as well as improve ductility, toughness, and corrosion resistance, 5‑10 percent d-ferrite concentration is advised (Kou, 2002).

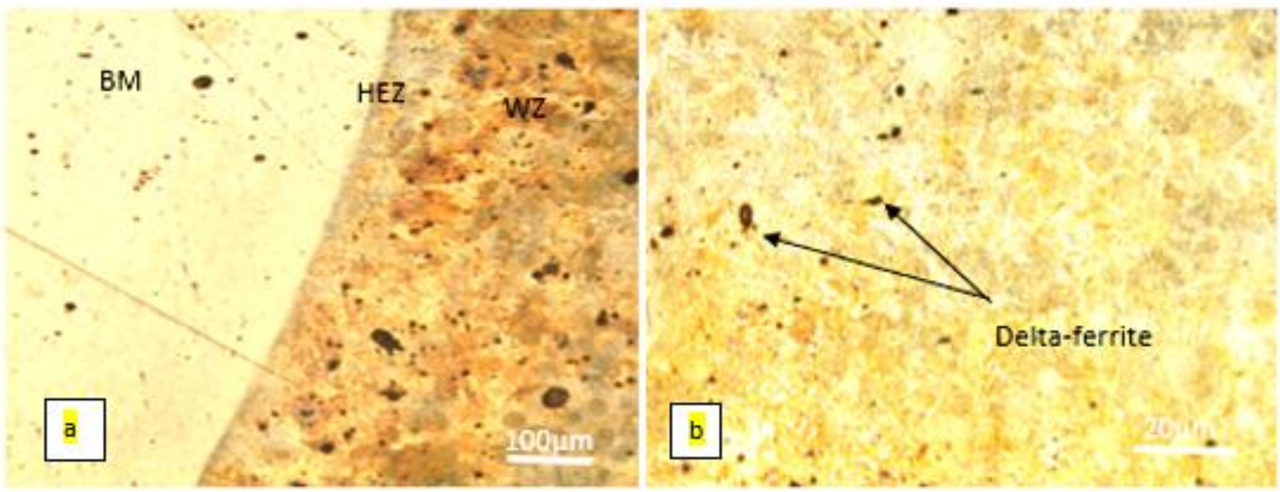

Figure 4.4 Microstructure of dissimilar welded joint of SS 316 and AISI 1020 (sample 1): a) welded joint, b) weld metal

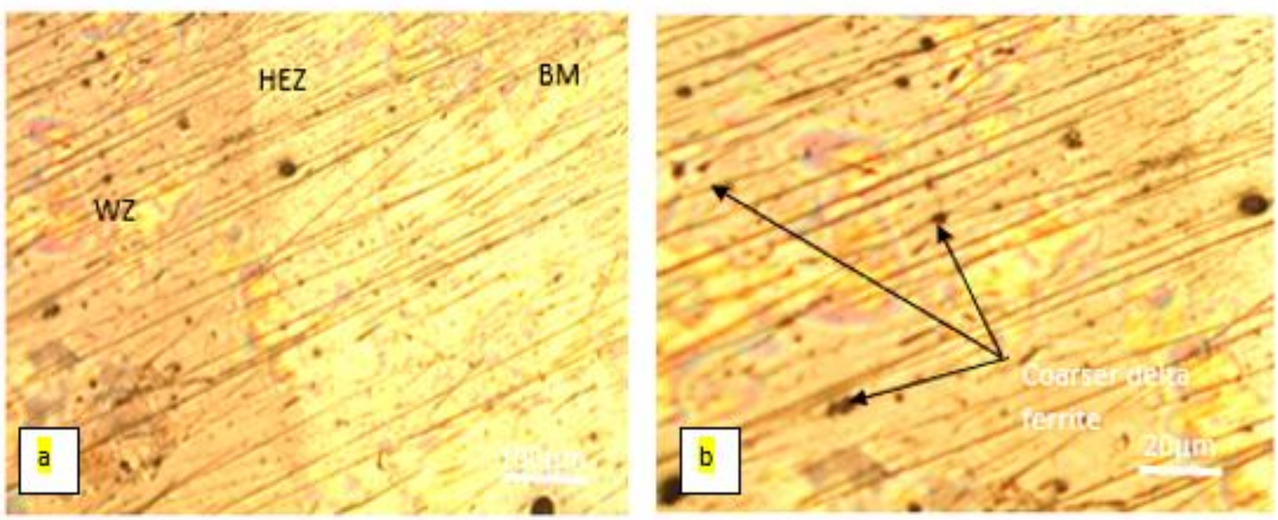

Figure 4.5 microstructure of similar welded joint of SS316 (sample 15): a) welded joint, b) weld metal

4.3.1. Fractography analysis

Scanning electron microscopy (SEM) was used to take micrographs of the fracture zone in the tensile test. For both situations, the specimens chosen for micrograph testing of fracture mechanisms were those with the highest ultimate tensile test results. The weld bead, penetration, and reinforcement of the weld were seen in figure 4.6, and the interface of the base and weld zone was joined also seen. According to the findings, the fracture location for both welds is in the base metal for all welded specimens, as illustrated in Figure 4.6. Both the comparable and dissimilar weld fracture micrographs reveal the same profile with the production of many dimples, indicating that the fracture is in the ductile mode, as illustrated in Figures 4.7 and 4.8, respectively.

It was discovered that the width of the weld generated by GTAW for similar and dissimilar metals had a full penetration from the face pass to the root pass. Weld bead shape can be better controlled by moderate current input utilizing filler metals ER-316 and ER-309 for similar and dissimilar welds, respectively, as seen in these two figures. As seen by (Moslemi et al., 2015) as its input was very low the weld pool depth and width were very small (low penetration) but at a moderate current, the weld pool width and area were controlled. The (AWS committee, 2000) also recommends using filler metal ER-316L for 316 stainless steel base metal so the result also agrees with them. AWS ER-309L filler is also recommended for dissimilar welding of stainless steel with low carbon steels, hence the result depicts that it is acceptable (ASM Handbook Committee, 2000).

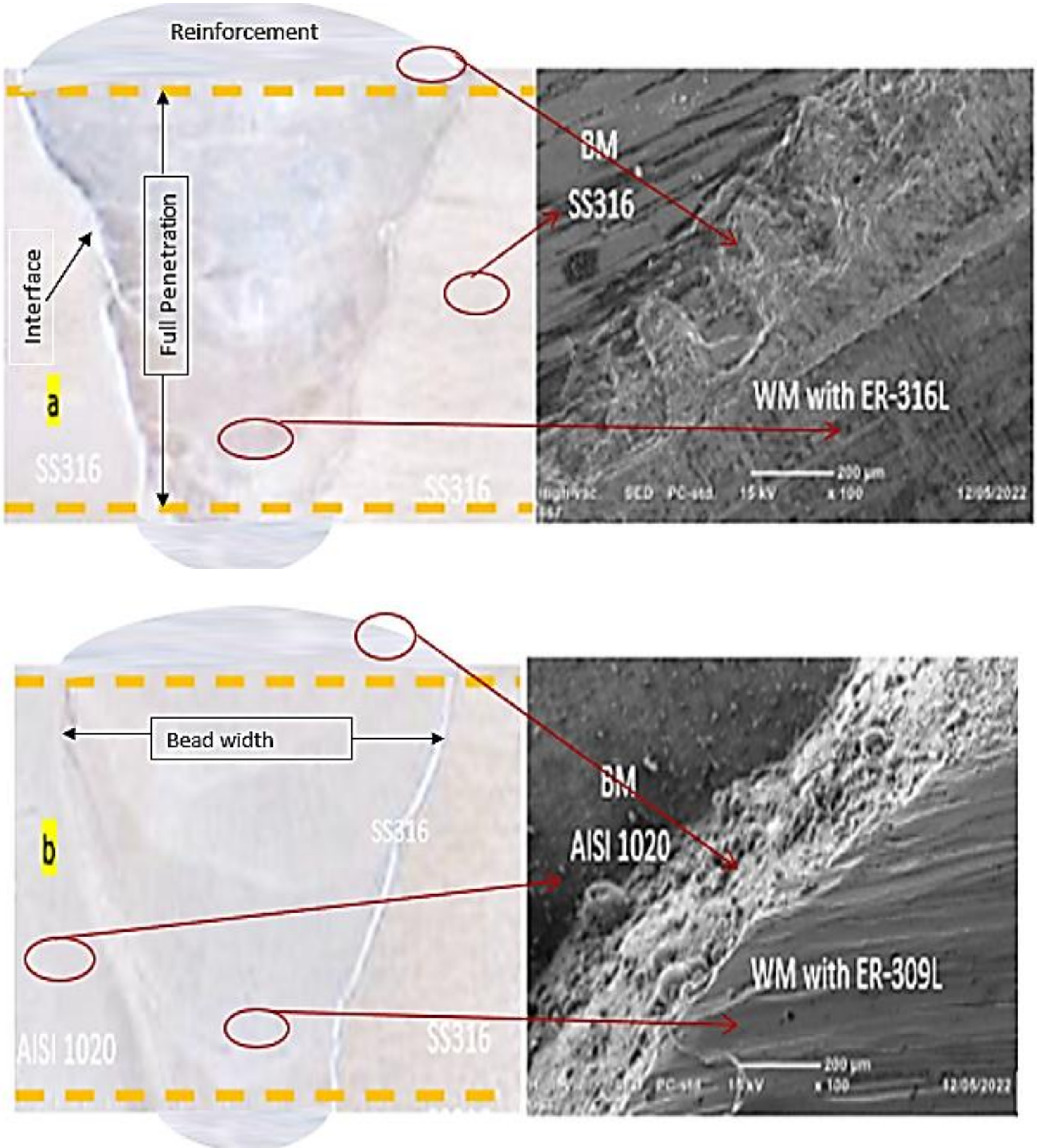

Figure 4.6:Cross-section of Weld bead and penetration of similar and dissimilar welded metals specimens; a)welded with ER-316, b) welded with ER-309

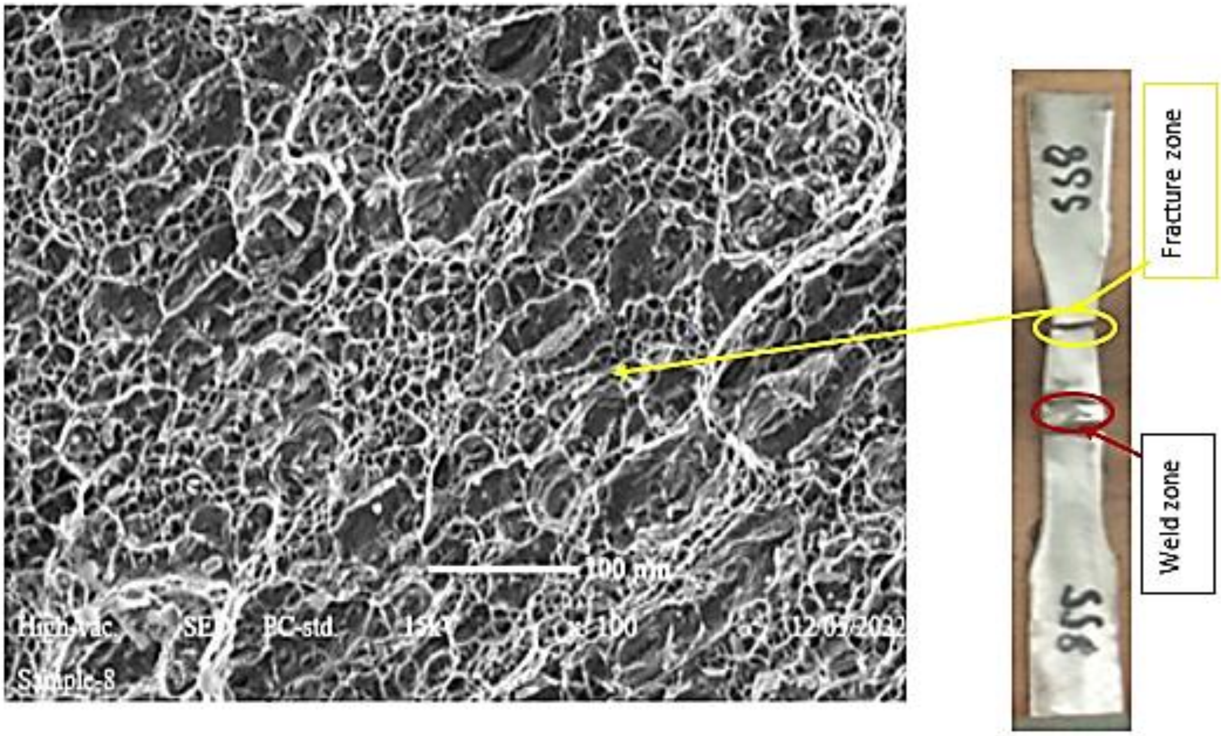

Figure 4.7 Tensile fracture surface, obtained in the base metal of 316 stainless steel

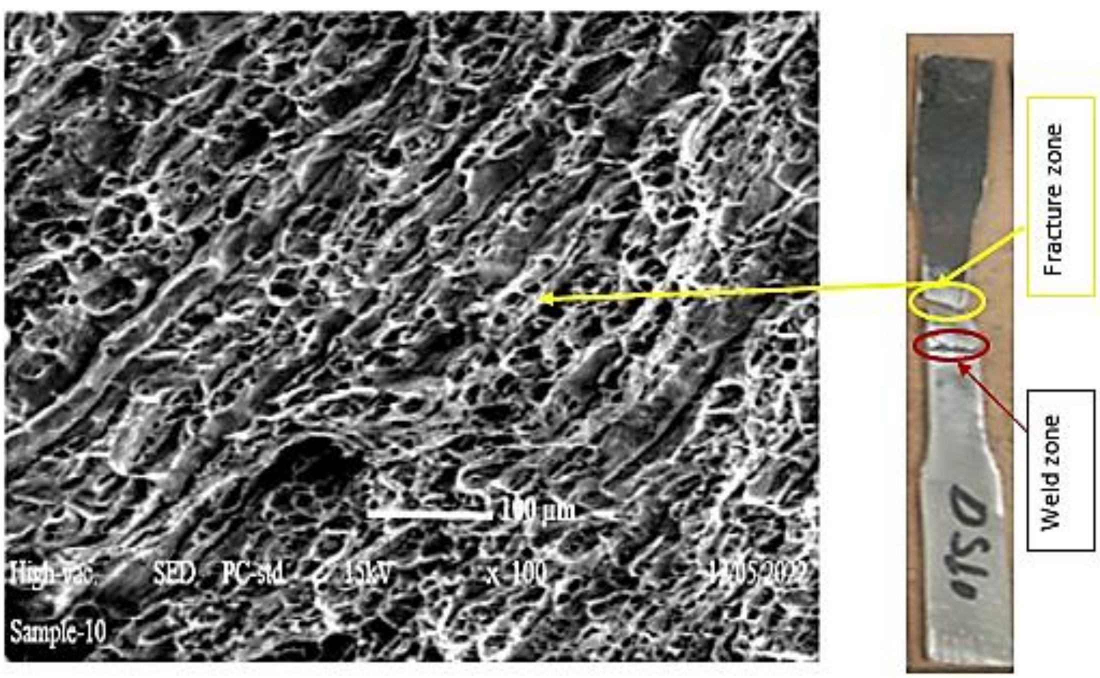

Figure 4.8 Tensile fracture surface, obtained in the base metal AISI 1020 low carbon steel

4.3.2. Micro-hardness analysis

Figure 4.9 depicts the differences in Vickers microhardness values as a function of distance from the weld center to the 316 stainless steels in sample 13 and in both in sample 14. In both similar and dissimilar joints, the hardness values of all weld areas are higher than the base metal hardness. In similar specimens, the weld has the highest hardness due to finer delta-ferrite. On the mild steel side, the highest hardness value was obtained in the weld zone near the fusion boundary, which was sample 14. This is caused by the creation of harder micro-constituents in this area, which is caused by carbon migration from the mild steel side into the weld metal. The average hardness value in the fusion zone of similar welded metals was (227 HV or 97 HRB). And average hardness in the fusion zone of dissimilar welded metals was (183 HV or 90 HRB).

Hardness values in the HAZs of both similar and dissimilar (SS316 and AISI 1020) sides were increased compared to the hardness values of the base metals. Hardness values in the HAZs of 316 stainless sheets of steel in similar welds (197 HV or 92 HRB) were greater than in dissimilar welds (162 HV or 85 HRB).

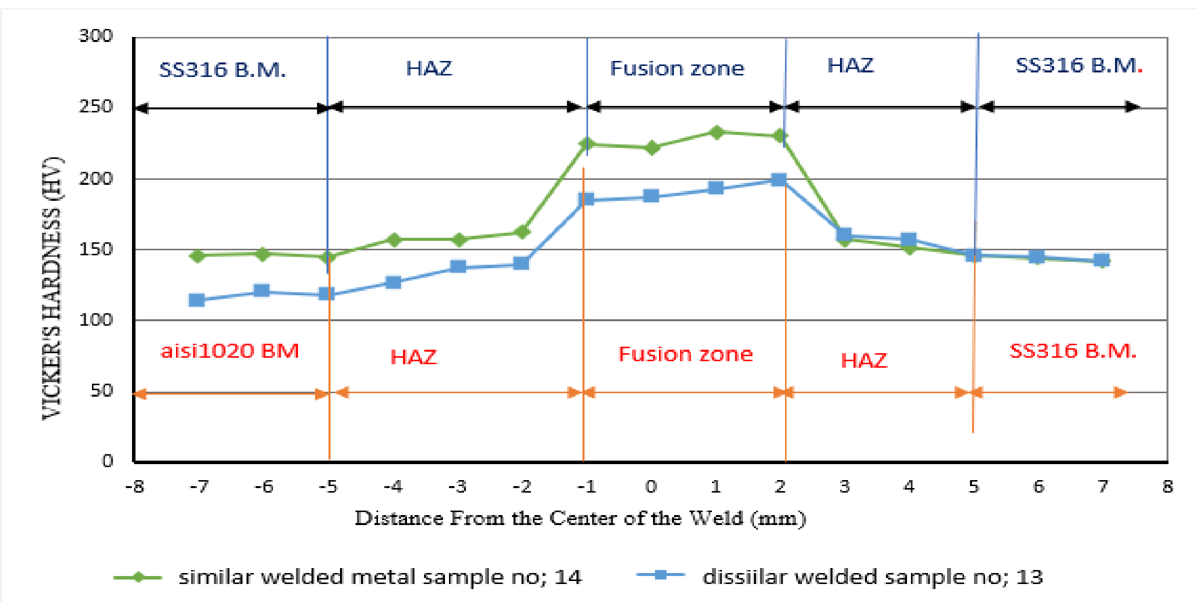

Figure 4.9 Micro-hardness graph for similar and dissimilar higher values

4.4. Mechanical Properties of Similar Welded Metals

The study focused on the investigation and parametric optimization of TIG welding settings employing the Taguchi L16 orthogonal array to weld similar and dissimilar metals. Here under this topic, the effect of welding parameters on mechanical properties and weld bead geometry has been analyzed. Next, the response parameters from the test will be analyzed using the Taguchi technique, and the percentage contribution of parameters was identified using analysis of variance (ANOVA). Finally, the parameters are optimized to the optimum parametric setting using a multi-response optimization technique using desirability function analysis (DFA). The welding control parameters and levels utilized during similar welding of stainless steel SS316 are shown in table 4.2 below.

Table 4.2: Selected Process parameters and levels

S. No	**Process parameter**	**Units**	**Levels**			
			1	**2**	**3**	**4**
1	Welding current (A)	Amp (A)	70	90	110	130
2	Gas flow rate (B)	L/Min	7	10	13	16
3	Root Gap (C)	mm	1	1.5	2	2.5
4	Type of filler metals (D)	Grade	ER-70S-3	ER-316	ER-309	ER-312

4.4.1. Tensile Strength Result Analysis

Tensile strength data were collected using a universal testing machine, and the stress formula was again manually calculated using equations (3.1 and 3.2). Each test consisted of two specimens, with the average value taken. Table 4.3 shows the measured experimental results of average tensile strength values for each trial experiment. Welding parameter setup optimization for both welding circumstances has been done individually using the DFA technique. The larger the performance qualities, the better the tensile strength (larger is the better).

Table 4.3: Mean tensile strength result

Sample No	*Welding Current (A)*	*Gas Flow Rate (B)*	*Root Gap (C)*	*Filler Type (D)*	*Tensile strength (MPa)*	*Signal to noise ratio*
1	70	7	1.0	ER70S-3	502	54.0141
2	70	10	1.5	ER316	560	54.9638
3	70	13	2.0	ER309	520	54.3494
4	70	16	2.5	ER312	525	54.4032
5	90	7	1.5	ER309	480	53.6248
6	90	10	1.0	ER312	525	54.4032
7	90	13	2.5	ER70S-3	531	54.5019

8	90	16	2.0	ER316	595	55.4903
9	110	7	2.0	ER312	450	53.0643
10	110	10	2.5	ER309	475	53.5339
11	110	13	1.0	ER316	485	53.7148
12	110	16	1.5	ER70S-3	490	53.8039
13	130	7	2.5	ER316	410	52.2557
14	130	10	2.0	ER70S-3	435	52.7698
15	130	13	1.5	ER312	375	51.4806
16	130	16	1.0	ER309	415	52.3610

4.4.1.1. Mean response analysis of tensile strength

A response table is calculated for each response characteristic, such as mean and signal-to-noise ratio. The response table can show which factors have the most impact on the response and which degree of the factor is associated with greater or lower response characteristic values as shown in equation (3.6). The steps for creating a response table are as follows:

1. Calculates the chosen response characteristic for each level's welding current, gas flow rate, root gap, and filler type.
2. After that, the delta values, which are the differences between the greatest average response characteristic value and the lowest average response characteristic value for levels of that factor, are determined.
3. The delta values are used to assign ranks from high to low. The factor with the highest delta value receives the top ranking.

- For example, for factor A, the mean was calculated by:

$$\text{At level 1}(A_1) = \frac{(502+560+520+525)}{4} = 526.8$$

$$\text{At level 2}(A_2) = \frac{(480+525+531+595)}{4} = 532.8$$

$$\text{At level 3}(A_3) = \frac{(450+475+485+490)}{4} = 475$$

$$\text{At level 4}(A_4) = \frac{(410+435+375+415)}{4} = 408.8$$

At each level, the mean for factors B, C, and D is calculated in the same way. The delta value is generated after the average means / S/N ratios for each factor have been obtained. The delta value is calculated by subtracting the minimum from the greatest value. Table (4.4) shows that welding current (A) has the highest value and is rated first, gas flow rate (B) is ranked second, filler type (D) is ranked third, and root gap (C) has the lowest value when compared to other parameters and is ranked fourth by Taguchi (means) analysis. These welding settings (A2B4C2D3) were chosen for TIG welding of stainless steel 316 with a thickness of 3mm as the initial parametric setting. Figure 4.11 shows the main effect plot for control factors for means of tensile strength value variations. The numerical value at the largest point in each graph of means of tensile strength represents the parameter's best value at that level. They also show the ideal conditions within the experimental conditions' range. When compared to other welding factors, the welding current weight percentage is the most effective at increasing tensile strength, while the root gap has the least effect.

Table 4.4: Response Table for Means of tensile strength

Level	Current (A)	GFR (B)	Root Gap (C)	Filler type (D)
1	526.8	460.5	481.8	489.5
2	**532.8**	498.8	476.3	**512.5**
3	475.0	477.8	**500.0**	472.5
4	408.8	**506.3**	485.3	468.8
Delta	124.0	45.8	23.8	43.8
Rank	**1**	**2**	**4**	**3**

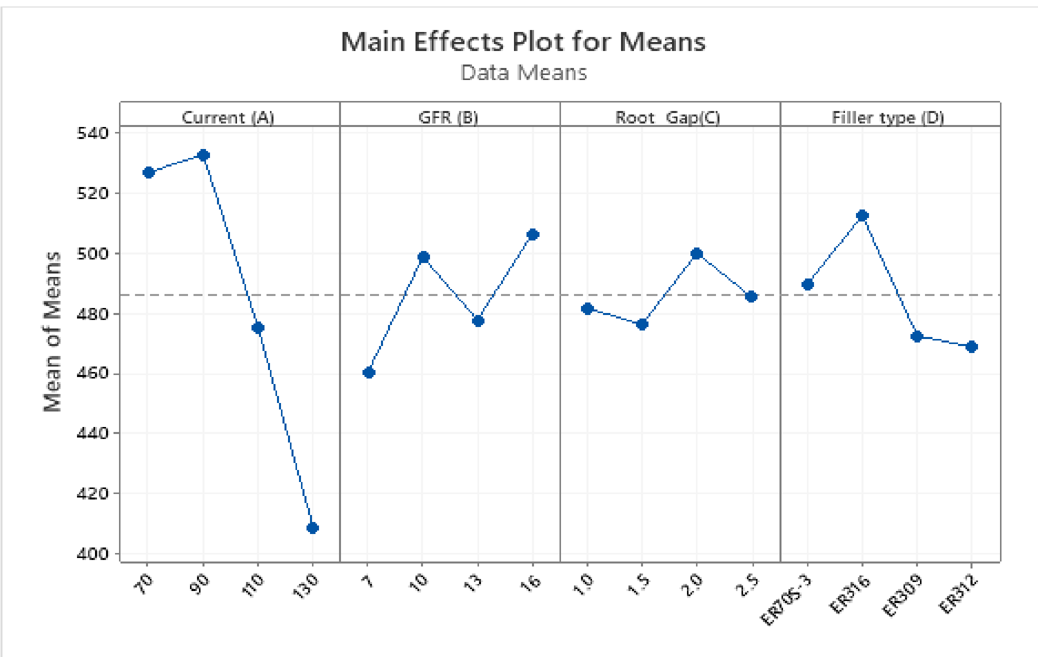

Figure 4.10 Main effect plot for means of tensile strength

4.4.1.2. Signal to noise ratio analysis for tensile strength

Taguchi evaluated the quality attribute that differed from the desired value using the S/N ratio. As a result, the larger the tensile strength, the better the quality. Based on the achieved tensile strength result, the effect of the above parameters on tensile strength was examined. Table 4.5 shows that the welding current has the biggest effect (Delta = 2.29, Rank =,1^{st}.) followed by gas flow rate and filler type (Delta =0.77, rank =,2^{nd} and 3^{rd}) respectively. Root gap (Delta = 0.44, Rank =,4^{th}.) has the smallest effect on the (S/N) ratio. To get a higher tensile strength value, the controlling of current will be the first essential work as shown by the signal to noise ratio.

Table 4.5: Response Table for Signal to Noise Ratios of UTS (Larger is better)

Level	Current (A)	GFR (B)	Root Gap (C)	Filler type (D)
1	54.43	53.24	53.62	53.77
2	**54.51**	53.92	53.47	**54.11**
3	53.53	53.50	**53.91**	53.46
4	52.22	**54.01**	53.67	53.34
Delta	2.29	0.77	0.44	0.77
Rank	**1**	**2**	**4**	**3**

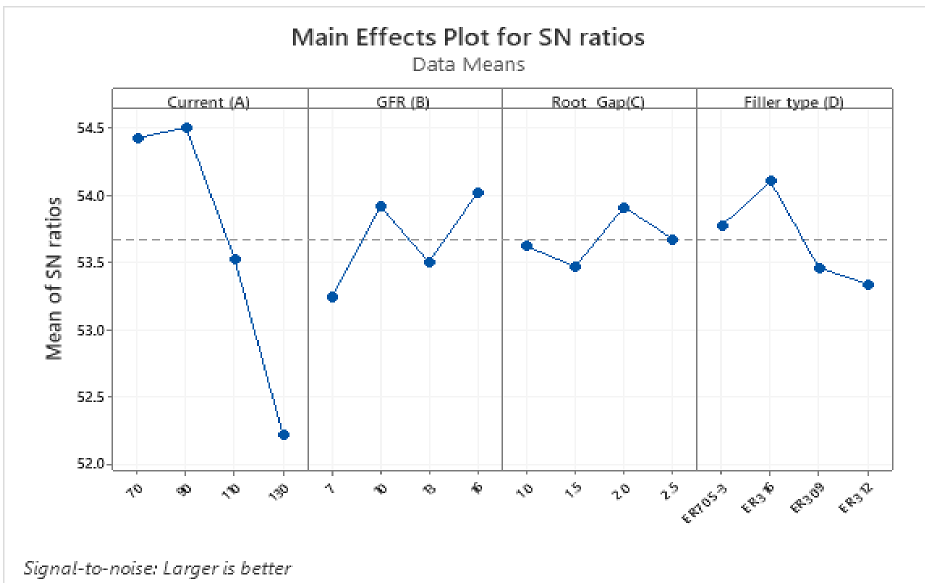

Figure 4.11 main effect plot for S/N ratio of UTS

4.4.1.3. Effect of parameters on tensile strength

The effect of welding parameters on tensile strength, as well as the optimum values based on their rank, are shown in Figure 4.12. The optimum values to maximize tensile strength, according to the analysis and the main effect plot graph for SN ratios, are current at level two (90A), the gas flow rate at level four (16L/min), root gap at level three (2mm), and filler metal at level two (SS 316), which has an initial parametric setting of A2B4C3D2. As seen from the graph above it was shown that the tensile strength was increased as the current raised from level 1(70A) to level 2 (90A). but the UTS significantly decreased from a higher value to a lower one at the current increased from level 2 to level 4 (130A). M. Naga Swapna et al., (2021) and Sanjay Kumar et al., (2019) also reported the same result that the current was the most significant welding parameter.

As gas flow rates increased from level 1 (7L/min) to level 2 (10L/min) the UTS was increased. When further GFR increased to level 3(13L/min) the UTS started decreasing but when further the GFR raised to level four then the UTS was increased to a higher value, (Ghadi & S., 2016) also get the same experimental result. The root gap at level 1 (1mm) was given minimum tensile strength, but the gap at level 3 (2mm) was given maximum tensile strength. Filler type at level two (ER-316L) was best for higher tensile strength and filler at level four (ER-312) was given the minimum value of tensile strength.

4.4.1.4. Analysis of variance (ANOVA) for tensile strength

The adequacy of the developed models is tested using the ANOVA. As per this technique, if the calculated value of the F_{ratio} (critical) of the developed model is less than the standard F_{ratio} (F-table value 3.49) value at the desired level of confidence of 95%, then the model is said to be adequate within the confidence limit. The coefficient of determination ' R2' for the ANOVA found was above 0.99. The most significant parameters that affect the tensile strength of the TIG welded steels are identified using analysis of variance (ANOVA). The study was performed based on their S / N ratios to obtain the percentage contribution of each of the factors.

Table 4.6: Analysis of Variance for UTS

Source	**DF**	**Seq SS**	**% Contr.**	**Adj SS**	**Adj MS**	**F**	**P**
Welding Current (A)	3	13.5979	79.89	13.5979	4.53264	499.24	0.000
Gas flow rate (B)	3	1.5707	9.23	1.5707	0.52356	57.67	0.004
Root Gap (C)	3	0.4041	2.37	0.4041	0.13469	14.84	0.026
Filler type (D)	3	1.4208	8.35	1.4208	0.47359	52.16	0.004
Residual Error	3	0.0272	0.16	0.0272	0.00908		
Total	**15**	**17.0207**	**100.00**				

S= 0.0953% **R-Sq**= 99.84% **R-Sq(adj) =** 99.20%

DF: Degree of freedom, SS: Sum of squares, %Contr.: percentage contribution, Adj SS: adjusted sum of squares, Adj MS: adjusted mean of squares, F-value: variance, P-value: calculated probability with a confidence interval of 95 percent is displayed in table 4.6.

F-value =3.49 < F-ratio, so the welding current weight percentage (79.9%), gas flow rate (9.23%), filler type (8.35%), and root gap (2.37%) all have a substantial impact on the tensile strength of TIG-welded 316 sheets of stainless steel with a thickness of 3mm, as shown in contribution graph 4.13. As a result, the welding current has a large impact on the tensile strength.

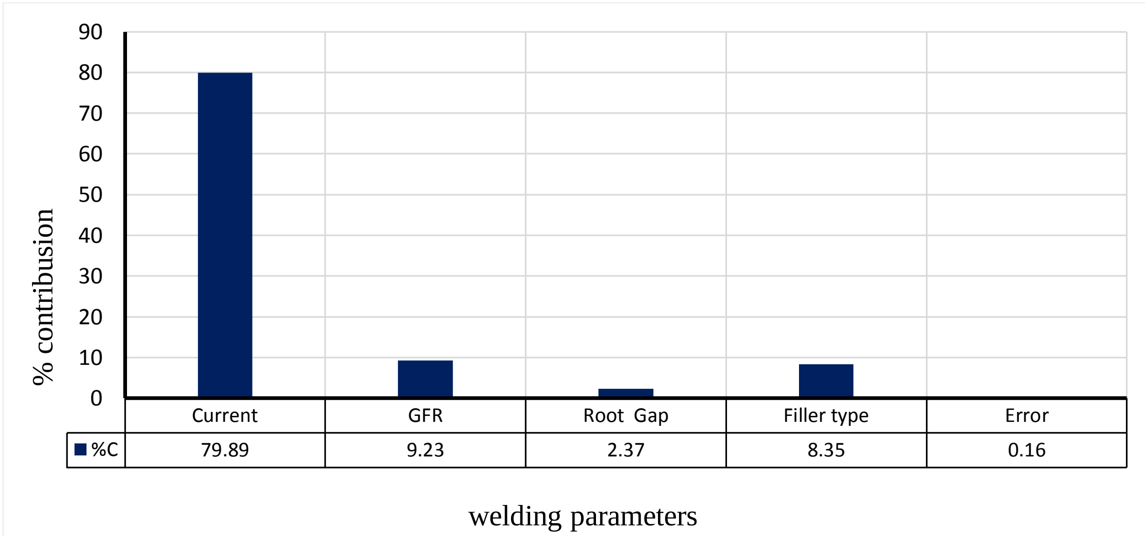

Figure 4.12 Percentage contribution of welding parameters on tensile strength

4.4.2. Hardness test results analysis

Hardness measurement data was obtained using a Rockwell B hardness testing machine, with each test performed from the base metal HAZ and the weld zone, each at 3mm from the weld zone's center. In each zone, three readings were recorded, and the average value was taken. For each trial experiment, Table 4.7 presents the measured average experimental results of hardness values. Larger hardness was projected to be the preferable option for better performance qualities (larger is the better).

4.4.2.1. Mean response analysis of hardness

welding current (A) at the fourth level has the highest value and is ranked first, followed by filler type (D), at the second level, root gap (C) at the third level, and gas flow rate (B) at the first level, as reveals in table 4.8. For TIG welding of stainless steel 316 with a thickness of 3mm, these welding settings (A4B1C3D2) were chosen as the initial parametric setting. For means of hardness value fluctuations, the main influence plot for control parameters is shown in Figure 4.14.

Table 4.7: Mean hardness testing result

Sample No	*Welding Current (A)*	*Gas Flow Rate (B)*	*Root Gap (C)*	*Filler Type (D)*	*Hardness (HRB)*	*Signal to noise ratio*
1	70	7	1.0	ER70S-3	71.0	37.0252
2	70	10	1.5	ER316	75.0	37.5012
3	70	13	2.0	ER309	75.3	37.5359
4	70	16	2.5	ER312	70.0	36.9020
5	90	7	1.5	ER309	83.0	38.3816
6	90	10	1.0	ER312	85.0	38.5884
7	90	13	2.5	ER70S-3	76.0	37.6163
8	90	16	2.0	ER316	95.0	39.5545
9	110	7	2.0	ER312	85.0	38.5884
10	110	10	2.5	ER309	86.0	38.6900
11	110	13	1.0	ER316	92.0	39.2758
12	110	16	1.5	ER70S-3	77.0	37.7298
13	130	7	2.5	ER316	**97.0**	**39.7354**
14	130	10	2.0	ER70S-3	84.0	38.4856
15	130	13	1.5	ER312	79.0	37.9525
16	130	16	1.0	ER309	87.0	38.7904

The parameter's best value at that level is shown by the maximum signifying point as numbered in each graph in the main effect plot figure below. They also display the optimal settings within the experiment's parameters.

Table 4.8: Response Table for Means of hardness

Level	Welding current (A)	GFR (B)	Root gap (C)	Filler type (D)
1	72.83	**84.00**	83.75	77.00
2	84.75	82.50	78.50	**89.75**
3	85.00	80.58	**84.83**	82.83
4	**86.75**	82.25	82.25	79.75
Delta	13.92	3.42	6.33	12.75
Rank	**1**	**4**	**3**	**2**

When compared to other welding variables, the welding current weight percent has the greatest impact on improving hardness, while the gas flow rate has the least impact, (Moi et al., 2018) also reported the same result. Welding current at level four (130A), gas flow rate (7 L/min) at level one, filler type (ER-316) at level two, and root gap at level three (2mm) were the optimum parameters.

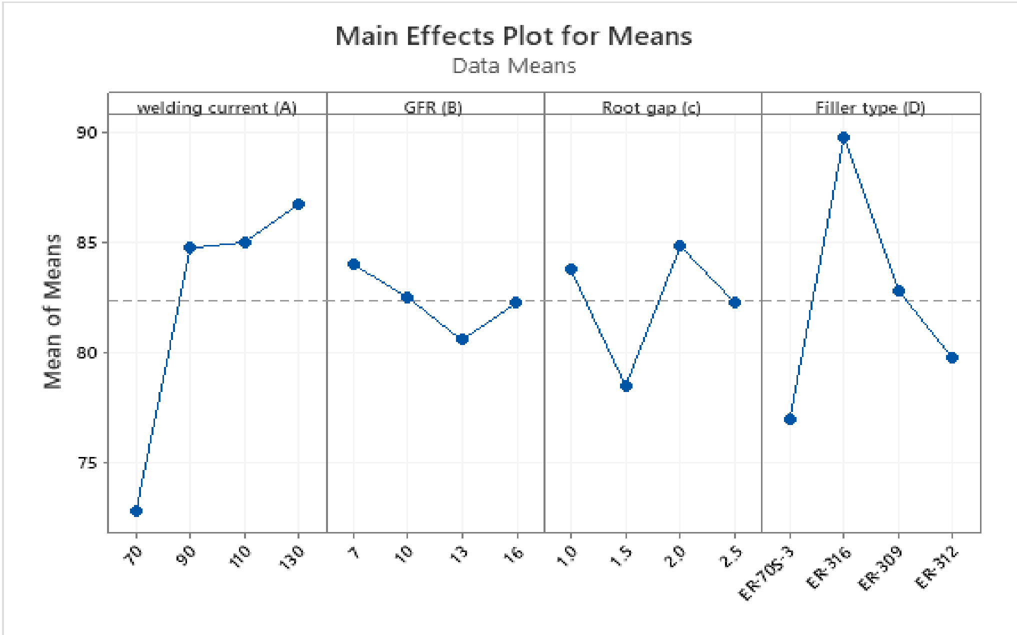

Figure 4.13 main effect plot for means of hardness

4.4.2.2. Signal to noise ratio analysis for hardness

From the S/N ratio analysis, it was observed that the welding current weight percentage has a higher effect (Delta = 1.50, Rank =,1^{st}.) followed by filler type (Delta =1.30, rank =,2^{nd}) root gap (Delta =0.65, rank 3^{rd}) as shown in table 4.9 below. Gas flow rate (Delta = 0.34, Rank =,4^{th}) has the smallest effect on the (S/N) ratio. On larger the better, hardness character, the initial parameter combination is (A4B1C3D2) for enhancing the hardness of TIG-welded 3mm 316 sheets of stainless steel are selected.

Table 4.9: Response Table for Signal to Noise Ratios of hardness(Larger is better)

Level	Welding current (A)	GFR (B)	Root gap (C)	Filler type (D)
1	37.24	**38.43**	38.42	37.71
2	38.54	38.32	37.89	**39.02**
3	38.57	38.10	**38.54**	38.35
4	**38.74**	38.24	38.24	38.01
Delta	1.50	0.34	0.65	1.30
Rank	**1**	**4**	**3**	**2**

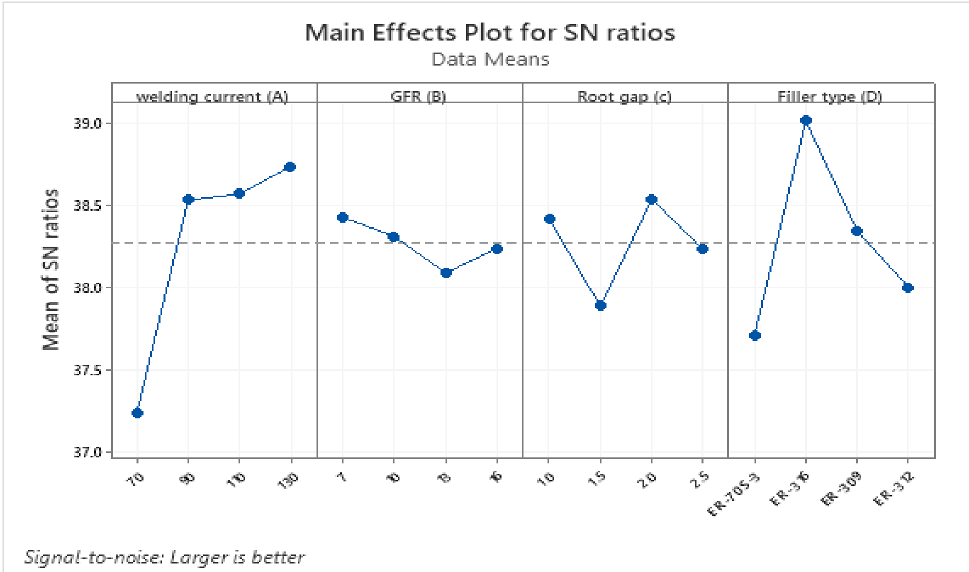

Figure: 4.14 main effect plot for S/N ratio of hardness

4.4.2.3. Effect of parameters on Hardness

Figure 4.16 depicts the effect of welding parameters on hardness, as well as the ideal values based on their rank. According to the analysis and the primary effect plot graph for SN ratios, the optimal values for maximizing hardness are current at level 4 (130A), gas flow rate at level 1 (7 L/min), root gap at level three (2mm), and filler metal at level two (SS 316). From the graph below, it can be seen that when the current rises from level one to level two, the hardness rises dramatically, but only somewhat increment as the current rises from level two to level three. When the current is increased from level three to four, the hardness increases again dramatically. The hardness of the material diminishes as the gas flow rate drops from level one to level three. However, as the gas flow rate rises from level three to level four, the hardness rises as well. The root gap was the third influential parameter; as the root gap increased from level one to two, the hardness fell from a higher value to a lower value. The hardness returns to growing as the game progresses from level two to three. However, when the gap is raised from level three to level four, the hardness decreases again. The filler metal type was the second important welding characteristic; when compared to other filler metals, level one filler metal had a lower hardness value. The filler at level two has the highest hardness value, followed by the fillers at levels three and four, each having a higher hardness value. As seen from the graph shown below the hardness is minimum at a lower current (Salehpour-Oskouei et al., 2021) also got the same experimental result depending on the current.

4.4.2.4. ANOVA for hardness

Using analysis of variance (ANOVA), the most significant parameters that determine the hardness of TIG-welded steels are found and displayed in table 4.10. To determine the percentage contribution of each of the components, the study was conducted using their S/N ratios.

Table 4.10: Analysis of Variance for SN ratios of hardness

Source	DF	Seq SS	%Contrib.	Adj SS	Adj MS	F	P
welding current (A)	3	5.7657	53	5.7657	1.92190	37.11	0.007
GFR (B)	3	0.2393	2	0.2393	0.07977	1.54	0.366
Root gap (c)	3	0.9621	9	0.9621	0.32071	6.19	0.084
Filler type (D)	3	3.7661	35	3.7661	1.25538	24.24	0.013
Residual Error	3	0.1554	1	0.1554	0.05180		
Total	**15**	**10.8887**	**100**				

S= 0.2276 **R-Sq =** 98.57% **R-Sq (adj) =** 92.86%

F-Value=3.49 < F-ratio so the parameters were significant, and as shown in the percentage graph in figure 4.17, the welding current weight percentage (53%), gas flow rate (2%), filler type (35%), and root gap (9%) all have a significant impact on the hardness of TIG-welded 316 sheets of stainless steel with a thickness of 3mm. As a result, the welding current and filler type has a highly significant impact on the hardness.

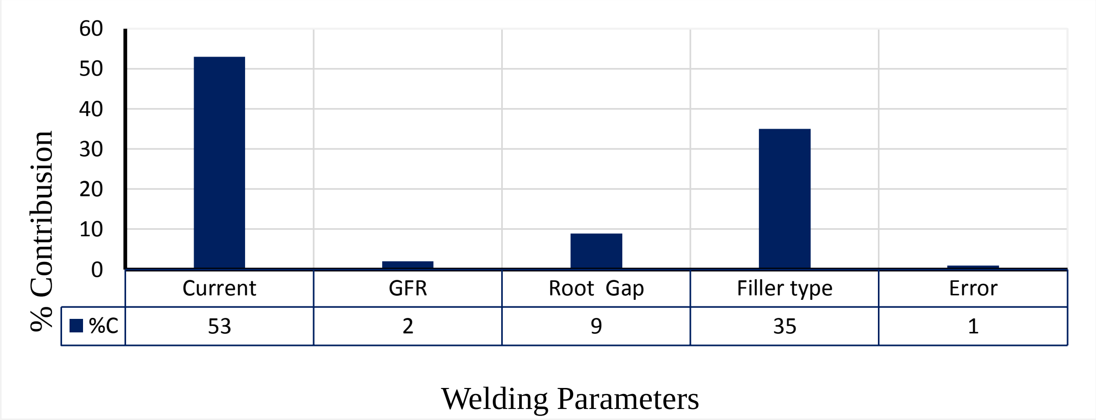

Figure 4.15 Percentage contribution of parameters on hardness

4.4.3. Flexural strength result Analysis

The maximum braking force was recorded from a 3-point bend test under the universal testing machine, and the flexural strength was computed using this force and cross-section area using the equation (3.4). Three readings were taken in each testing trial, and the average value was calculated. Table 4.11 shows the measured experimental results of mean flexural strength values for each trial experiment. Both welding situations have had their welding parameter setup optimized separately. For superior performance qualities, larger flexural strength was predicted to be the preferred alternative.

4.4.3.1. Mean response analysis of flexural strength

Table 4.12 shows that the highest value is showing gas flow rate (B) at the fourth level, followed by welding current (A) at the third level, filler type (D) at the third level, and root gap (C) at the first level. These welding parameters (A3B4C1D3) were chosen as the initial parametric setting for TIG welding of stainless steel 316 with a thickness of 3mm to get larger, better results from experimental results. The principal main effect plot for control parameters was shown in Figure 4.19 for the means of flexural strength value.

Table 4.11: flexural strength test result

Sample No	*Welding Current (A)*	*Gas Flow Rate (B)*	*Root Gap (C)*	*Filler Type (D)*	*Flexural strength (MPa)*	*Signal to noise ratio*
1	70	7	1.0	ER703	718	57.1195
2	70	10	1.5	ER316	599	55.5534
3	70	13	2.0	ER309	633	56.0304
4	70	16	2.5	ER312	723	57.1778
5	90	7	1.5	ER309	755	57.5613
6	90	10	1.0	ER312	633	56.0304
7	90	13	2.5	ER703	636	56.0635
8	90	16	2.0	ER316	776	57.7998
9	110	7	2.0	ER312	730	57.2645
10	110	10	2.5	ER309	749	57.4916
11	110	13	1.0	ER316	667	56.4825
12	110	16	1.5	ER703	766	57.6855
13	130	7	2.5	ER316	630	55.9868
14	130	10	2.0	ER703	609	55.6923
15	130	13	1.5	ER312	520	54.3201
16	130	16	1.0	ER309	760	57.6163

Table 4.12: Response Table for Means of flexural

Level	Welding current (A)	GFR (B)	root gap (C)	Filler type (D)
1	668.2	708.2	**694.5**	682.1
2	700.0	647.7	660.2	668.1
3	**728.0**	613.9	687.1	**724.4**
4	629.8	**756.2**	684.3	651.4
Delta	98.3	142.3	34.3	73.0
Rank	**2**	**1**	**4**	**3**

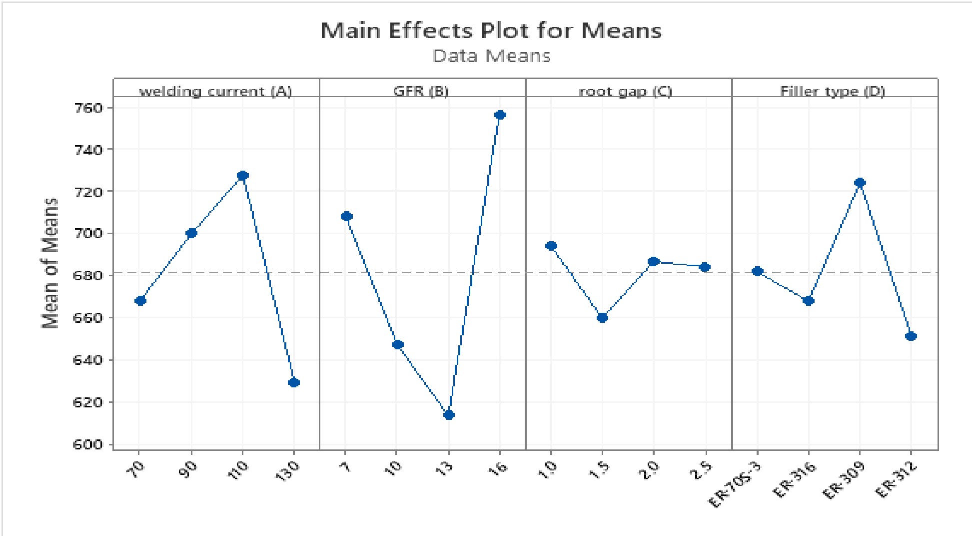

Figure 4.16 main effect plot for means of flexural strength

In the main effect plot graph above, the indicating number at the largest point in each graph represents the parameter's best value at that level. They also display the optimal settings within the experiment's parameters. The gas flow rate weight percent has the greatest impact on flexural strength enhancement when compared to other welding variables, While the root gap has the least. The best parameters were welding current at level three (110A), gas flow rate (16 L/min) at level four, filler type (ER-309) at level three, and root gap at level one (1mm)

4.4.3.2. Signal to noise ratio analysis for flexural strength

The welding gas flow rate weight percentage has the greatest influence (Delta = 1.64, Rank =,1^{st}) followed by welding current (Delta =1.09, Rank =,2^{nd}), and filler type (Delta =0.77, Rank =,3^{rd}) as shown in table 4.13. The minimum effect on the (S/N) ratio is the root gap (Delta = 0.32, Rank =, 4^{th}.) The initial best parameter combination for enhancing the rupture strength of TIG-welded 316 stainless sheets of steel is A3B4C1D3 based on the larger the better, flexural strength character.

Table 4.13: Response Table for Signal to Noise Ratios of flexural (Larger is better)

Level	Welding current (A)	GFR (B)	root gap (C)	Filler type (D)
1	56.47	56.98	56.81	56.64
2	56.86	56.19	56.28	56.46
3	57.23	55.72	56.70	57.17
4	55.90	57.57	56.68	56.20
Delta	1.33	1.85	0.53	0.98
Rank	**2**	**1**	**4**	**3**

4.4.3.3. Effect of parameters on flexural strength

Figure 4.20 shows how welding factors affect flexural strength, as well as the ideal values depending on their rank. The optimal values for maximizing flexural strength, according to the analysis and the primary effect plot graph for SN ratios, are current at the third level (110A), the gas flow rate at the fourth level (16 L/min), root gap at the first level (1mm), and filler metal at the third level (SS 309), with an initial parametric setting of (A3B4C1D3). The flexural strength increases proportionally with current input as the current climbs from level one to level three, as shown in the graph above. The flexural strength drops substantially as the current is increased from level three to level four. As the gas flow rate decreases from level one to level three, the material's flexural strength decreases. The rupture strength increases as the gas flow rate increases from level three to level four. The root gap was the list influential parameter; as the root gap increased from level one to two, the flexural strength fell from a higher value to a lower value. The flexural strength somewhat returns to growing as the game progresses from level two to three. However, when the gap is raised from level three to level four, the strength decreases slightly (Sanjay Kumar et al., 2017) also reported the same result. The filler metal type was the third important welding characteristic; when compared to other filler metals, level four filler metal had a lower rupture strength value. The filler at level three has the highest rupture strength value, followed by the fillers at levels one and two respectively (Anand Rao & Deivanathan, (2014) also get the same result for another type of austenite stainless steel.

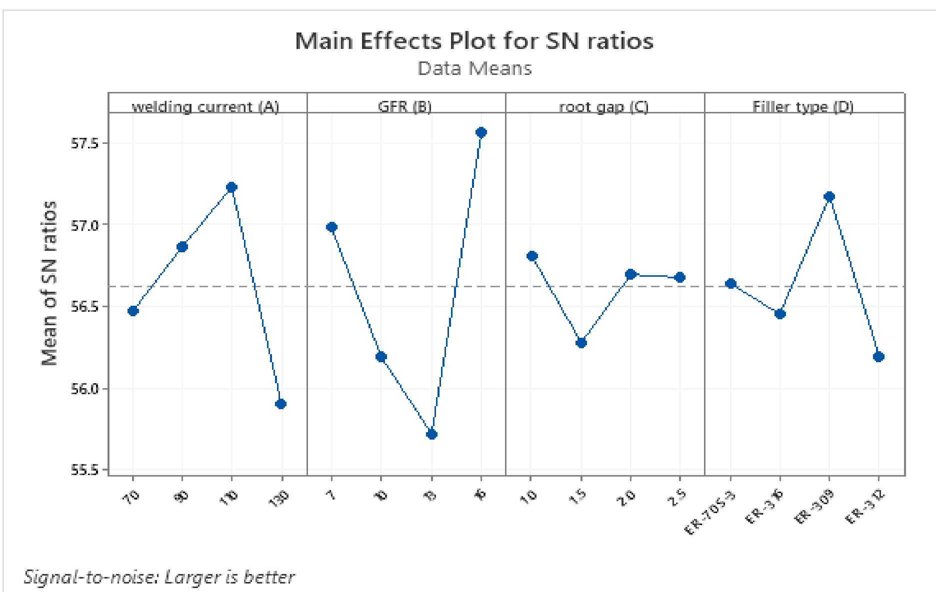

Figure 4.17 main effect plot for the signal to ratio of flexural

4.4.3.4. ANOVA for flexural strength

The most critical factors (most significant parameters) that determine the flexural strength of TIG-welded steels are discovered using analysis of variance (ANOVA) using table 4.14. The study used their S/N ratios to establish the percentage contribution of each of the components.

Table 4.14: Analysis of Variance for SN ratios of flexural

Source	**DF**	**%Contrib.**	**Seq SS**	**Adj SS**	**Adj MS**	**F**	**P**
welding current (A)	3	26	3.8720	3.8720	1.29066	19.14	0.018
GFR (B)	3	54	8.0795	8.0795	2.69316	39.95	0.006
root gap (C)	3	5	0.6477	0.6477	0.21590	3.20	0.182
Filler type (D)	3	14	2.0529	2.0529	0.68431	10.15	0.044
Residual Error	3	1	0.2023	0.2023	0.06742		
Total	**15**	**100**	**14.8543**				

S= 0.2597 **R-Sq** = 98.64% **R-Sq (adj)** = 93.19%

F-value =3.49 < F-ratio, hence the parameters have a significant effect , and the gas flow rate (54%) welding current (26%) has a highly significant impact and filler metals type (14%) has significant effect on the flexural strength as shown in the figure 4.21.

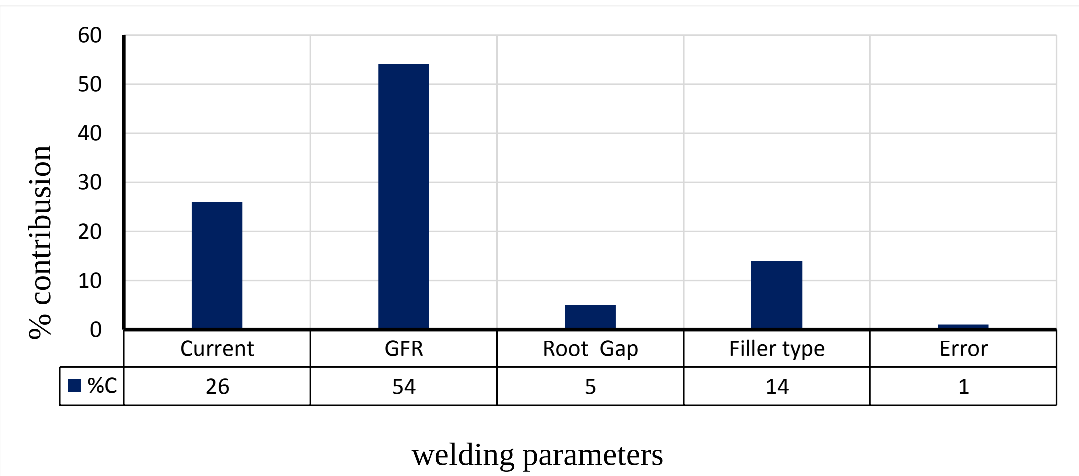

Figure 4.18 Percentage contribution of parameters on flexural strength

4.4.4. Bead width result Analysis

The greatest width of the deposited weld metal is the weld bead width. The welded metal's bead width was determined by measuring the width of the material deposited between the base metals with vernier calipers with a 0.01 accuracy. In each welded specimen, three readings were collected, and the average value was calculated. For each trial experiment, Table 4.15 shows the measured average experimental results of bead width geometry values. Smaller bead width was projected to be the preferable option for the higher economic performance of bead width.

Table 4.15: the experimental result of bead width

Sample No	*Welding Current (A)*	*Gas Flow Rate (B)*	*Root Gap (C)*	*Filler Type (D)*	*Bead width (mm)*	*Signal to noise ratio*
1	70	7	1.0	ER703	6.80	-16.6502
2	70	10	1.5	ER316	6.52	-16.2850
3	70	13	2.0	ER309	6.30	-15.9868
4	70	16	2.5	ER312	7.10	-17.0252
5	90	7	1.5	ER309	6.74	-16.5732
6	90	10	1.0	ER312	6.75	-16.5861
7	90	13	2.5	ER703	7.15	-17.0861
8	90	16	2.0	ER316	6.80	-16.6502
9	110	7	2.0	ER312	6.82	-16.6757
10	110	10	2.5	ER309	7.20	-17.1466
11	110	13	1.0	ER316	7.10	-17.0252
12	110	16	1.5	ER703	7.20	-17.1466
13	130	7	2.5	ER316	8.50	-18.5884
14	130	10	2.0	ER703	7.60	-17.6163
15	130	13	1.5	ER312	7.82	-17.8641
16	130	16	1.0	ER309	7.80	-17.8419

4.4.4.1. Mean response analysis of bead width

Table 4.16 shows that current (A) at the first level has the highest value, followed by root gap (C) at the third level, filler type (D) at the third level, and gas flow rate (B) at the second level. Figure 4.22 shows the main influence plot for control parameters for the mean bead width value. From the means graph, the numerical number at the minimum point in each graph in the main effect plot graph shows the parameter's best value at that level. They also show the best settings within the parameters of the experiment. When compared to other welding variables, the welding current weight percent has the greatest impact on improving bead width, followed by the root gap. Welding current (70A) at level one, gas flow rate (10 L/min) at level two, root gap (2mm) at level three, and filler type (ER-309) at level three were the optimum parameters (A1B2C3D3).

Table 4.16: Response Table for Means of bead width

Level	Welding current (A)	Gas flow rate (B)	Root gap (c)	Filler type (D)
1	**6.680**	7.215	7.112	7.188
2	6.860	**7.018**	7.070	7.230
3	7.080	7.092	**6.880**	**7.010**
4	7.930	7.225	7.487	7.123
Delta	1.250	0.207	0.607	0.220
Rank	**1**	**4**	**2**	**3**

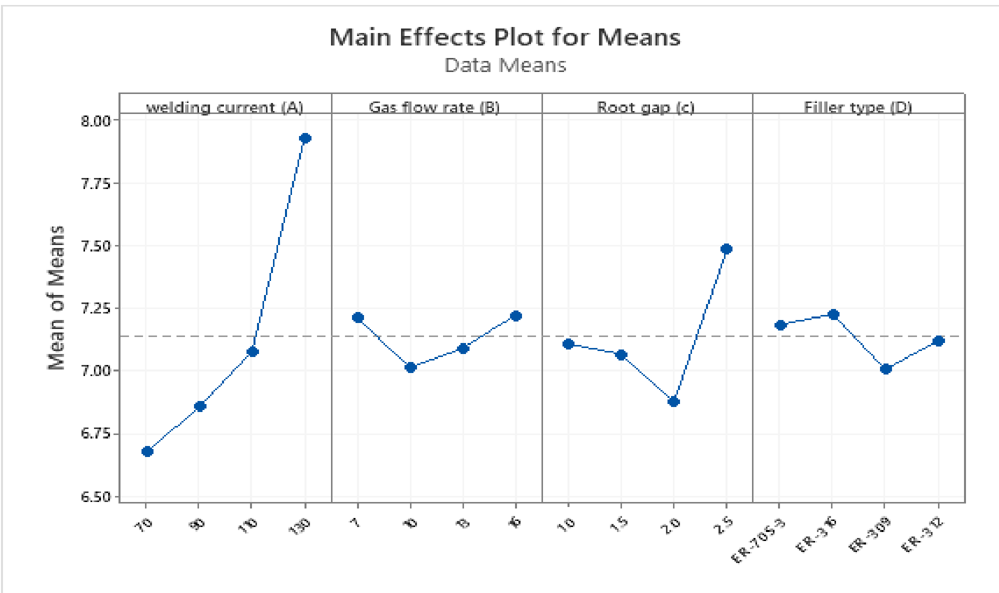

Figure 4.19 main effect plot for means of bead width

4.4.4.2. Signal to noise ratio analysis of Bead width

The welding current weight percentage has the major influence, according to the signal to noise ratio value indicated in table 4.17 (Delta = 1.49, Rank =,1^{st}) followed by root gap (Delta =0.73, Rank =,2^{nd}), and gas flow rate (Delta =0.26, Rank =,3^{rd}). The filler type has the smallest impact on the (S/N) ratio (Delta = 0.25, Rank =, 4^{th}.) The parameter combinations A1B2C3D3 based on the smaller the better, weld width character is the first optimum parameter combination for enhancing the bead width with the smallest the better response.

Table 4.17: Response table for Signal to Noise Ratios of bead (Smaller is better)

Level	Welding current (A)	Gas flow rate (B)	Root gap (c)	Filler type (D)
1	**-16.49**	-17.12	-17.03	-17.12
2	-16.72	**-16.91**	-16.97	-17.14
3	-17.00	-16.99	**-16.73**	**-16.89**
4	-17.98	-17.17	-17.46	-17.04
Delta	1.49	0.26	0.73	0.25
Rank	**1**	**3**	**2**	**4**

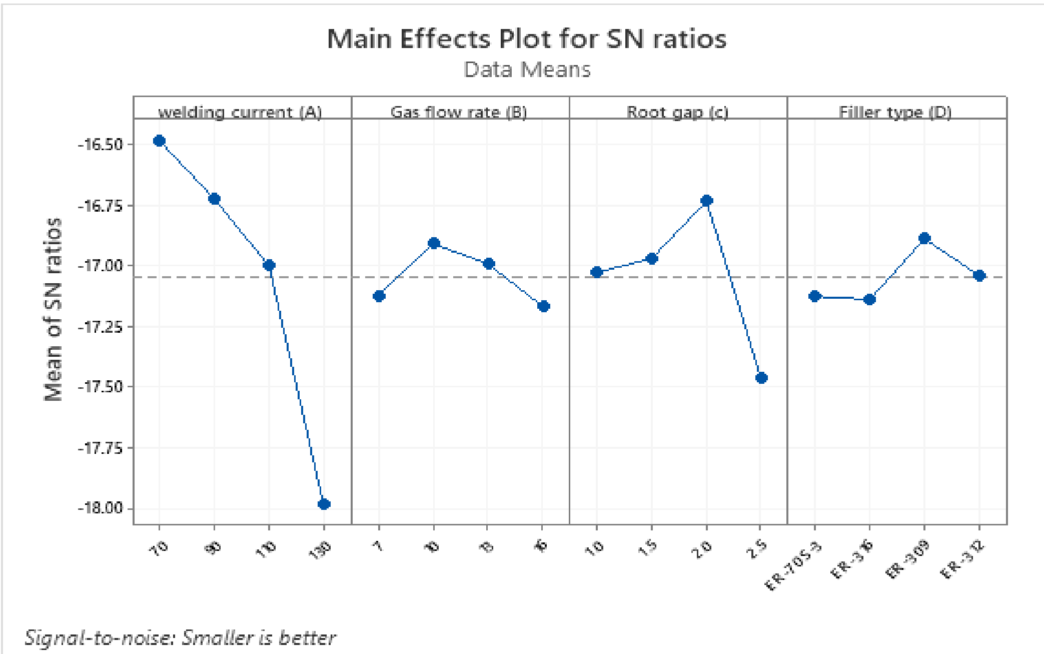

Figure 4.20 main effect plot for S/N ratio of bead width

4.4.4.3. Effects of parameters on bead width size

Figure 4.24 depicts how welding factors influence bead width, as well as the best values for each factor based on their rank. According to the analysis and primary effect plot graph for SN ratios, the optimal values for minimizing bead width are current at level 1 (70A), gas flow rate at level 2 (10 L/min), root gap at level three (2mm), and filler metal at level three (SS 309), with an initial parametric setting of A1B2C3D3. As the current rises from level one to level three, the bead width of the weld grows proportionally with the current input, as seen in the graph above. As the current is increased from level three to level four, the bead width (weld width) increases significantly Ramachandran, (2015). The width of the weld narrows as the gas flow rate rises from level one to level two, which is desirable. As the gas flow rate rises from level two to level four, the bead gets bigger. The second influential component was the root gap; when the root gap climbed from level one to three, the bead width decreased from a greater to a smaller amount. When gaps rise from level three to level four, the bead diameter widens considerably. As a result, the best bead width was chosen at stage three. The filler metal type was the list relevant welding attribute; level two filler metal had a wider bead width value than other filler metals. The level three filler has the narrower bead width value, followed by the levels four and one filler, respectively.

4.4.4.4. ANOVA for Bead width

Using analysis of variance (ANOVA) the most significant parameters that determine the weld width was shown in table 4.18. The percentage contribution of each of the components was calculated using their S/N ratios. The result F-Value=3.49 less than the experimental F-ratio, this shows that the parameters have a significant effect. The welding current weight percentage (77.8%) and root gap (16.8%) have a highly significant impact and gas flow rate (2.5%) and filler type (2.4%) have a significant influence on the bead width, as illustrated in figure 4.25.

Table 4.18: Analysis of Variance for SN ratios

Source	DF	Seq SS	% Cont.	Adj SS	Adj MS	F	P
welding current (A)	3	5.14697	77.8	5.14697	1.71566	168.99	0.001
Gas flow rate (B)	3	0.16852	2.5	0.16852	0.05617	5.53	0.097
Root gap (c)	3	1.11105	16.8	1.11105	0.37035	36.48	0.007
Filler type (D)	3	0.15930	2.4	0.15930	0.05310	5.23	0.104
Residual Error	3	0.03046	0.5	0.03046	0.01015		
Total	**15**	**6.61629**	**100.0**				

S= 0.1008 **R-Sq** = 99.54% **R-Sq (adj)** = 97.70%

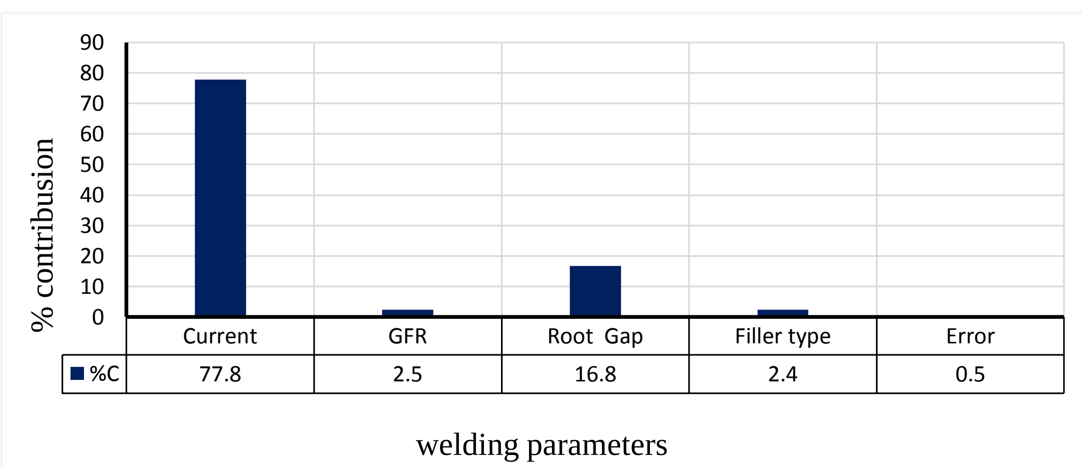

Figure 4.21 Percentage contribution of parameters on bead width

4.5. Multi-response parametric optimization of similar metals

In today's industry, multi-response optimization is more profitable than single-response optimization. The goal of this study is to use a multi-objective approach termed desirability function analysis to investigate the effect of TIG welding parameters on different responses.

4.5.1. Desirability function analysis (DFA)

It's a common method for large-scale industries to optimize multi-responses by combining multiple response characteristics into a single response characteristic. In this study, Taguchi methodology was used to determine the best process parameters for single performance characteristics only, whereas desirability function analysis was used to determine the best process parameters for multiple performance characteristics at the same time. The original parametric set was computed using the Taguchi technique to get the anticipated parametric set by using desirability these values were used in each result and analysis of tensile strength, hardness, flexural strength, and bead width.

4.5.1.1. Steps in Desirability function analysis for optimization

First: The design of a decision matrix to reflect performance characteristics in connection to numerous variables, as well as the identification of goals and their features. There are four responses in table 4.19, however, the expected positive reaction in each response was different depending on the aims that were needed. For example, the goal (objective) for tensile strength was maximization, and the bead width goal was minimization. Each answer is calculated according to its objective.

Table 4.19: result table for all responses

Sample No	*Welding Current (A)*	*Gas Flow Rate (B)*	*Root Gap (C)*	*Filler Type (D)*	*Tensile strength (MPa)*	*Hardness (HRB)*	*Flexural strength (MPa)*	*Bead width (mm)*
1	70	7	1.0	ER70S-3	502	71.0	718	6.80
2	70	10	1.5	ER316	560	75.0	599	6.52
3	70	13	2.0	ER309	590	75.3	633	6.30
4	70	16	2.5	ER312	525	70.0	723	7.10
5	90	7	1.5	ER309	480	83.0	755	6.74
6	90	10	1.0	ER312	525	85.0	633	6.75
7	90	13	2.5	ER70S-3	531	76.0	636	7.15
8	90	16	2.0	ER316	595	95.0	776	6.80
9	110	7	2.0	ER312	450	85.0	730	6.82

10	110	10	2.5	ER309	475	86.0	749	7.20
11	110	13	1.0	ER316	485	92.0	667	7.10
12	110	16	1.5	ER70S-3	490	77.0	766	7.20
13	130	7	2.5	ER316	410	97.0	630	8.50
14	130	10	2.0	ER70S-3	435	84.0	609	7.60
15	130	13	1.5	ER312	375	79.0	520	7.82
16	130	16	1.0	ER309	415	87.0	760	7.80

Second: The individual desirability index (di) value is calculated for each response. Di value is determined by the type of the relevant output. Using equation (4.3) for Maximization and equation (4.4) for minimization.

$$di = \begin{cases} 0, & if \quad \hat{y} \le \widehat{ymin} \\ \left(\frac{\hat{y} - ymin}{ymax - ymin}\right)^r, & ymin \le \hat{y} \le ymax, r \ge 0; \\ 1, & if \quad \hat{y} \ge ymax \end{cases} \tag{4.3}$$

$$di = \begin{cases} 1, & \hat{y} \le ymin \\ \left(\frac{\hat{y} - ymax}{ymin - ymax}\right)^r, & ymin \le \hat{y} \le ymax, r \ge 0; \\ 0, & \hat{y} \ge ymax \end{cases} \tag{4.4}$$

Where the $ymin$ represents the lower tolerance limit of ŷ, the $ymax$ represents the upper tolerance limit of ŷ and r represents the weight.

- The larger is the better: So, for Tensile strength, hardness, and flexural strength the objectives are maximization

For tensile strength: Specimen no 1:

$$d1(tensile) = \left(\frac{502 - 375}{595 - 375}\right)^{0.5} = 0.7598$$

For hardness: specimen no 1:

$$d1(hardness) = \left(\frac{71 - 70}{97 - 70}\right)^{0.5} = 0.19245$$

For flexural strength: specimen no1:

$$d1(flexural) = \left(\frac{718 - 520}{776 - 520}\right)^{0.5} = 0.5051$$

Since the previous three responses maximize the response variables, this is how all of the responses for trials 2 through 16 for each response parameter were done as shown in table 4.20.

- The smaller the better: The objective of the bead width response parameter is minimization. As a result, the equation used to calculate the individual desirability index for bead width differed from the responses above.

For bead width: specimen no 1:

$$d1\ (bead\ width) = \left(\frac{6.8 - 8.5}{6.3 - 8.5}\right)^{0.5} = 0.8790$$

The individual desirability index for smaller is the better was calculated using the above equation for all 2 to 16 trials as shown in table 4.20.

Third: Compute the Composite desirability index: To calculate the total desirability, the individual desirability values were added together.

$$Dg_1 = \sqrt[w]{d1^{w1} * d2^{w2} * \ldots * di^{wi}} \quad (4.5)$$

Where Di and *Wi* are the individual desirability and weight of the response Yi. W is the sum of the individual weights and Dg is the Composite Desirability or overall desirability. So, from the above individual desirability index, the composite desirability index was computed.

$$D1 = \sqrt[w]{d1^{w1} * d2^{w2} * d3^{w3} * d4^{w4}} = 0.2548$$

Table 4.20: individual desirability index and Composite desirability index with the rank

sample	UTS	Hardness	Flexural	BW	Individual Desirability Index (Di)					
no	MPa	HRB	MPa	mm	UTS	Hardness	Flexural	Bead width	CDI (dg)	Rank
1	502	71	718	6.8	0.7598	0.19245	0.5051	0.8790	0.2548	13
2	560	75	599	6.52	0.9170	0.43033	0.3191	0.9487	0.3456	10
3	590	75.3	633	6.3	0.9886	0.44305	0.3816	1.0000	0.4088	7
4	525	70	723	7.1	0.8257	0.00000	0.5115	0.7977	0.0000	14
5	480	83	755	6.74	0.6908	0.69389	0.5503	0.8944	0.4857	2
6	525	85	633	6.75	0.8257	0.74536	0.3816	0.8919	0.4577	5

7	531	76	636	7.15	0.8421	0.47140	0.3866	0.7833	0.3467	9
8	595	95	776	6.8	1.0000	0.96225	0.5744	0.8790	0.6970	1
9	450	85	730	6.82	0.5839	0.74536	0.5202	0.8739	0.4448	6
10	475	86	749	7.2	0.6742	0.76980	0.5432	0.7687	0.4655	4
11	485	92	667	7.1	0.7071	0.90267	0.4352	0.7977	0.4708	3
12	490	77	766	7.2	0.7230	0.50918	0.5630	0.7687	0.3992	8
13	410	97	630	8.5	0.3989	1.00000	0.3765	0.0000	0.0000	14
14	435	84	609	7.6	0.5222	0.72008	0.3387	0.6396	0.2854	12
15	375	79	520	7.82	0.0000	0.57735	0.0000	0.5560	0.0000	14
16	415	87	760	7.8	0.4264	0.79349	0.5561	0.5641	0.3258	11

CDI (dg) were analyzed after their composite desirability index (dg) was determined based on their rank. The CDI (dg) in the first rank was used as the CDI's initial parameter setting as shown in table 4.21.

Table 4.21: initial parametric setting

Initial setting	UTS (MPa)	HARDNESS (HRB)	FS (MPa)	BW (mm)	CDI (dg)
A2 B4 C3 D2	595	95	776	6.8	0.6970

Fourth: Determine the optimal parameter and its level combination. The higher composite desirability value implies better product quality. Conduct Taguchi's experimental work with this CDI value as the response parameter to obtain the best parametric configuration.

Table 4.22: Response Table for Means of CDI

Level	Welding current (A)	gas flow rate (B)	root gap (C)	Filler type (D)
1	0.2523	0.2963	0.3773	0.3215
2	**0.4968**	**0.3886**	0.3076	0.3783
3	0.4451	0.3066	**0.4590**	**0.4215**
4	0.1528	0.3555	0.2031	0.2256
Delta	0.3440	0.0922	0.2559	0.1959
Rank	**1**	**4**	**2**	**3**

The Taguchi method is now used to analyze the composite desirability values. The means of the di and dg values are shown in table 4.22. On the multiple responses, the main effect plot was used to find the main influencing (most significant) parameter. Figure 4.16

shows that the highest influencing parameter for dg is welding current, followed by root gap and filler type.

Figure 4.22 main effect plot for means of CDI (dg)

Fifth: compute Analysis of variance (ANOVA) for CDI (dg)

The influence of the process factors on the multi-response (dg) is tested using an analysis of variance. Welding current, root gap, and filler metal have higher significance, but GFR has a low significance effect on composite desirability dg, as shown in table 4.23.

Table 4.23: Analysis of Variance of dg

Source	DF	Adj SS	%Cont.	Adj MS	F-Value	P-Value
welding current (A)	3	0.313256	55	0.104419	34.76	0.008
gas flow rate (B)	3	0.022316	4	0.007439	2.48	0.238
root gap (C)	3	0.141226	25	0.047075	15.67	0.024
filler type (D)	3	0.085965	15	0.028655	9.54	0.048
Error	3	0.009013	1	0.003004		
Total	**15**	**0.571776**	**100%**			

S= 0.05481 **R-Sq** = 98.42% **R-Sq (adj)** = 92.12%

The welding current (55%) has a highly significant impact on the CDI (dg) of TIG-welded 316 stainless sheets of steel and the root gap (25%) and filler metal (15%) have a significant impact on the CDI (dg) of TIG-welded 316 stainless sheets of steel with a thickness of 3mm, as shown in the figure 4.27. As a result, the welding current has a big influence on the responses (dg) of TIG-welded 316 stainless sheets of steel.

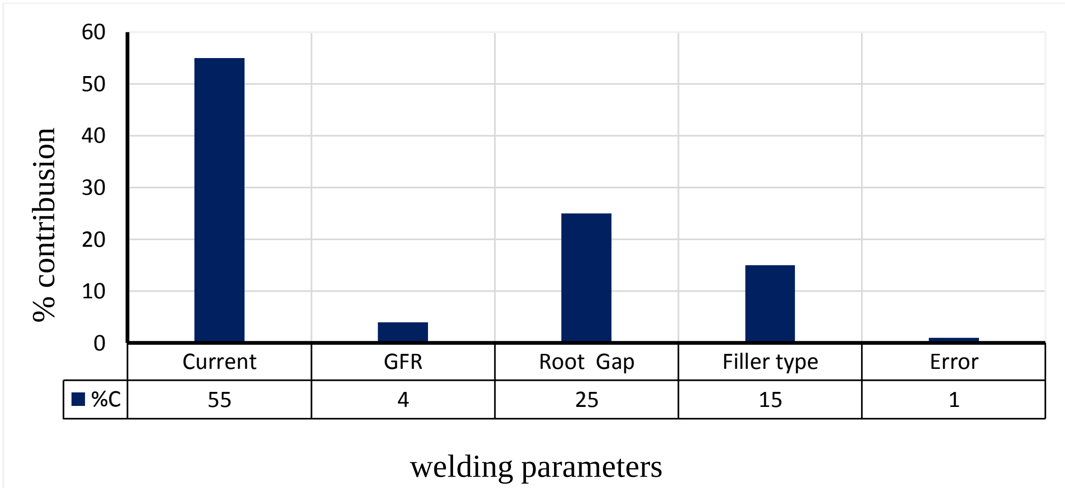

Figure 4.23 Percentage contribution of parameters on CDI

Sixth: Finally, using the ideal level of design parameters, predict and validate the quality features.

Table 4.24:The optimum parametric setting

Optimum setting	UTS(MPa)	HARDNESS (HRB)	FS(MPa)	BW (mm)	CDI (dg)
A2 B2 C3 D3	602	96.4	780	6.1	0.7556

Table 4.25: Improvement in UTS, FS, HARDNESS, and BW

Initial setting				Optimum setting				**% Improvement**			
A2 B4 C3 D2				A2 B2 C3 D3							
UTS	HRD	FS	BW	UTS	HRD	FS	BW	UTS	HRD	FS	BW
595	95	776	6.8	602	96.4	780	6.1	**1.18%**	**1.47%**	**0.52%**	**10.29%**
Composite desirability											
0.697				**0.7556**				**8.41%**			

UTS:- ultimate tensile strength, **HRD:-** hardness, **FS:-** flexural strength, **BW:-** bead width

4.6. Mechanical Properties of Dissimilar Welded Metals

The goal of this study was to see if dissimilar welding of AISI 316 austenitic stainless steel and AISI 1020 mild steel sheets was possible. These two metals are typical austenitic stainless-steel grades and mild steel grades, respectively. This research looked at the microstructure, mechanical properties (hardness, tensile, flexural bending, properties), and bead width of weldments produced by TIG. And further investigate and optimize TIG process parameters for dissimilar welding between AISI 316 and AISI 1020.

4.6.1. Tensile strength results analysis

Table 4.26 shows the ultimate tensile strengths of samples made from TIG-produced weldments. The failure of the testing sample following the test on the carbon steel side. These findings matched the hardness profile, which indicated that carbon steel had the lowest hardness.

Table 4.26: Mean Tensile testing result

Sample No	*Welding Current (A)*	*Gas Flow Rate (B)*	*Root Gap (C)*	*Filler Type (D)*	*Tensile strength (MPa)*	*Signal to noise ratio*
1	70	7	1.0	ER-70S-3	390	51.8213
2	70	10	1.5	ER-316	420	52.4650
3	70	13	2.0	ER-309	460	53.2552
4	70	16	2.5	ER-312	442	52.9084
5	90	7	1.5	ER-309	450	53.0643
6	90	10	1.0	ER-312	410	52.2557
7	90	13	2.5	ER-70S-3	478	53.5886
8	90	16	2.0	ER-316	445	52.9672
9	110	7	2.0	ER-312	410	52.2557
10	110	10	2.5	ER-309	502	54.0141
11	110	13	1.0	ER-316	483	53.6789
12	110	16	1.5	ER-70S-3	486	53.7327
13	130	7	2.5	ER-316	398	51.9977
14	130	10	2.0	ER-70S-3	395	51.9319
15	130	13	1.5	ER-312	412	52.2979
16	130	16	1.0	ER-309	435	52.7698

4.6.1.1. Mean response analysis of tensile strength

Current (A) at level 3 is the highest value in Table 4.26, followed by gas flow rate (B), filler type (D), and root gap (C) at level 3. For TIG welding of stainless steel 316 and AISI 1020 with a thickness of 3mm, Taguchi employed these welding parameters (A3B3C4D3) as the initial parametric setup. That means it's possible to use that as a parameter combination to create larger and better results. The main influence plot for control factors for mean tensile strength value variations is shown in Figure 4.28.

Table 4.27: Response Table for Means of UTS

Level	Welding current (A)	gas flow rate (B)	root gap (C)	Filler type (D)
1	428.0	412.0	429.5	437.3
2	445.8	431.8	442.0	436.5
3	**470.3**	**458.3**	427.5	**461.8**
4	410.0	452.0	**455.0**	418.5
Delta	60.3	46.3	27.5	43.3
Rank	**1**	**2**	**4**	**3**

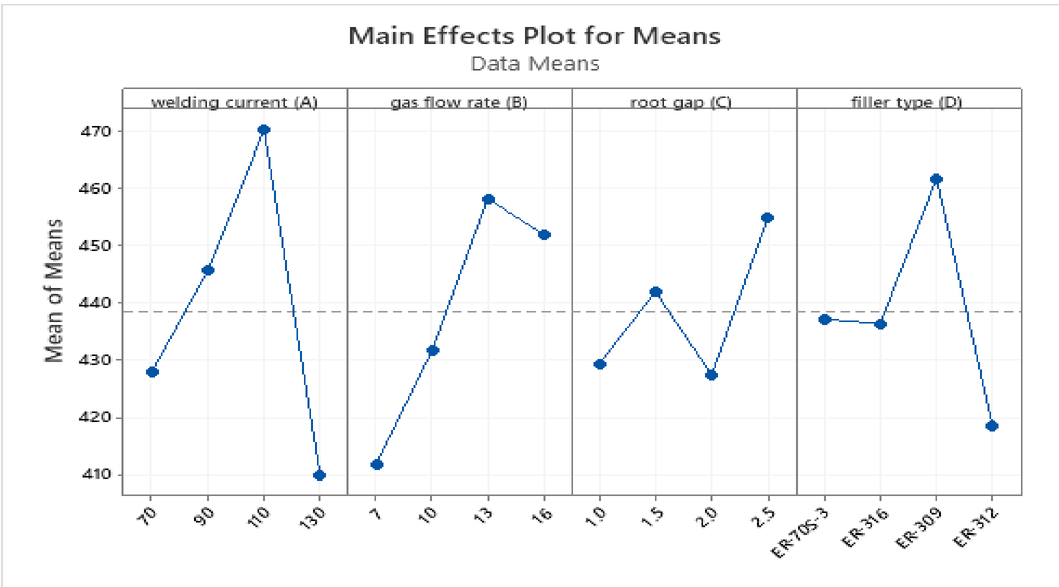

Figure 4.24 main effect plot for means of UTS

In the main effect plot graph figure 4.27 above, the numerical number at the maximum point in each graph represents the parameter's best value at that level. They also display the optimum settings within the experiment's parameters. When compared to other welding variables, the welding current weight percentage, followed by the gas flow rate, has the largest impact on improving tensile strength. The ideal parameters were welding current (110A) at level four, gas flow rate (13 L/min) at level three, root gap (2.5mm) at level four, and filler type (ER-309) at level three.

4.6.1.2. Signal to noise ratio analysis of tensile properties

According to the signal to noise ratio value in table 4.28, the welding current weight percentage has the highest influence, (Delta = 1.17, Rank =,1^{st}) followed by gas flow rate (Delta =0.92, Rank =,2^{nd}), and filler metal (Delta =0.85, Rank =,3^{rd}). The (S/N) ratio is least affected by the root gap (Delta = 0.52, Rank =, 4^{th}.) according to the experimental result. The initial best parameter combination for increasing weld metal stiffness with the greater the better responsiveness of TIG-welded 316 stainless steel and AISI 1020 steel sheets is **A3B3C4D3**.

Table 4.28: Response Table for Signal to Noise Ratios of UTS (Larger is better)

Level	Welding current (A)	gas flow rate (B)	root gap (C)	Filler type (D)
1	52.61	52.28	52.63	52.77
2	52.97	52.67	52.89	52.78
3	**53.42**	**53.21**	52.60	**53.28**
4	52.25	53.09	**53.13**	52.43
Delta	1.17	0.92	0.52	0.85
Rank	**1**	**2**	**4**	**3**

4.6.1.3. Effect of process parameters on tensile strength

Figure 4.28 shows how welding factors affect metal stiffness, as well as the ideal values for each factor depending on their ranking. The optimal values for enhancing tensile strength, according to the analysis and primary effect plot graph for SN ratios, are current at level 3 (110A), the gas flow rate at level 3 (13 L/min), root gap at level four (2.5mm), and filler metal at level three (SS 309), with an initial parametric setting of A3B3C4D3. The tensile strength increases dramatically as the current climbs from level one to level three, as shown in the graph above. The tensile strength decreases drastically as the current is increased from level three to level four. As the gas flow rate increases from level one to level three, the tensile strength value increases (Pasupathy & Ravisankar, 2013) report the same result. However, as the gas flow is increased from level two to level four, the material's tensile characteristics decrease. The root gap was another important factor; when the root gap expanded from level one to two, the tensile strength increased from a low to a high number. The tensile characteristic of the metal decreases as gaps increases from level two to level three. However, widening the gap from level three to level four maximizes the material's tensile property (Wahule & Wasankar, 2018). The third important welding attribute was the filler metal type; level one and two filler metal had nearly identical tensile strengths. The tensile strength of the level three filler is the highest of all the fillers employed. However, the filler at level four was worthless.

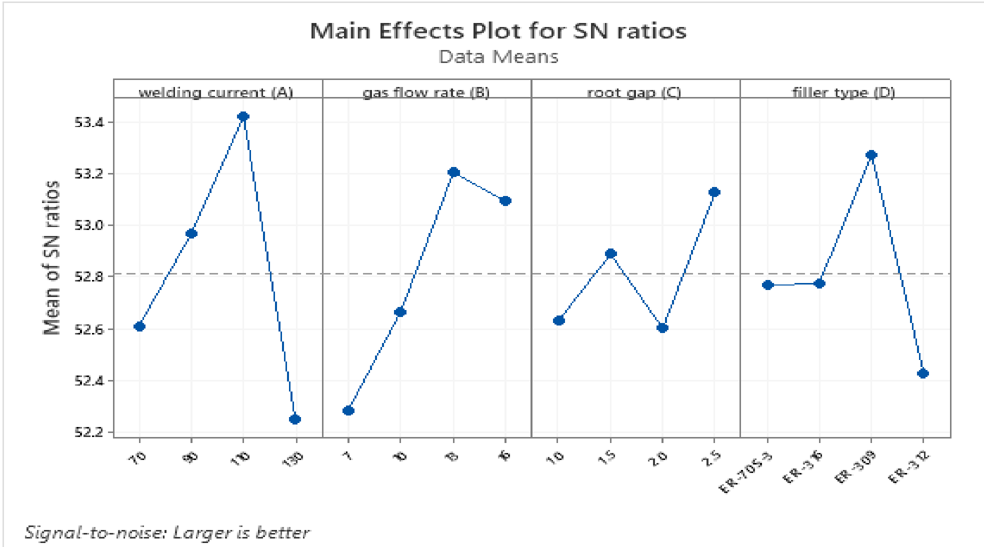

Figure 4.25 main effects plots for a signal to noise ratio of UTS

4.6.1.4. ANOVA for tensile strength

The most significant parameters that impact the tensile strength of TIG-welded steels are determined using analysis of variance (ANOVA), as shown in table 4.29.

Table 4.29: Analysis of Variance for SN ratios of UTS

Source	**DF**	**Seq SS**	**% Cont.**	**Adj SS**	**Adj MS**	**F**	**P**
welding current (A)	3	3.00449	40.80	3.00449	1.00150	73.76	0.003
Gas flow rate (B)	3	2.13415	29.00	2.13415	0.71138	52.39	0.004
Root gap (c)	3	0.72768	9.90	0.72768	0.24256	17.86	0.020
Filler type (D)	3	1.45828	19.80	1.45828	0.48609	35.80	0.008
Residual Error	3	0.04073	0.50	0.04073	0.01358		
Total	**15**	**7.36534**	**100.00**				

S= 0.1165 **R-Sq** = 99.45% **R-Sq (adj)** = 97.23%

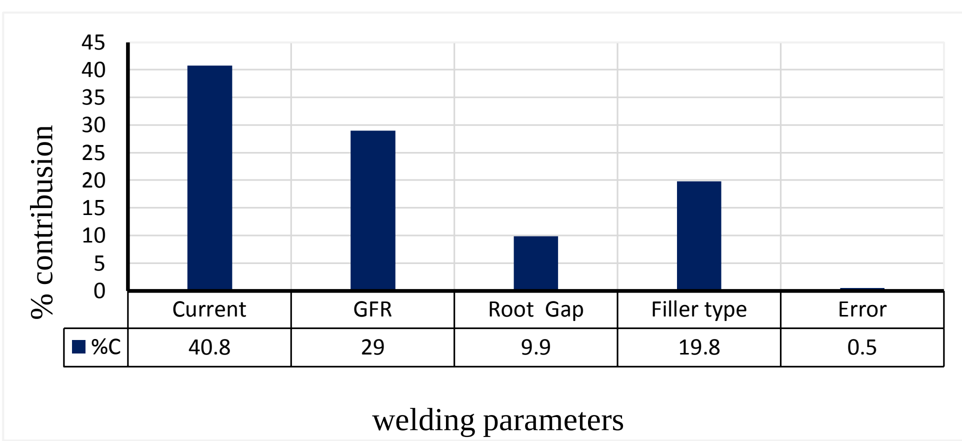

Figure 4.26 Percentage contribution of parameter

Since the F- value from the table is 3.49, the F-ratio gained from the ANOVA table is much greater than the critical F-ratio, so all parameters have a significant effect on tensile strength. As shown in figure 4.30, the welding current weight percentage (40.8%), gas flow rate (29%), filler metal (19.80), and root gap (9.90) all have a substantial impact on the tensile strength of TIG-welded SS316 and AISI 1020 steel sheets with a thickness of 3mm.

4.6.2. Hardness result analysis

Rockwell and Vickers's hardness can be used to determine the material's hardness. From the weld center to HAZ and WZ, the specimens are tested. Three readings were taken in each zone, and the average value was used for each trial experiment. The measured experimental results of hardness values are presented in Table 4.30. For superior performance qualities, larger hardness was predicted to be the preferred alternative.

4.6.2.1. Mean response analysis of hardness

The greatest value in Table 4.31 is current (A) at level 4, followed by root gap (C) at level 3, the gas flow rate at level 4, and filler type at level 4. These welding parameters (A4B4C3D4) were chosen as the first parametric setup for hardness when TIG welding stainless steel 316 and AISI 1020 mild steel with a thickness of 3mm. That implies using that as a parameter combination to achieve larger, better hardness outcomes is a viable option. The main influence plot for control parameters for mean hardness value fluctuations is shown in Figure 4.30.

Table 4.30: Hardness test mean result

Sample No	*Welding Current (A)*	*Gas Flow Rate (B)*	*Root Gap (C)*	*Filler Type (D)*	*Hardness (HRB)*	*Signal to noise ratio*
1	70	7	1.0	ER703	64	36.1236
2	70	10	1.5	ER316	72	37.1466
3	70	13	2.0	ER309	75	37.5012
4	70	16	2.5	ER312	76	37.6163
5	90	7	1.5	ER309	78	37.8419
6	90	10	1.0	ER312	75	37.5012
7	90	13	2.5	ER703	75	37.5012
8	90	16	2.0	ER316	83	38.3816
9	110	7	2.0	ER312	86	38.6900
10	110	10	2.5	ER309	84	38.4856
11	110	13	1.0	ER316	81	38.1697
12	110	16	1.5	ER703	86	38.6900
13	130	7	2.5	ER316	83	38.3816
14	130	10	2.0	ER703	88	38.8897

15	130	13	1.5	ER312	90	39.0849
16	130	16	1.0	ER309	87	38.7904

Table 4.31: Response Table for Means of hardness

Level	Welding current (A)	GFR (B)	root gap (C)	Filler type (D)
1	71.75	77.75	76.75	78.25
2	77.75	79.75	81.50	79.75
3	84.25	80.25	**83.00**	81.00
4	**87.00**	**83.00**	79.50	**81.75**
Delta	15.25	5.25	6.25	3.50
Rank	**1**	**3**	**2**	**4**

In the main effect plot graph below, the indicating number at the maximum point in each graph represents the parameter's best value at that level. They also display the optimum settings within the experiment's parameters. When compared to other welding variables, the welding current weight percent, followed by the root gap, has the biggest impact on improving hardness. According to the response data means of the experiment, the optimum parameters were welding current (130A) at level four, gas flow rate (16 L/min) at level four, root gap (2mm) at level three, and filler type (ER-312) at level four.

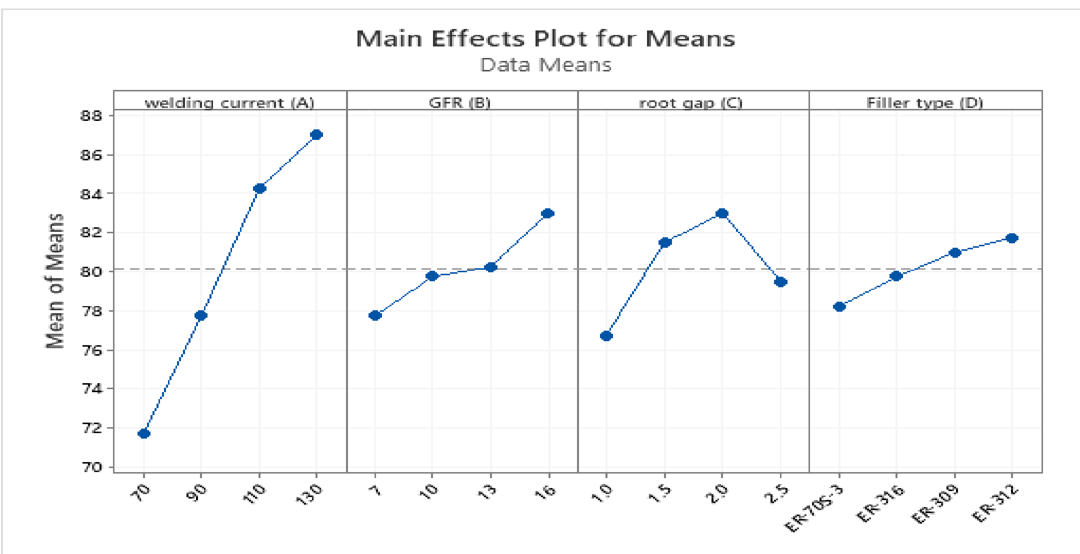

Figure 4.27 main effects graph for means of hardness

4.6.2.2. Signal to noise ratio analysis for hardness

According to the signal to noise ratio value in table 4.32, the welding current weight percentage has the greatest impact (Delta = 1.69, Rank =,1^{st}) followed by root gap (Delta =0.72, Rank

=,2^{nd}), and gas flow rate (Delta =0.61, Rank =,3^{rd}). The filler type has the smallest impact on the (S/N) ratio (Delta = 0.42, Rank =, 4^{th}.) The Taguchi initial optimum parameter combination for boosting the hardness of dissimilar TIG-welded 316 stainless steel and AISI 1020 mild steel is A4B4C3D4 based on the larger the better, hardness character.

Table 4.32: Response Table for Signal to Noise Ratios (Larger is better)

Level	Welding current (A)	GFR (B)	root gap (C)	Filler type (D)
1	37.10	37.76	37.65	37.80
2	37.81	38.01	38.19	38.02
3	38.51	38.06	**38.37**	38.15
4	**38.79**	**38.37**	38.00	**38.22**
Delta	1.69	0.61	0.72	0.42
Rank	**1**	**3**	**2**	**4**

4.6.2.3. Effect of process parameters on hardness

The influence of welding settings on hardness is depicted in Figure 4.31, as well as the optimal values depending on their rank. The optimal values for maximizing hardness are current at level 4 (130A), the gas flow rate at level 1 (16 L/min), root gap at level three (2mm), and filler metal at level two (SS 312), according to the analysis and the primary effect plot graph for SN ratios, with an initial parametric setting of **A4B4C3D4**. As the current rises from level one to level four, the hardness rises proportionally with it, as indicated in the graph above. The harder the metal was at level four, the harder it was as shown by (L. S. Kumar et al., 2011). The material's hardness increases as the gas flow rate increases from level one to level four. The same result has been identified by (Anbarasu et al., 2020) for mild steel using duplex stainless steel filler. The second influential parameter was the root gap; as the root gap climbed from one to three, the hardness increased from the lower limit to the maximum value. When the gap reached level four, the hardness of the metal began to decrease. However, according to the experimental results, the gap at level three provided the optimal opening between the base metals. The fourth and most essential welding attribute was the filler metal type; when compared to other filler metals, level four filler metal had a greater hardness value, followed by level three and level two fillers. The list hardness value is in the filler at level one.

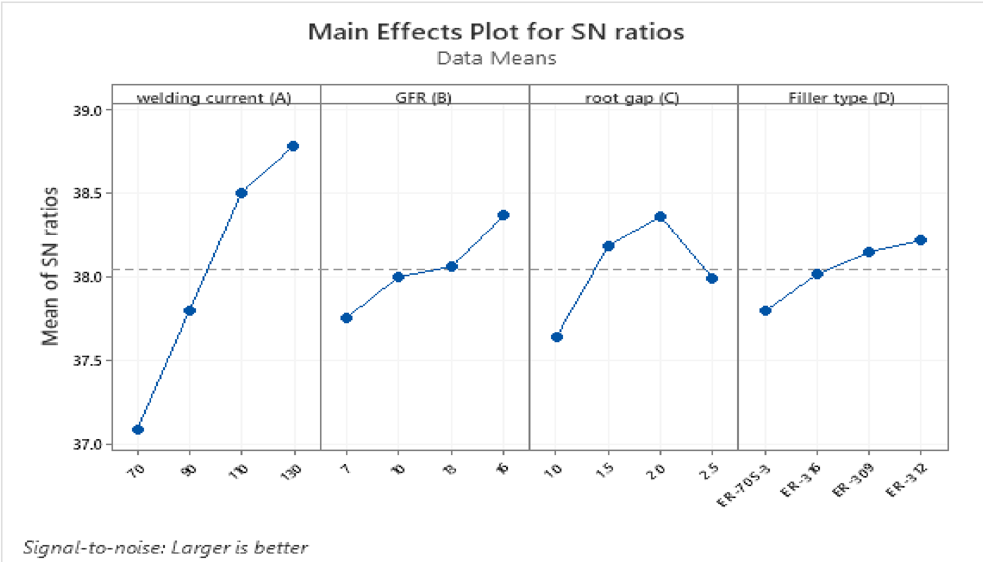

Figure 4.28 main effects graph for a signal to noise ratio of hardness

4.6.2.4. ANOVA for hardness

The ANOVA was developed for hardness to determine whether the developed experiment was adequate. since the determined F-ratio of the produced model is greater than the standard F-ratio (F-table value 3.49) value at the required degree of confidence of 95 percent, so the model is deemed to be inadequate within the confidence limit, according to this technique. The coefficient of determination, R2, is greater than 0.99.

Table 4.33: Analysis of Variance for SN ratios of hardness

Source	DF	Seq SS	% Cont.	Adj SS	Adj MS	F	P
Welding current (A)	3	6.88294	74.57	6.88294	2.29431	200.49	0.001
GFR (B)	3	0.75520	8.52	0.75520	0.25173	22.00	0.015
root gap (C)	3	1.14149	12.37	1.14149	0.38050	33.25	0.008
Filler type (D)	3	0.41515	4.50	0.41515	0.13838	12.09	0.035
Residual Error	3	0.03433	0.04	0.03433	0.01144		
Total	**15**	**9.22910**	**100**				

S= 0.1070 **R-Sq** = 99.63% **R-Sq (adj)** = 98.14%

Since the F-ratio of the ANOVA table shown above was higher than the F-critical, so all the parameters have a highly significant effect on hardness. As shown in figure 4.33, the welding current weight percentage (74.57%), gas flow rate (8.52%), filler metal (4.50), and root gap

(12.52) have a considerable impact on the hardness of TIG-welded 316 stainless steel and AISI 1020 mild steel sheets with a thickness of 3mm.

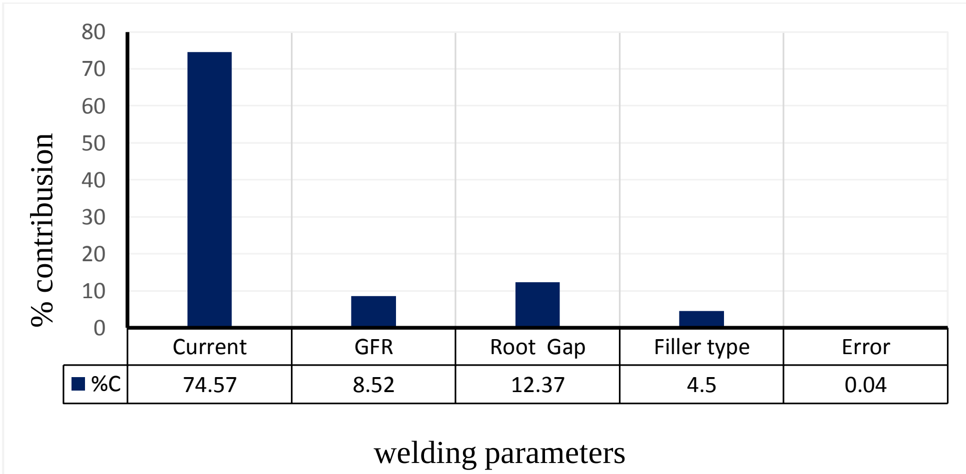

Figure 4.29 percentage contribution graph

4.6.3. Flexural strength results analysis

Flexural bending through a 3-point bend test on universal testing equipment can be used to measure the welded material's bending strength (UTM). The bend test bends the specimens into a U shape. The maximum force from the universal testing equipment was recorded, and the flexural strength was calculated using this maximum force and cross-section area. Each testing trial had three readings, with the average value determined. The measured experimental results of mean flexural strength values for each trial experiment are shown in Table 4.34.

Table 4.34: Mean flexural strength testing result

Sample No	*Welding Current (A)*	*Gas Flow Rate (B)*	*Root Gap (C)*	*Filler Type (D)*	*Flexural strength (MPa)*	*Signal to noise ratio*
1	70	7	1.0	ER703	555	54.8859
2	70	10	1.5	ER316	605	55.6351
3	70	13	2.0	ER309	670	56.5215
4	70	16	2.5	ER312	640	56.1236
5	90	7	1.5	ER309	692	56.8021
6	90	10	1.0	ER312	655	56.3248
7	90	13	2.5	ER703	620	55.8478
8	90	16	2.0	ER316	679	56.6374
9	110	7	2.0	ER312	545	54.7279
10	110	10	2.5	ER309	662	56.4172
11	110	13	1.0	ER316	505	54.0658

12	110	16	1.5	ER703	440	52.8691
13	130	7	2.5	ER316	588	55.3875
14	130	10	2.0	ER703	525	54.4032
15	130	13	1.5	ER312	480	53.6248
16	130	16	1.0	ER309	595	55.4903

4.6.3.1. Mean response analysis of flexural strength

The welding current (A) at level 2 has the highest value, followed by filler metal (D) at level 3, root gap (C) at level 4, and gas flow rate (B) at level 2. For TIG welding of stainless steel 316 with AISI 1020 mild steel with a thickness of 3mm, these welding parameters (A2B2C4D3) were chosen as the initial parametric setup. That suggests that using that as a parameter combination to generate larger, flexural strength outcomes is possible. Figure 4.34 shows the major influence plot for control parameters for means of flexural strength value fluctuations.

Table 4.35: Response Table for Means of flexural strength

Level	Welding current (A)	GFR (B)	root gap (C)	Filler type (D)
1	617.5	595.0	577.5	535.0
2	**661.5**	**611.8**	554.3	594.3
3	538.0	568.8	604.8	**654.8**
4	547.0	588.5	**627.5**	580.0
Delta	123.5	43.0	73.3	119.8
Rank	**1**	**4**	**3**	**2**

The numerical means value at the greatest point in each graph represents the parameter's best value at that level, as seen in the main effect plot graph below. They also show the best options within the parameters of the trial. When compared to other welding variables, the welding current weight percent has the greatest impact on improving flexural strength, while the gas flow rate has the least. Welding current (90A) at level two, gas flow rate (10 L/min) at level two, filler type (ER-309) at level three, and root gap (2.5mm) at level four (which has a combination of factors) were the best.

Figure 4.30 main effects graph for means flexural strength

4.6.3.2. Signal to noise ratio analysis for flexural strength

The most important factor is the welding current weight % (Delta = 1.88, Rank =,1^{st}) followed by filler metal type (Delta =1.81, Rank =,2^{nd}), and root gap (Delta =1.21, Rank =,3^{rd}) as shown in table 4.36. The last influential effect on the (S/N) ratio is the gas flow rate (Delta = 0.68, Rank =, 4^{th}) Based on the larger the better, flexural strength character, the initial optimum parameter combination for boosting the rupture strength of TIG-welded 316 stainless steel with AISI 1020 mild sheets of steel was A2B2C4D3.

Table 4.36: Response Table for Signal to Noise Ratios of flexural(Larger is better)

Level	Welding current (A)	GFR (B)	root gap (C)	Filler type (D)
1	55.85	**55.45**	55.09	54.42
2	**56.36**	55.30	54.99	55.47
3	54.37	55.31	**55.61**	**56.28**
4	54.73	55.23	55.61	55.13
Delta	1.99	0.22	0.62	1.86
Rank	**1**	**4**	**3**	**2**

4.6.3.3. Effect of process parameters on flexural strength

Figure 4.34 depicts the effects of welding factors on flexural strength, as well as the optimal values for each rank. According to the analysis and the primary effect plot graph for SN ratios, the optimal values for maximizing flexural strength are Current at level 2 (90A), the gas flow rate at level 2 (10 L/min), root gap at level four (2.5mm), and filler metal at level three (SS 309), with an initial parametric setting of **A2B1C3D3**. As the current rises from level one to level two, as illustrated in the graph above, the flexural strength increases proportionally with the current input. As the current is increased from level two to level three, the flexural strength of the metal backs decreases significantly, while the rupture strength of the metal backs increases (Vennimalai Rajan et al., 2020) reported the same value. The flexural strength of the material increases as the gas flow rate increases from level one to level two. As you progress through the levels, the rupture strength decreases. When the purging gas was increased to level four, however, material strength began to increase again. The root gap was the most important factor; as the root gap went from one to two, the flexural strength decreased significantly. When the gap between levels two and four is increased, the flexural strength increases dramatically. The filler metal type was the second most important welding attribute; level one filler metal had a lower rupture strength rating than other filler metals. The level three filler has the maximum rupture strength, followed by the levels two and four fillers, respectively.

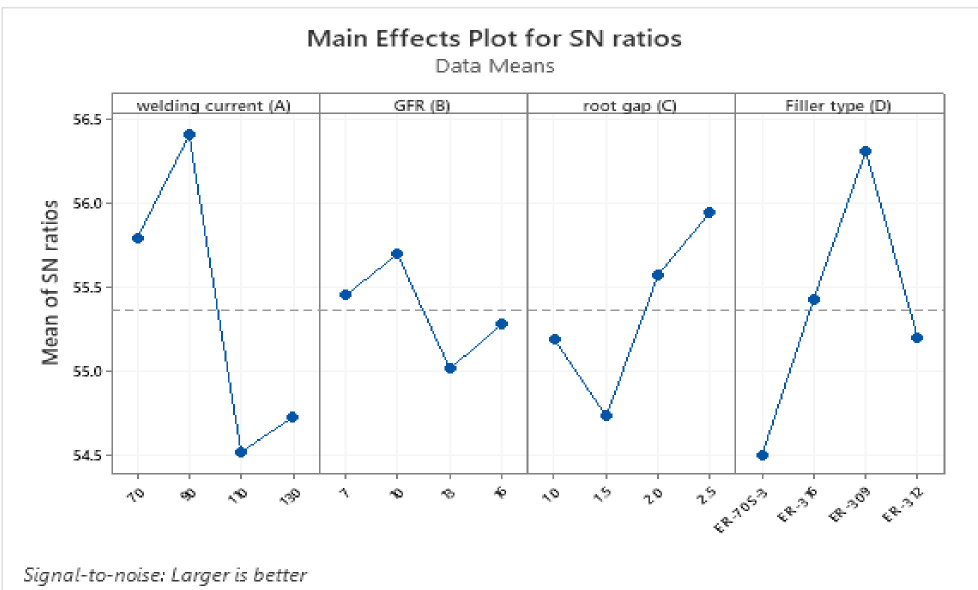

Figure 4.31 main effects graph for a signal to ratio of flexural

4.6.3.4. ANOVA flexural strength

The determined value of the F-ratio of the produced model is greater than the standard F-ratio (F-table value 3.49) value at the desired level of confidence of 95%, the model is inadequate within the confidence limit, according to this technique. The coefficient of determination, or R2, is greater than 0.99.

Table 4.37: Analysis of Variance for SN ratios of flexural

Source	DF	Seq SS	% Cont.	Adj SS	Adj MS	F	P
Welding current (A)	3	9.5245	46.57	9.52446	3.17482	190.89	0.001
GFR (B)	3	0.9838	4.8	0.98376	0.32792	19.72	0.018
root gap (C)	3	3.2319	15.80	3.23193	1.07731	64.77	0.003
Filler type (D)	3	6.6638	32.58	6.66380	2.22127	133.55	0.001
Residual Error	3	0.0499	0.25	0.04990	0.01663		
Total	**15**	**20.4538**	**100**				

S= 0.1290 **R-Sq** = 99.76% **R-Sq (adj)** = 98.78%

According to the experimental results, all parameters have a significant effect on flexural strength because F-critical=3.49 is less than the F-ratio of parameters. When seeing the contribution of each parameter, the welding current (46.57 percent), filler metal type (32.58 percent), and root gap (15.8%) have a highly significant impact, while the gas flow rate (4.80 percent) has a significant impact on the flexural strength of TIG-welded 316 stainless steel and AISI 1020 mild steel sheets.

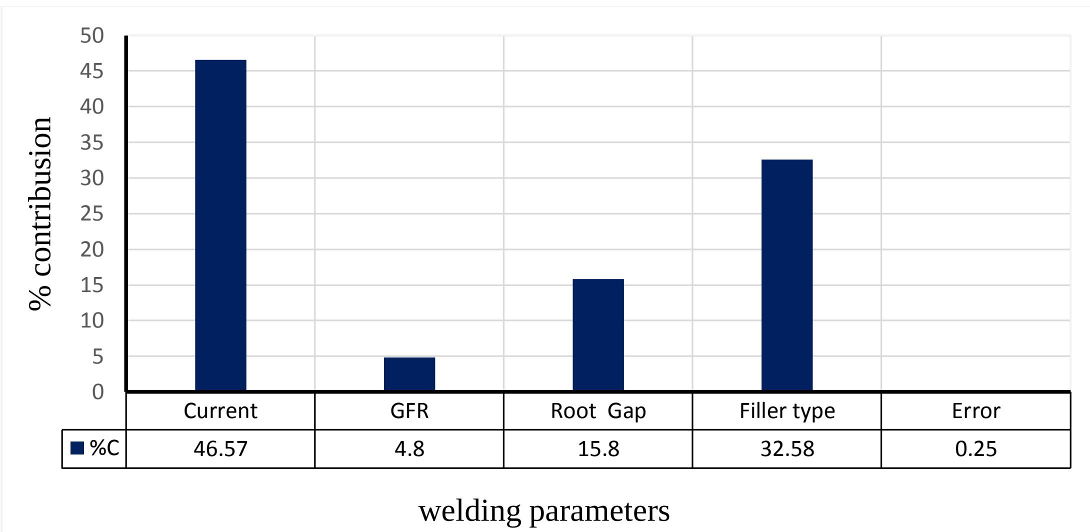

Figure 4.32 percentage contribution graph

4.6.4. Bead width result analysis

Three readings were taken in each welded specimen, and the average value was calculated. Table 4.38 presents the measured experimental results of mean bead width geometry values for each trial experiment. According to the experimental results, specimen number 8 has the smallest width value, making it the best of the specimens.

Table 4.38: Mean test result of bead width of dissimilar metals

Sample No	*Welding Current (A)*	*Gas Flow Rate (B)*	*Root Gap (C)*	*Filler Type (D)*	*Bead width (mm)*	*Signal to noise ratio*
1	70	7	1.0	ER703	7.50	-17.5012
2	70	10	1.5	ER316	7.05	-16.9638
3	70	13	2.0	ER309	6.90	-16.7770
4	70	16	2.5	ER312	6.90	-16.7770
5	90	7	1.5	ER309	7.00	-16.9020
6	90	10	1.0	ER312	7.80	-17.8419
7	90	13	2.5	ER703	6.80	-16.6502
8	90	16	2.0	ER316	6.21	-15.8618
9	110	7	2.0	ER312	7.70	-17.7298
10	110	10	2.5	ER309	7.50	-17.5012
11	110	13	1.0	ER316	8.00	-18.0618
12	110	16	1.5	ER703	7.10	-17.0252
13	130	7	2.5	ER316	7.45	-17.4431
14	130	10	2.0	ER703	7.80	-17.8419
15	130	13	1.5	ER312	7.90	-17.9525
16	130	16	1.0	ER309	8.00	-18.0618

4.6.4.1. Mean response analysis of Bead width

The greatest value in Table 4.38 is current (A) at level 2, followed by root gap (C) at level 3, filler type (D) at level 2, and gas flow rate (B) at level 4. These welding settings (A2B4C3D2) were chosen as the initial parametric setup from the result for dissimilar TIG welding of stainless steel 316 and AISI 1020 steel with a thickness of 3mm. This implies that using this as a parameter combination to create smaller but better results is viable. The main influence plot for control parameters for mean bead width value variations is shown in Figure 4.38. In the main effect plot graph of the parameters below, the numerical number at the minimum point in each graph represents the parameter's best value at that level. They also display the optimum settings within the experiment's parameters. When compared to other welding variables, the welding current weight percent, followed by the root gap, has the biggest impact on enhancing bead width.

Table 4.39: Response Table for Means of bead width

Level	Welding current (A)	GFR (B)	root gap (C)	Filler type(D)
1	7.088	7.412	7.825	7.300
2	**6.953**	7.538	7.262	**7.177**
3	7.575	7.400	**7.152**	7.350
4	7.787	**7.053**	7.162	7.575
Delta	0.835	0.485	0.673	0.397
Rank	**1**	**3**	**2**	**4**

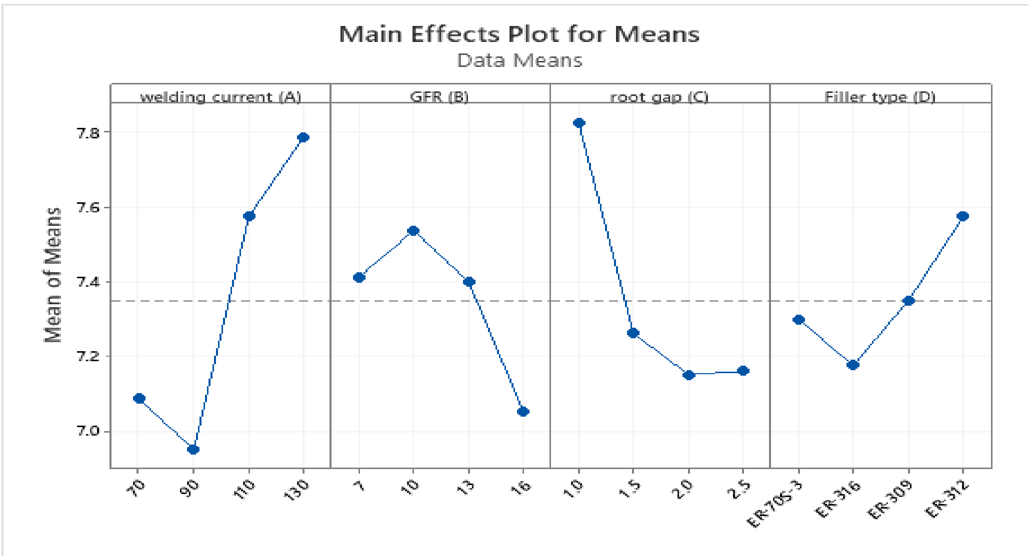

Figure 4.33: main effects graph for means of bead width

4.6.4.2. Signal to noise ratio analysis for Bead width

According to the signal to noise ratio value shown in table 4.39, the welding current weight percentage has the most impact (Delta = 1.01, Rank =,1^{st}) followed by root gap (Delta =0.81, Rank =,2^{nd}), and gas flow rate (Delta =0.61, Rank =,3^{rd}). The filler type has the smallest impact on the (S/N) ratio (Delta = 0.49, Rank =, 4^{th})

Table 4.40: Response Table for Signal to Noise Ratios (Smaller is better)

Level	Welding current (A)	GFR (B)	root gap (C)	Filler type (D)
1	-17.00	-17.39	-17.87	-17.25
2	**-16.81**	-17.54	-17.21	**-17.08**
3	-17.58	-17.36	**-17.05**	-17.31
4	-17.82	**-16.93**	-17.09	-17.58
Delta	1.01	0.61	0.81	0.49
Rank	**1**	**3**	**2**	**4**

4.6.4.3. Effect of process parameters on bead width size

Figure 4.37 demonstrates how welding factors influence bead width, as well as the optimal values for each factor depending on their rank. The optimal values for minimizing bead width are current at level 2 (90A), the gas flow rate at level 4 (16 L/min), root gap at level three (2mm), and filler metal at level two (SS 316), according to the analysis and primary effect plot graph for a signal to noise ratios, with an initial parametric setting of **A2B4C3D2**. The bead diameter of the weld reduces as the current climbs from level one to level two, as shown in the graph above. The bead width (weld width) increases dramatically as the current is increased from level two to level four, reaching its maximum value (Patil & Waghmare, 2013) showing similar identification. As the gas flow rate rises from level one to level two, the width of the weld widens, which is undesirable. The bead of the weld narrows substantially as the gas flow rate climbs from level two to level four, and the gas flow rate at level four was the optimal flow for minimal bead width. The root gap was the second important process parameter; when the root gap increased from level one to three, the bead width fell from a larger to a smaller number. The bead width grows gradually as gaps arise from level three to level four. As a result, at third level, the ideal bead width was picked. The list of relevant welding properties was the filler metal type; level two filler metal had a narrower bead width value than other filler metals. Level four filler metal has the widen bead width value, followed by levels three and one filler metal.

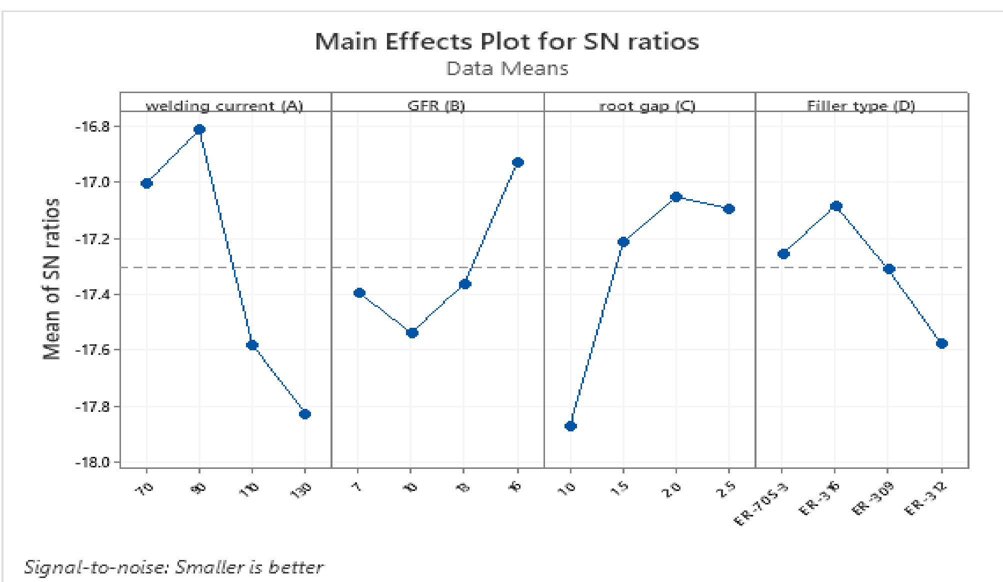

Figure 4.34 main effects graph for a signal to noise ratio of bead width

4.6.4.4. ANOVA for bead width

Here the determined F-ratio of the produced model is higher than the standard F-ratio (F-table value 3.49) value at the required degree of confidence of 95 percent, so the model is deemed to be inadequate within the confidence limit, according to this technique. The coefficient of determination, or R2, is determined to be greater than 0.98 as shown in table 4.41.

Table 4.41: Analysis of Variance for SN ratios

Source	**DF**	**Seq SS**	**% Cont.**	**Adj SS**	**Adj MS**	**F**	**P**
Welding current (A)	3	2.70740	46.35	2.70740	0.90247	31.29	0.009
GFR (B)	3	0.81780	14.00	0.81780	0.27260	9.45	0.049
root gap (C)	3	1.73212	29.64	1.73212	0.57737	20.02	0.017
Filler type (D)	3	0.50032	8.56	0.50032	0.16677	5.78	0.092
Residual Error	3	0.08652	1.45	0.08652	0.02884		
Total	**15**	**5.84416**	**100**				

S= 0.1698 **R-Sq** = 98.52% **R-Sq (adj)** = 92.60%

F-value =3.49, But F-ratio from the ANOVA table is much higher than the critical F-value, so the parameters used under this investigation have a highly significant on weld bead.

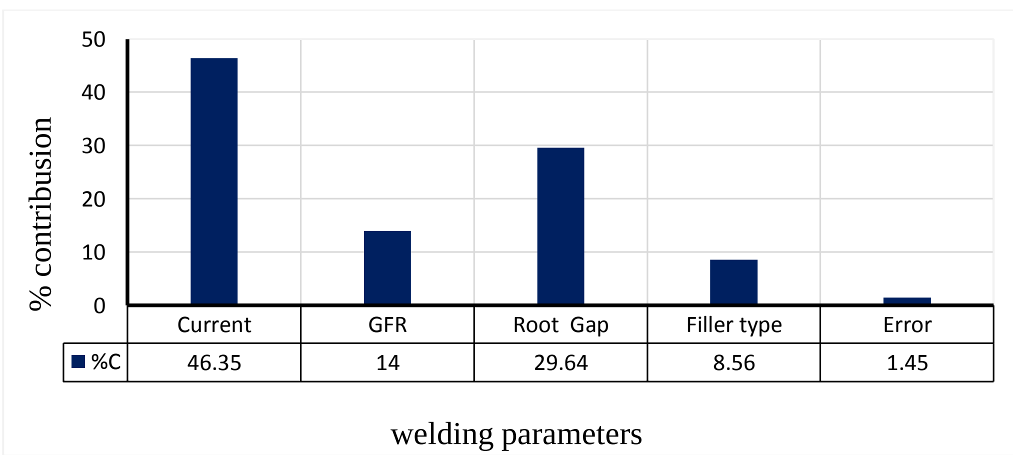

Figure 4.35 Parameters percentage contribution graph

The above plot in figure 4.38 shows that the welding current (46.35 percent), root gap (29.64percent), gas flow rate (14 percent), and filler metal type (8.56 percent) have a highly significant impact, while the type of filler metals (4.80 percent) has a significant impact on the bead width of dissimilar TIG-welded 316 stainless steel and AISI 1020 mild steel.

4.7. Multi-response parametric optimization of dissimilar metals

Multi-response optimization is more profitable than single-response optimization in today's industry. The purpose of this study is to explore the effect of TIG welding parameters on various responses using a multi-objective technique known as desirability function analysis.

4.7.1. Desirability function analysis (DFA)

Taguchi methodology was used to determine the best process parameters for single performance characteristics only, while desirability function analysis was used to determine the best process parameters for multiple performance characteristics at the same time, as was done in this study on similar welding. The predicted parametric set was generated using the Taguchi technique, and these values were employed in each result and analysis of tensile strength, hardness, flexural strength, and bead width as shown in table 4.42. The above-mentioned calculation of similar welding approach for composite desirability was also applied to dissimilar types.

Table 4.42: response table for all output parameters

Sample No	*Welding Current (A)*	*Gas Flow Rate (B)*	*Root Gap (C)*	*Filler Type (D)*	*Tensile strength (MPa)*	*Hardness (HRB)*	*Flexural strength (MPa)*	*Bead width (mm)*
1	70	7	1.0	ER70S-3	390	64	555	7.50
2	70	10	1.5	ER316	420	72	605	7.05
3	70	13	2.0	ER309	460	75	670	6.90
4	70	16	2.5	ER312	442	76	640	6.90
5	90	7	1.5	ER309	450	78	692	7.00
6	90	10	1.0	ER312	410	75	655	7.80
7	90	13	2.5	ER70S-3	478	75	620	6.80
8	90	16	2.0	ER316	445	83	679	6.21
9	110	7	2.0	ER312	410	86	545	7.70
10	110	10	2.5	ER309	502	84	662	7.50
11	110	13	1.0	ER316	483	81	505	8.00
12	110	16	1.5	ER70S-3	486	86	440	7.10
13	130	7	2.5	ER316	398	83	588	7.45
14	130	10	2.0	ER70S-3	395	88	525	7.80
15	130	13	1.5	ER312	412	90	480	7.90
16	130	16	1.0	ER309	435	87	595	8.00

The individual desirability index (di) value is calculated for each response. Di value is determined by the type of the relevant output. Using equation (4.3) for Maximization and equation (4.4) for minimization.

Table 4.43: composite desirability index and rank

sample no	UTS	HARD	FLEX.	BW	Individual desirability index (Di)					
	MPa	HRB	MPa	mm	UTS	Hardness	Flexural	Bead width	CDI (dg)	Rank
1	390	64	555	7.5	0.0000	0.0000	0.6755	0.5285	0.0000	13
2	420	72	605	7.05	0.5175	0.5547	0.8092	0.7285	0.4114	7
3	460	75	670	6.9	0.7906	0.6504	0.9554	0.7839	0.6206	5
4	442	76	640	6.9	0.6814	0.6794	0.8909	0.7839	0.5686	6
5	450	78	692	7	0.7319	0.7338	1.0000	0.7474	0.6336	3
6	410	75	655	7.8	0.4226	0.6504	0.9237	0.3343	0.2913	10
7	478	75	620	6.8	0.8864	0.6504	0.8452	0.8188	0.6316	4
8	445	83	679	6.21	0.7008	0.8549	0.9739	1.0000	0.7638	1
9	410	86	545	7.7	0.4226	0.9199	0.6455	0.4094	0.3205	8
10	502	84	662	7.5	1.0000	0.8771	0.9386	0.5285	0.6596	2
11	483	81	505	8	0.9112	0.8086	0.5079	0.0000	0.0000	13
12	486	86	440	7.1	0.9258	0.9199	0.0000	0.7091	0.0000	13
13	398	83	588	7.45	0.2673	0.8549	0.7664	0.5543	0.3115	9
14	395	88	525	7.8	0.2113	0.9608	0.5808	0.3343	0.1985	12
15	412	90	480	7.9	0.4432	1.0000	0.3984	0.2364	0.2043	11
16	435	87	595	8	0.6339	0.9405	0.7843	0.0000	0.0000	13

4.7.2. Initial parametric setting condition

The initial parametric setting for composite desirability was current at (90A), flow rate at (16L/min), root gap at (2.5mm) and filler type (ER-316L) as shown in table 4.44.

Table 4.44: initial predicted parametric setting

Initial setting	UTS (MPa)	HARDNESS (HRB)	FS (MPa)	BW (mm)	CDI (dg)
A2 B4 C3 D2	445	83	679	6.21	0.7638

4.7.3. Mean response analysis for composite desirability (dg)

Root gap (C) at level 4, welding current (A) at level 2, filler metal (D) at level 3, and gas flow rate (B) at level 2 had the highest values, as shown in Table 4.43. These welding parameters (**A2B2C4D3**) were chosen as the optimal parametric setting for CDI of TIG welding of dissimilar metals of stainless steel 316 and AISI 1020 mild steel. The feasibility of using this as a parameter combination to generate larger, better outcomes was demonstrated using the desirability function-based optimization. Figure 4.39 shows the main influence plot for control parameters for the means of composite desirability index (dg).

Table 4.45: Response Table for Means of CDI (dg)

Level	Welding current (A)	GFR (B)	root gap (C)	Filler type (D)
1	0.40013	0.31641	0.07283	0.20754
2	**0.58009**	**0.39020**	0.31232	0.37168
3	0.24503	0.36413	0.47585	**0.47844**
4	0.17859	0.33310	**0.54284**	0.34617
Delta	0.40150	0.07380	0.47001	0.27090
Rank	**2**	**4**	**1**	**3**

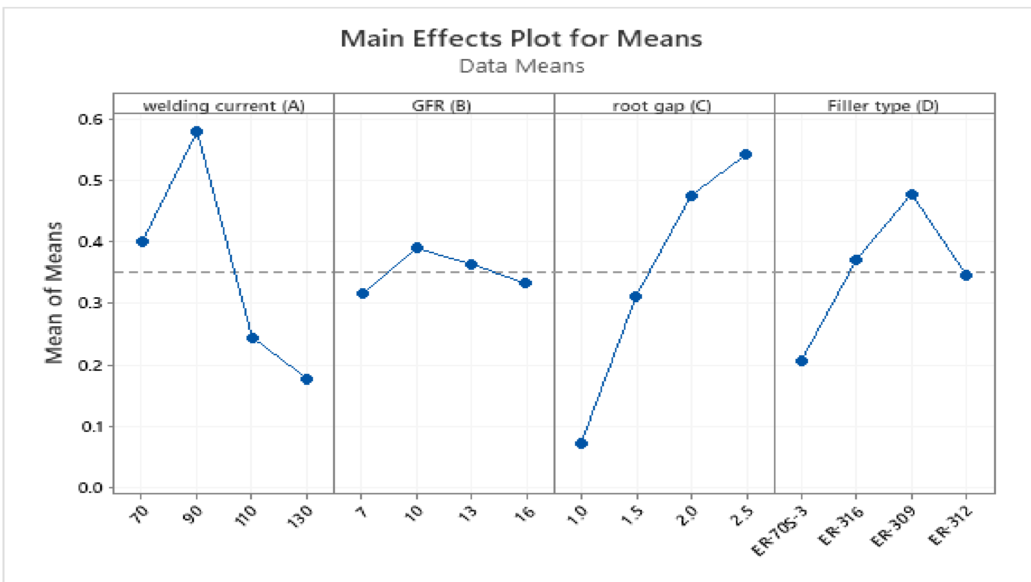

Figure 4.36 Main effects plot for CDI (dg)

The parameter's best value at that level is indicated by the number at the maximum point in each graph in the main effect plot graph above. They also show which settings are best within the experiment's parameters. The root gap and welding current weight percent have the greatest impact on all response parameters when compared to other welding variables. The best predicted optimal parameter combinations for the composite desirability index (dg) were welding current (90A) at level two, gas flow rate (16 L/min) at level four, root gap (2mm) at level three, and filler type (ER-316) at level two (**A2B4C3D2**).

4.7.4. ANOVA for composite desirability.

Using analysis of variance(ANOVA), the most important characteristics that determine the composite desirability index of TIG-welded dissimilar steels are found. According to the ANOVA table 4.46 of CDI, the root gap, and welding current have the greatest contribution, followed by filler wire type. Also figure 4.40 below show that the root gap (48 percent), welding current (35 percent), and filler metal type (14 percent) have a highly significant impact, while the gas flow rate (14 percent) has a less significant impact on the CDI (dg) of dissimilar TIG-welded 316 stainless steel and AISI 1020 mild steel.

Table 4.46: Analysis of Variance for Means

Source	DF	Seq SS	%Cont.	Adj SS	Adj MS	F	P
welding current (A)	3	0.38341	35	0.38341	0.127803	18.19	0.020
GFR (B)	3	0.01291	1.20	0.01291	0.004302	0.61	0.652
root gap (C)	3	0.52506	48	0.52506	0.175020	24.91	0.013
Filler type (D)	3	0.14909	14	0.14909	0.049697	7.07	0.071
Residual Error	3	0.02107	1.80	0.02107	0.007025		
Total	**15**	**1.09154**	**100**				

S= 0.0838 **R-Sq** = 98.07% **R-Sq (adj)** = 90.35%

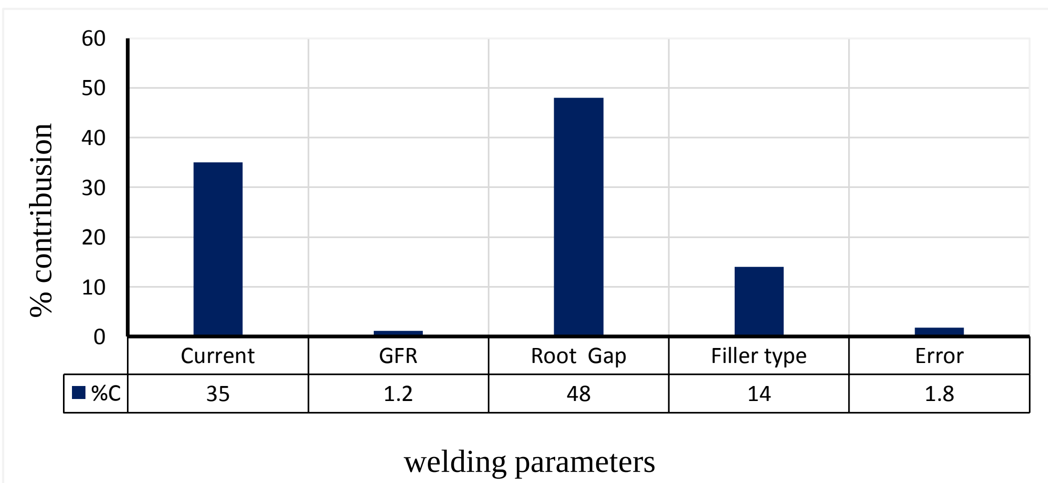

Figure 4.37 parameters percentage contribution graph

4.7.5. Optimal condition

The optimal condition for composite was current (90A), flow rate (10L/min), root gap (2.5mm) and filler metal (ER-309L) as shown in table 4.47. And improvement between initial and optimal condition was shown in table 4.48.

Table 4.47:The optimum parametric setting

Optimum setting	UTS(MPa)	HARDNESS (HRB)	FS(MPa)	BW (mm)	CDI (dg)
A2 B2 C4 D3	493.2	86	691	5.8	0.9387

Table 4.48: Improvement in UTS, FS, HARDNESS, and BW

Initial setting				Optimum setting				**% Improvement**			
A2 B4 C3 D2				**A2 B2 C4 D3**							
UTS	HRD	FS	BW	UTS	HRD	FS	BW	UTS	HRD	FS	BW
445	83	679	6.21	493.2	86	691	5.8	**10.83%**	**3.61%**	**1.77%**	**6.60%**
Composite desirability											
0.7638				0.9387				**22.90%**			

4.8. Confirmation test

The confirmation test is required after the experimental optimization to validate whether the optimized parametric configuration is accepted or not. As a result, the confirmation experimental test was carried out at the Ethiopian Technical Institute's center of excellence for engineering (CEE) at the welding training center. So, from the conformity test, it was gained that the experimental parametric setting results were agreed with the predicted optimum parametric setting result with a minimum accepted validation error of less than 1% for similar welded metals and 3.42% percent for dissimilar welded metals, according to the results of the confirmation test.

Table 4.49: confirmation test with Validation error

Type of samples	**Optimum setting**	**UTS (MPa)**	**HARDNESS (HRB)**	**FS (MPa)**	**BW (mm)**	**CDI (dg)**	Error
Similar	A2 B2 C3 D3	602	96.4	780	6.10	0.7556	**0.622%**
	Exp. setting A2 B2 C3 D3	609.50	98	781	5.93	0.7603	
Dissimilar	A2 B2 C4 D3	493.2	86	691	5.80	0.9387	**3.42%**
	Exp. setting A2 B2 C4 D3	498	88	691.45	5.25	0.9708	

CHAPTER - 5

CONCLUSION AND RECOMMENDATION

5.1. Conclusion

This research investigated and optimized the parameters of tungsten inert gas welding on similar steels (SS316) and dissimilar (SS316 with AISI 1020) steels. The experimental results were analyzed using a Taguchi L16 orthogonal array and the signal-to-noise ratio method, and ANOVA was used to determine the influential effect of each parameter. To minimize their effect on mechanical and microstructural qualities and bead geometry, DFA was utilized to perform multi-response optimization of input parameters such as welding current, gas flow rate, root gap, and filler type. As a result of the experimental findings, the following conclusions were drawn: For similar and dissimilar metals, non-destructive testing was performed using PT for welding faults, and problems such as porosity, lack of fusion, and lack of penetration were identified on a few samples. The weld zone of sample numbers 8 and 10 for similar and dissimilar welding methods exhibits a very fine skeletal ferrite along with grain, sub-grain, and migrating boundaries in the plain austenitic matrix due to moderate heat input and moderate cooling rate. Due to very low welding heat inputs, i.e., high cooling rates, sample number 1 for dissimilar weld metals includes δ -ferrite in the form of dendritic lathy-ferrite. The delta ferrite (δ) in the TIG weld zone of sample number 15 is coarser. The heat input was increased to 130A on this sample.

- At the combinations of welding conditions A2B4C3D2 (90A welding current, 16L/min gas flow rate, 2mm root gap, and ER-316L filler metal), a higher tensile strength of 595 MPa was produced in a similar weld. The most significant parameter affecting tensile strength was welding current, followed by gas flow rate, according to ANOVA.
- With a combination of 130A welding current, 7L/min gas flow rate, 2.5mm root gap, and ER-316 filler metals, a maximum hardness of 97 HRB or 227HV was reached. Welding current was the most significant factor for hardness, followed by filler type, according to an analysis of variance (ANOVA).
- A combination of factors, including 90A welding current, 16L/min, 2mm root gap, and ER-316L filler metal, yielded a maximum flexural strength of 776MPa. The most

influential parameter of flexural strength was gas flow rate, followed by welding current, according to an analysis of variance (ANOVA).

- Minimum bead width of 6.30mm was achieved at a parametric combination of 70A welding current, 13L/min gas flow rate, 2mm root gap, and ER-309 filler metal. Analysis of variance (ANOVA) shows welding current was the most significant parameter for bead width followed by root gap.

From the optimization result, it was shown that all responses were improved from initial setting value to optimum parametric setting value i.e., UTS was improved from 595MPa to 602MPa (1.18%), hardness was improved from 95HRB to 96.4HRB (1.47%), flexural strength was improved to 776 to 780(0.52%) and bead width was improved from 6.8mm to 6.1mm (10.29%) and overall composite desirability was improved from 0.6970 to 0.7556 (8.41%) at an optimum parametric setting of (A2B2C3D3). This parameter combination results were agreed with the confirmation test results.

- In dissimilar weld, a higher tensile strength of 502 was achieved at the parametric combination of 110A welding current, 10L/min gas flow rate, 2.5mm root gap, and ER-309L filler wire. Analysis of variance (ANOVA) shows welding current was the most significant parameter for tensile strength followed by gas flow rate.
- With a parametric setup of 130A welding current, 10L/min gas flow rate, 1.5mm root gap, and ER-312 filler wire, a maximum hardness of 90HRB or 183HV was reached. Welding current was the most important characteristic for hardness, followed by root gap, according to an analysis of variance (ANOVA).
- At a parametric setup of 90 welding currents, 7L/min gas flow rate, 1.5mm root gap, and ER-309L filler metals, the maximum flexural strength of 692 was attained. Welding current was the most significant characteristic for flexural strength, followed by filler type, according to an analysis of variance (ANOVA).
- A parametric combination of 90A welding current, 16L/min gas flow rate, 2mm root gap, and ER-316L filler metals were used to obtain a minimum weld width of 6.21mm. The most important characteristic for weld width was welding current, followed by root gap, according to an analysis of variance (ANOVA).

According to the optimization results, all responses improved from the initial setting value to the optimum parametric setting value, which enhanced UTS from 445MPa to 493.2MPa (10.83%), hardness was improved from 83 HRB to 86 HRB (3.61%), flexural strength was improved to 679 MPa to 691 MPa (1.77%) and bead width was improved from 6.21 mm to 5.8 mm (6.60%) and overall composite desirability was improved from 0.7638 to 0.9387 (22.90%) at an optimum parametric setting of (A2B2C4D3). This parameter combination results were agreed with the confirmation test result.

5.2. Recommendation

The following recommendations are made based on the study's findings and conclusions.

- TIG welding of 316 and AISI 1020 was employed in this study, and it can be extended to other materials types to investigate the effect of welding parameters on the mechanical and microstructural properties of TIG welding processes in various welding environments.
- During similar welding of SS316 steel materials, welding workshops and other industrial sectors can employ the optimal welding process parameters of welding current 90A, gas flow rate 10L/min, root gap 2mm, and filler type ER-309L. In addition, during dissimilar welding of SS316 with AISI1020 steel materials having a thickness of 3mm, welding current of 90A, the gas flow rate of 10L/min, root gap of 2.5mm, and ER-309L filler metals were used.

5.3. Scope for future work

The following will be investigated further as part of future research.:

- Only four welding parameters were studied in this study: welding current, gas flow rate, root gap, and filler type. Future research could investigate the effects and analyses of welding voltage, welding speed, base metal thickness, and base and electrode distance and interaction effect of them during TIG welding of similar and dissimilar metals.
- The focus of these experiments was on the effects of welding parameters on mechanical and microstructural properties of similar and dissimilar metals, but this can be further investigated using other TIG welding processes such as activating flux tungsten inert gas welding (ATIG) pulsed current for further TIG welding process parameter optimization.

Research fund Acknowledgment

This research project is funded by Adama Science and Technology University under the grant number ASTU/SM-R586/22, Adama, Ethiopia.

REFERENCES

Akbari Mousavi, S. A. A., & Miresmaeili, R. (2008). Experimental and numerical analyses of residual stress distributions in TIG welding process for 304L stainless steel. *Journal of Materials Processing Technology*, *208*(1–3), 383–394. https://doi.org/10.1016/j.jmatprotec.2008.01.015

Anand Rao, V., & Deivanathan, R. (2014). Experimental investigation for welding aspects of stainless steel 310 for the process of TIG welding. *Procedia Engineering*, *97*, 902–908. https://doi.org/10.1016/j.proeng.2014.12.365

Anbarasu, P., Yokeswaran, R., Godwin Antony, A., & Sivachandran, S. (2020). Investigation of filler material influence on hardness of TIG welded joints. *Materials Today: Proceedings*, *21*(xxxx), 964–967. https://doi.org/10.1016/j.matpr.2019.09.061

Aravinth, P., Kumar, M. T., Dakshinamoorthy, A., & Kumar, A. N. (2012). A criticality study by design failure mode and Effect analysis (FMEA) procedure in LINCOLN V350 PRO welding machine. *International Journal of Advances in Engineering & Technology*, *4*(1), 611.

Arora, H., Singh, R., & Brar, G. S. (2020). On mechanical and morphological investigations of tungsten inert gas welded SS 304 thin pipe joints. *Measurement and Control*, *53*(1–2), 61–72.

ASM Handbook Committee. (2000). mechanical testing and evaluation. *ASM Handbook*, *8*, 143–151.

Avery, R. E. (1991). *Pay attention to dissimilar-metal welds: guidelines for welding dissimilar metals*. Nickel Development Institute.

AWS committee. (2000). *Welding Inspection Handbook (3rd Edition).*

Ayoola, W. A., Suder, W. J., & Williams, S. W. (2019). Effect of beam shape and spatial energy distribution on weld bead geometry in conduction welding. *Optics and Laser Technology*, *117*(April), 280–287. https://doi.org/10.1016/j.optlastec.2019.04.025

Balaji, C., Kumar, S. V. A., Kumar, S. A., Sathish, R., & Nadu, T. (2012). Evaluation of Mechanical Properties of Ss 316 L Weldments Using Tungsten Inert Gas Welding. *International Journal of Engineering Science and Technology*, *4*(5), 2053–2057.

Balram, Y., Vishu Vardhan, T., Sridhar Babu, B., Venkat Ramana, G., & Preethi, C. (2019).

Thermal stress analysis of AISI 316 stainless steels weldments in TIG and pulse TIG welding processes. *Materials Today: Proceedings*, *19*(xxxx), 182–187. https://doi.org/10.1016/j.matpr.2019.06.695

Bharath, P., & Sridhar, V. G. (2014). Optimization of 316 stainless steel weld joint characteristics using Taguchi technique. *Procedia Engineering*, *97*, 881–891.

Chaudhari, R., Loharkar, P. K., & Ingle, A. (2020). Applications and challenges of arc welding methods in dissimilar metal joining. *IOP Conference Series: Materials Science and Engineering*, *810*(1). https://doi.org/10.1088/1757-899X/810/1/012006

Choudhary, A., Kumar, M., & Unune, D. R. (2019). Experimental investigation and optimization of weld bead characteristics during submerged arc welding of AISI 1023 steel. *Defence Technology*, *15*(1), 72–82. https://doi.org/10.1016/j.dt.2018.08.004

Dak, G., & Pandey, C. (2021). Experimental investigation of the effect of welding current, voltage and gas flow rate on welding characteristics of tig welded s31603 material. *International Journal of Pressure Vessels and Piping*, *194*, 104536. https://doi.org/10.1016/J.IJPVP.2021.104536

Davis, J. R. (2004b). *Tensile testing*. ASM international.

Derringer, G., & Suich, R. (1980). Simultaneous optimization of several response variables. *Journal of Quality Technology*, *12*(4), 214–219.

Devakumar, D., & Jabaraj, D. B. (2014). Research on gas tungsten arc welding of stainless steel–an overview. *International Journal of Scientific & Engineering Research*, *5*(1), 1612–1618.

Devakumar, D., Jabaraj, D. B., Bupesh Raja, V. K., & Jayaprakash, J. (2016). Experimental Investigation of DSS/HRS GTAW Weldments. *Indian Journal of Science and Technology*, *9*(43), 1–6. https://doi.org/10.17485/ijst/2016/v9i43/101986

Dr. Dmitri, K. (2021). *Flexural strength tests of ceramics [SubsTech]*. https://www.substech.com/dokuwiki/doku.php?id=flexural_strength_tests_of_ceramics

eFunda. (2012). *Definition of Low-Carbon Steels*. http://www.efunda.com/materials/alloys/carbon steels/low_carbon.cfm

Esme, U., Bayramoglu, M., Kazancoglu, Y., & Ozgun, S. (2009). *Optimization of weld bead geometry in TIG welding process using grey relation analysis and Taguchi method Optimization Of Weld Bead Geometry In Tig Welding Process Using Grey Relation Analysis And*

Taguchi Method Optimizacija Geometrije Tig-Varkov Z Greyje. *March 2017*.

Flagg, M., & Krebs, D. (2004). Welding Wisdom. *Modern Steel Construction*, *44*(8), 43–45.

Ganesh, C. S., Vigraman, T., Sujith, D., Velmanikandan, M., & Vetrivel, T. (n.d.). *Microstructural And Transient Thermal Analysis Of Tig Welded Joint Sae 2205 With Aisi 304 With Aisi 308 Filler Metal*.

Ghadi, G., & S., D. S. (2016). Analysis of TIG Welding Process Parameters for Stainless Steel (SS202). *International Journal of Advanced Engineering Research and Science*, *3*(10), 66–70. https://doi.org/10.22161/ijaers/3.10.13

Gohel, V., Makwana, J., & Ranjan, R. (2016). Thermo-Mechanical analysis in TIG welding of SS 304. *International Journal of Engineering Development and Research*, *4*(2), 1704–1710.

Greyjevo, O., & Metodo, A. I. T. (2009). Optimization of weld bead geometry in TIG welding process using grey relation analysis and Taguchi method. *Materiali in Tehnologije*, *43*(3), 143–149.

Gupta, S. (2016). Optimization Condition for Performing GMAW Welding on Ultra 904L Specimens. *International Journal of Scientific and Technical Advancements ISSN*, 1532–2454.

Halil İbrahim, K. (2013). Study on Microstructure, Tensile Test and Hardness 316 Stainless Steel Jointed by TIG Welding. *International Journal of Advances in Engineering, Science and Technology (IJAEST) Vol*, *3*.

Hannerz, N. (2002). Svetsningens materialteknologi. *Industirell Produktion-Kungliga Tekniska Hogskolan*.

Harrington, Edwin, C. (1965). The desirability function. *Industrial Quality Control*, *21*(10), 494–498.

Hazari, H. R., Balubai, M., Suresh Kumar, D., & Haq, A. U. (2019). Experimental investigation of TIG welding on AA 6082 and AA 8011. *Materials Today: Proceedings*, *19*, 818–822. https://doi.org/10.1016/j.matpr.2019.08.137

Hedhibi, A. C., Touileb, K., Djoudjou, R., Ouis, A., Alrobei, H., & Ahmed, M. M. Z. (2021). Mechanical properties and microstructure of TIG and ATIG welded 316L austenitic stainless steel with multi-components flux optimization using mixing design method and particle swarm optimization (PSO). *Materials*, *14*(23). https://doi.org/10.3390/ma14237139

Inweld.com. (n.d.). *Data Sheet for 1.4301 Stainless Steel*. https://www.inweldcorporation.com/ downloads/312-16 Data Sheet.pdf

Inweld.com. (n.d.). *data sheet for 309L*. 94621. https://www.inweldcorporation. com/ downloads/309L-15 Data Sheet.pdf

Inweld.com. (n.d.). *Data sheet for 316L stainless steel*. 94621. https://inweldcorporation. com/ downloads/316L Data Sheet.pdf

Jebaraj, A. V., & Ajaykumar, L. (2013). Influence of microstructural changes on impact toughness of weldment and base metal of duplex stainless steel AISI 2205 for low temperature applications. *Procedia Engineering*, *64*, 456–466.

Jeevahan, J., Joseph, G. B., Mageshwaran, G., & Manikandan, N. (2016). Experimental investigation of the effect of welding current, voltage and gas flow rate on welding characteristics of TIG welded S31603 material. *Journal of Chemical and Pharmaceutical Sciences*, *9*(2), 734–737.

Jeng, S. L., Lee, H. T., Weirich, T. E., & Rebach, W. P. (2007). Microstructual study of the dissimilar joints of alloy 690 and SUS 304L stainless steel. *Materials Transactions*, *48*(3), 481–489. https://doi.org/10.2320/matertrans.48.481

Jeyaprakash, N., Haile, A., & Arunprasath, M. (2015). The Parameters and Equipments Used in TIG Welding: A Review. *The International Journal Of Engineering And Science*, 2319–1813. www.theijes.com

Johnson, L. (2022). *How to Calculate Flexural Strength | Sciencing*. https://sciencing.com/ calculate-flexural-strength-5179141.html

Kah, P., & Jukka Martikainen, M. S. (2013). Trends in joining dissimilar metals by welding. *Applied Mechanics and Materials*, *440*, 269–276. https://doi.org/10.4028/www.scientific .net/AMM.440.269

Kailas A. Gite & Ramkisan S. Pawar. (2016). *Effect of Welding Geometry Parameter on Hardness for Aisi304 Tig*. *4*, 735–744.

Karna, S. K., & Sahai, R. (2012). An overview on Taguchi method. *International Journal of Engineering and Mathematical Sciences*, *1*(1), 1–7.

Karunakaran, N., & Balasubramanian, V. (2011). Effect of pulsed current on temperature distribution, weld bead profiles and characteristics of gas tungsten arc welded aluminum alloy joints. *Transactions of Nonferrous Metals Society of China (English Edition)*, *21*(2), 278–286. https://doi.org/10.1016/S1003-6326(11)60710-3

Kausar, A. (2019). Study of Weld Quality characteristics of Tungsten Inert Gas Welding of Dissimilar Metals SS 316L and IS 2062 Plates. *International Journal for Research in Applied Science and Engineering Technology*, *7*(6), 759–767. https://doi.org/10.22214/ijraset.2019.6131

Kazi, J., Zaid, S., Talha, S. M., Yasir, M., & Akib, D. (2015). A review on various welding techniques. *International Journal of Modern Research*, *5*(2), 22–28.

Kou, S. (2002). *Weld metall*.

Krishna, D. V., Mahesh, E., Kiran, G., Suchethan, G. S., & Mouli, G. C. (2016). Numerical Analysis on the effect of welding parameters in TIG welding for INCONEL 625 alloy. *International Journal of Engineering and Techniques*, *2*(5).

Krishnaiah, K., & Shahabudeen, P. (2012). *Applied design of experiments and Taguchi methods*. PHI Learning Pvt. Ltd.

Kumar, A., Sharma, V., & Baruaole, N. S. (2017). Experimental Investigation of TIG welding of Stainless Steel 202 and Stainless Steel 410 using Taguchi Technique. *Mody University International Journal of Computing and Engineering Research*, *1*(2), 96–99. https://ijcer.in/ojs/index.php/IJCER/article/view/18

Kumar, L. S., Verma, S. M., Prasad, P. R., Kumar, P. K., & Shanker, T. S. (2011). Experimental investigation for welding aspects of AISI 304 & 316 by Taguchi technique for the process of TIG & MIG welding. *International Journal of Engineering Trends and Technology*, *2*(2), 28–33.

Kumar, R., Ramesh Mevada, N., Rathore, S., Agarwal, N., Rajput, V., & Barad, A. S. (2017). Experimental Investigation and Optimization of TIG Welding Parameters on Aluminum 6061 Alloy Using Firefly Algorithm. *IOP Conference Series: Materials Science and Engineering*, *225*, 012153. https://doi.org/10.1088/1757-899x/225/1/012153

Kumar, S. S., Maheswaran, C. B., & Kannan, T. D. B. (2021). Experimental investigation on a pulsed TIG welding of Inconel 625. *Materials Today: Proceedings*, *45*(xxxx), 2109–2114. https://doi.org/10.1016/j.matpr.2020.09.724

Kumar, Sanjay, Jena, S., Lahoty, V., Paswan, M. K., Sharma, B., Patel, D., Prasad, S. B., &

Kumar Sharma, V. (2019). Experimental investigation on the effect of welding parameters of TIG welded joints using ANOVA. *Materials Today: Proceedings*, *22*, 3181–3189. https://doi.org/10.1016/j.matpr.2020.03.455

Kumar, Sanjay, Singh, P., Patel, D., & Prasad, S. B. (2017). Optimization of TIG welding process parameters using Taguchi's analysis and response surface methodology. *International Journal of Mechanical Engineering and Technology*, *8*(11), 932–941.

Kumar, Subodh, & Shahi, A. S. (2011). Effect of heat input on the microstructure and mechanical properties of gas tungsten arc welded AISI 304 stainless steel joints. *Materials & Design*, *32*(6), 3617–3623.

Lakshminarayanan, A. K., Shanmugam, K., & Balasubramanian, V. (2009). Effect of welding processes on tensile and impact properties, hardness and microstructure of AISI 409M ferritic stainless joints fabricated by duplex stainless steel filler metal. *Journal of Iron and Steel Research, International*, *16*(5), 66–72.

Leonghuat. (2015). *Effects of Mn, P, S, Si & V on the Mechanical Properties of Steel* (pp. 10–11). http://www.leonghuat.com/articles/elements.htm

Lippold, J. C., & Kotecki, D. J. (2005). *Welding metallurgy and weldability of stainless steels*.

Lu, Y., Huang, J. Y., Wang, C., Sun, S., & Lou, J. (2010). Cold welding of ultrathin gold nanowires. *Nature Nanotechnology*, *5*(3), 218–224.

M. Naga Swapna, Anusha Peyyala, B. Purna Chandra Sekhar, & N. Venkata Krishna. (2021). Experimental investigation of GTA Welded SS316L plates using shape memory alloy as a filler material. *Global Journal of Engineering and Technology Advances*, *6*(3), 042–048. https://doi.org/10.30574/gjeta.2021.6.3.0033

M, I. R., & Marpu, R. N. (2012). *Effect of Pulsed Current Tig Welding Parameters on Mechanical Properties of J-Joint Strength of Aa6351*. 1–5.

Maalekian, M. (2007). Effects of alloying elements on electromigration. *Microelectronics Reliability*, *38*(6–8), 1015–1020. https://doi.org/10.1016/S0026-2714(98)00110-3

MakeItFrom.com. (n.d.). *AISI 316 (S31600) Stainless Steel*. https://www.makeitfrom.com/material-properties/AISI-316-S31600-Stainless-Steel

Mandavia, R. B. (2017). *Experimental Investigation of TIG Welding for Stainless Steel using Design of Experiment*. *2*(6), 53–56.

Maneiah, D., Rao, K. P., & Raju, K. B. (2019). Experimental Investigation On Tig Welded Butt Joints Of Aluminium Alloy 6061-T6 To Obtain Tensile Strength. *IOSR Journal of Mechanical and Civil Engineering*, *May*.

Miller Electric Mfg. (2013). Gas Tungsten Arc Welding (GTAW). *Shock*. https://web.archive .org/web/20151208054411/https://www.millerwelds.com/~/media/miller electric/files/ pdf/resources/bookspamphlets/gtawbook.pdf

Mohanavel, V., Ravichandran, M., & Suresh Kumar, S. (2018). Optimization of tungsten inert gas welding parameters to attain maximum impact strength in AA6061 alloy joints using Taguchi Technique. *Materials Today: Proceedings*, *5*(11), 25112–25120. https://doi.org/ 10.1016/j.matpr.2018.10.312

Moi, S. C., Pal, P. K., & Bandyopadhyay, A. (2019). Design optimization of TIG welding process for AISI 316L stainless steel. *International Journal of Recent Technology and Engineering*, *8*(2), 5348–5354. https://doi.org/10.35940/ijrte.B2709.078219

Moi, S. C., Pal, P. K., Bandyopadhyay, A., & Rudrapati, R. (2018). Determination of tungsten inert gas welding input parameters to attain maximum tensile strength of 316L austenitic stainless steel. *Strojnicky Casopis*, *68*(3), 231–248. https://doi.org/10.2478/scjme-2018-0037

Moi, S. C., Rudrapati, R., Pal, P. K., & Bandyopadhyay, A. (2019). Analysis of Impact Behaviour of TIG Weldment by Using Hybrid RSM and CSO. *Strojnicky Casopis*, *69*(4), 105–114. https://doi.org/10.2478/scjme-2019-0046

Moslemi, N., Redzuan, N., Ahmad, N., & Hor, T. N. (2015). Effect of current on characteristic for 316 stainless steel welded joint including microstructure and mechanical properties. *Procedia CIRP*, *26*, 560–564. https://doi.org/10.1016/j.procir.2015.01.010

Msomi, V., & Mabuwa, S. (2020). Experimental investigation of bending and tensile strength of friction stir processed TIG-welded AA5083-H111 joint. *Engineering Research Express*, *2*(4). https://doi.org/10.1088/2631-8695/abbd8b

Nagesh, D. S., & Datta, G. L. (2002). Prediction of weld bead geometry and penetration in shielded metal-arc welding using artificial neural networks. *Journal of Materials Processing Technology*, *123*(2), 303–312. https://doi.org/10.1016/S0924-0136(02)00101-2

Naik, A. B., & Reddy, A. C. (2016). Experimental Analysis of TIG Welding and Comparison between Activated-TIG and TIG on Duplex Stainless Steel (2205). *International Journal of*

Scientific & Engineering Research, *7*, 115–122.

Natrayan, L., Anand, R., & Kumar, S. S. (2020). Optimization of process parameters in TIG welding of AISI 4140 stainless steel using Taguchi technique. *Materials Today: Proceedings*, *37*(Part 2), 1550–1553. https://doi.org/10.1016/j.matpr.2020.07.150

Ondieki, L. N. A. M. C., & Odhong, E. (2021). *Experimental Investigation Of TIG Welding Parameters In Butt- Joint Configuration Of Mild Steel*. *8*(8).

Oxford instruments. (2007). *ARC-MET 8000 SPECTROMETER*. 1–4. https://mfe-is.com/wp-content/uploads/2017/11/Oxford-Instruments_ARC-MET8000.pdf

Panwar, G. S., & Kakirde, A. (2021). *Experimental Investigation of Tungsten Inert Gas Arc Welding Process Parameter of Mild Steel*. *2*, 169–173.

Pardeshi, S. (2020). Parametric Study of the TIG Welding Parameter for SS317L Steel. *International Journal for Research in Applied Science and Engineering Technology*, *8*(11), 64–67. https://doi.org/10.22214/ijraset.2020.32031

Pasupathy, J., & Ravisankar, V. (2013). Parametric Optimization of TIG Welding Parameters using Taguchi Method for Dissimilar Joint. *International Journal of Scientific & Engineering Research*, *4*(11), 25–28.

Patel, A. B., & Patel, S. P. (2014). The effect of activating fluxes in TIG welding by using Anova for SS 321. *International Journal of Engineering Research and Applications*, *4*(5), 41–48.

Patil, S. R., & Waghmare, C. A. (2013). Optimization of MIG welding parameters for improving strength of welded joints. *Int. J. Adv. Engg. Res. Studies/II/IV/July-Sept*, *14*, 16.

Products, S. P. (2019). *TECH TALK_ Back Purging Welds - What and Why*. https://soulpp.com/2019/09/17/tech-talk-back-purging-welds-what-and-why/

Ramachandran, R. (2015). *Analysis and Experimental Investigations of Weld Characteristics for a Tig Welding With Ss316L*. *10*, 9–25.

Rohit, I. J., Ajithraj, R., & Anand, M. D. (2017). Experimental analysis of TIG Welded 304 stainless steel using artificial intelligence tool. *International Journal of Pure and Applied Mathematics*, *116*(22), 365–373.

Ross, P. J. (1996). *Taguchi techniques for quality engineering: loss function, orthogonal experiments, parameter and tolerance design*.

Ruggiero, A., Tricarico, L., Olabi, A. G., & Benyounis, K. Y. (2011). Weld-bead profile and costs optimisation of the CO2 dissimilar laser welding process of low carbon steel and austenitic steel AISI316. *Optics and Laser Technology*, *43*(1), 82–90. https://doi.org/10.1016/j.optlastec.2010.05.008

S. Raissi and R- Eslami Farsani. (2009). *Statistical Process Optimization Through Multi-Response Surface Methodology*. *3*(3), 247–251.

Sagar, P., Gope, D. K., & Chattopadhyaya, S. (2018). Thermal analysis of TIG welded Ti-6Al-4V plates using ANSYS. *IOP Conference Series: Materials Science and Engineering*, *377*(1), 12113.

Saha, M. (2020). Effect of Welding Parameter of Welded Joint of Stainless Steel 304 by TIG Welding. *SSRN Electronic Journal*, *March*. https://doi.org/10.2139/ssrn.3643709

Salehpour-Oskouei, F., Nematifard, V., Marami, G., & Afkar, A. (2021). Experimental investigation of tungsten inert gas welding input parameters effects on mechanical characteristics. *International Journal of Engineering, Transactions B: Applications*, *34*(2), 564–571. https://doi.org/10.5829/IJE.2021.34.02B.30

Satputaley, S. S., Waware, Y., Ksheersagar, K., Jichkar, Y., & Khonde, K. (2021). Experimental investigation on effect of TIG welding process on chromoly 4130 and aluminum 7075-T6. *Materials Today: Proceedings*, *41*, 991–994.

Sayed, A. R., Kumbhare, Y. V, Ingole, N. G., Dhengale, P. T., & Dhanorkar, N. R. (2019). A Review Study of Dissimilar Metal Welds of Stainless Steel and Mild Steel by TIG Welding Process. *Int. J. Res. Appl. Sci. Eng. Technol.*, *7*, 370–373.

Senthil Kumar, T., Balasubramanian, V., & Sanavullah, M. Y. (2007). Influences of pulsed current tungsten inert gas welding parameters on the tensile properties of AA 6061 aluminium alloy. *Materials and Design*, *28*(7), 2080–2092. https://doi.org/10.1016/j.matdes.2006.05.027

Singh, A. K., Dey, V., & Rai, R. N. (2017). Techniques to improveweld penetration in TIG welding (A review). *Materials Today: Proceedings*, *4*(2), 1252–1259. https://doi.org/10.1016/j.matpr.2017.01.145

Singh, P., & Singh, R. (2014). Experimental Investigation of Deposition Rate in Tig Welding of Grade 304 Stainless Steel. *International Journal of Advanced Engineering Technology E-*

Int J Adv Engg Tech V/Issue II, *3*, 31–33.

Singh, Sewa, Chawla, V., & Brar, G. (2019). The performance of tig welded similar and dissimilar weldments under tensile loading: an experimental investigation. *International Journal of Mechanical and Production Engineering Research and Development*, *9*(4), 1015–1026. https://doi.org/10.24247/ijmperdaug2019103

Singh, Surjeet, Soni, G., & Shivesh, C. (2016). *International Journal Of Engineering Sciences & Research Technology Experimental Investigation Of Tensile Strength Of Aa 6082 Using Tig Welding At Different Process Parameters*.

SMI. (2022). *The Challenges of Welding Stainless Steel | Steelmor*. https://www.steelmor.co.za/challenges-welding-stainless-steel/

Taban, E., Deleu, E., Dhooge, A., & Kaluc, E. (2007). Gas metal arc welding of modified X2CrNi12 ferritic stainless steel. *Kovove Materialy-Metallic Materials*, *45*(2), 67–74.

Trewiler, G. E. (2006). *Fusion welding method and welded article*. Google Patents.

Unibraze corporation. (2000). *Er70S-3 Carbon Steel Welding Wire*. 1–2. http://www.unibraze.com/DataSheets/Data70S-3.pdf

Uthayakumar, M., Balasubramanian, V., Rani, A. M. A., & Hadzima, B. (2018). Effects of welding on the fatigue behaviour of commercial aluminum AA-1100 joints. *IOP Conference Series: Materials Science and Engineering*, *346*(1), 12065.

Vennimalai Rajan, A., Mathalai Sundaram, D. C., Vembathurajesh, A., Nagaraja, R., Chakravarthy Samy Durai, J., & Nagaraja, R. (2020). Analysis and Experimental investigation of Weld Characteristics for TIG Welding in Dissimilar Metals. *International Journal Of Recent Trends In Engineering & Research*, *Special Is*, 278–287. https://doi.org/10.23883/ijrter.conf.20200315.039.aisyd

Wahule, A., & Wasankar, K. (2018). Multi-response optimization of process parameters of TIG welding for dissimilar metals (SS-304 and Fe-410) using grey relational analysis. *Int. Res. J. Eng. Technol*, *5*(6), 986–993.

Walak, S. E., Cronin, M. J., & Grobstein, T. (1992). *Heat pipe fatigue test specimen: Metallurgical evaluation*.

Weman, K. (2011). *Welding processes handbook*. Elsevier.

APPENDICES

Appendix 1: Tensile Test of Stress-Strain Graph for Similar and Dissimilar Weld Metal

EN-02-Metallic materials-Tensile test-2

(Test data record sheet)

Sample No.	SS1	Test Standard	ASTM
Laboratory	Ethiopian Technical Institute	Customer	student
Temperature		Tester	
Humidity		Checker	
Test Date	06/04/2022		

No.	width	thicknes	Lo	Fm	FeH	FeL	Fp0.2	Ft1.0	Lu
	mm	mm	mm	kN	kN	kN	kN	kN	mm
1	12.5	3	200	19.5	9.2	8.74	0.0	0.0	
No.	A	Rm	ReH	ReL	Rp0.2	Rt1.0			
	%	MPa	MPa	MPa	MPa	MPa			
1	100.0	502	245	233	0	0			

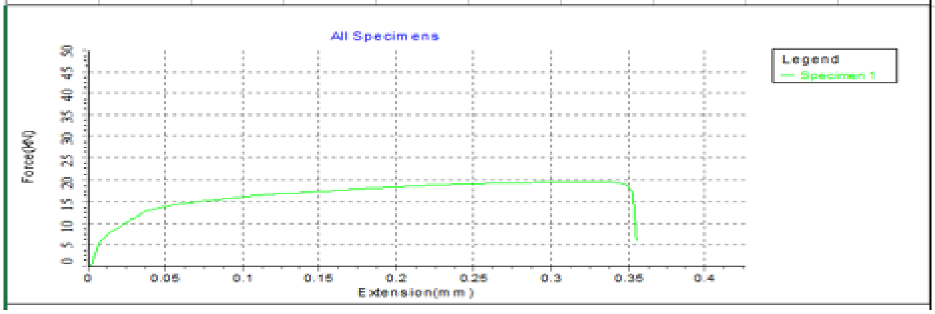

EN-02-Metallic materials-Tensile test-2

(Test data record sheet)

Sample No.	DS3	Test Standard	ASTM
Laboratory	ETVI	Customer	Student
Temperature		Tester	
Humidity		Checker	
Test Date	06/04/2022		

No.	width	thicknes	Lo	Fm	FeH	FeL	Fp0.2	Ft1.0	Lu
	mm	mm	mm	kN	kN	kN	kN	kN	mm
1	12.5	3	200	17.25	0.0	0	0.0	0.0	
No.	A	Rm	ReH	ReL	Rp0.2	Rt1.0			
	%	MPa	MPa	MPa	MPa	MPa			
1	100.0	460							

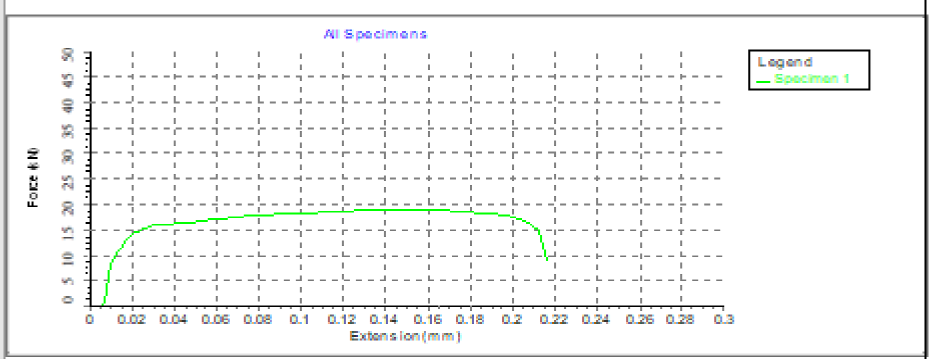

Appendix 2: DOE Minitab software and Taguchi L16 orthogonal array design

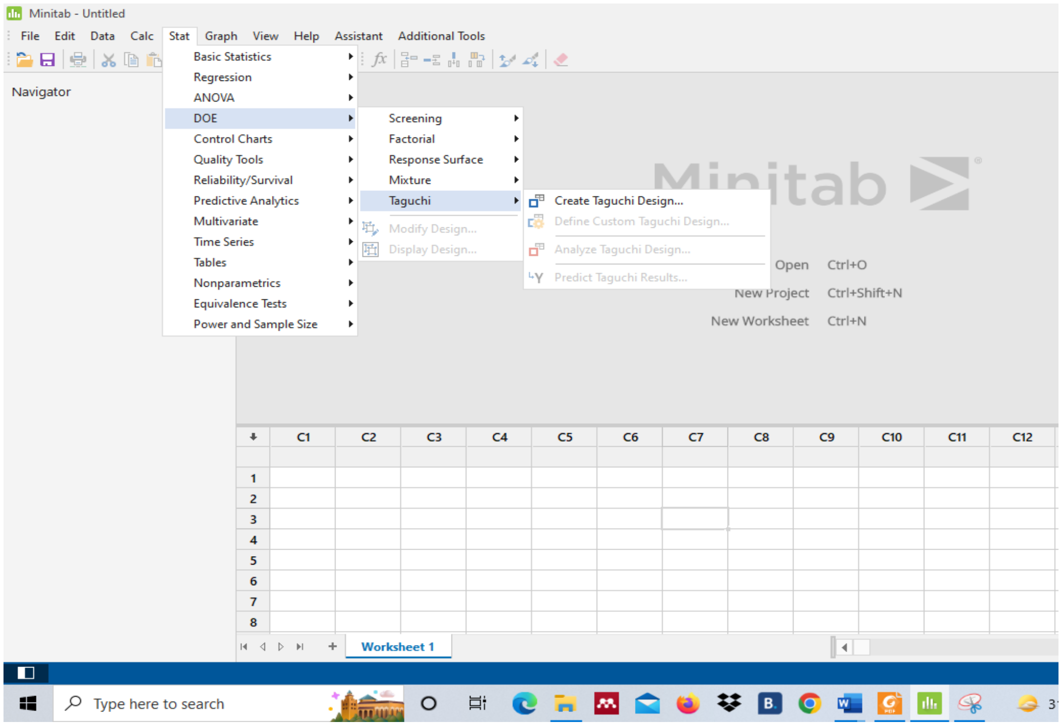

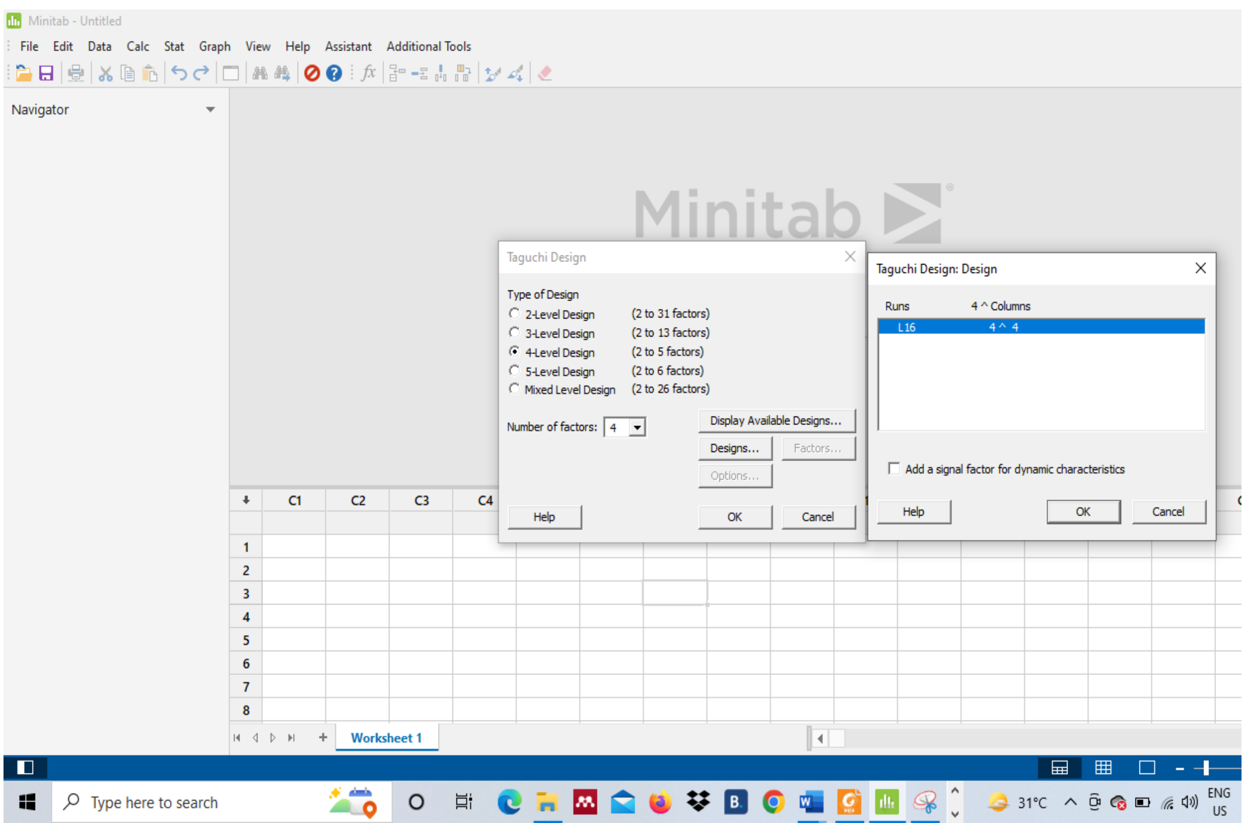

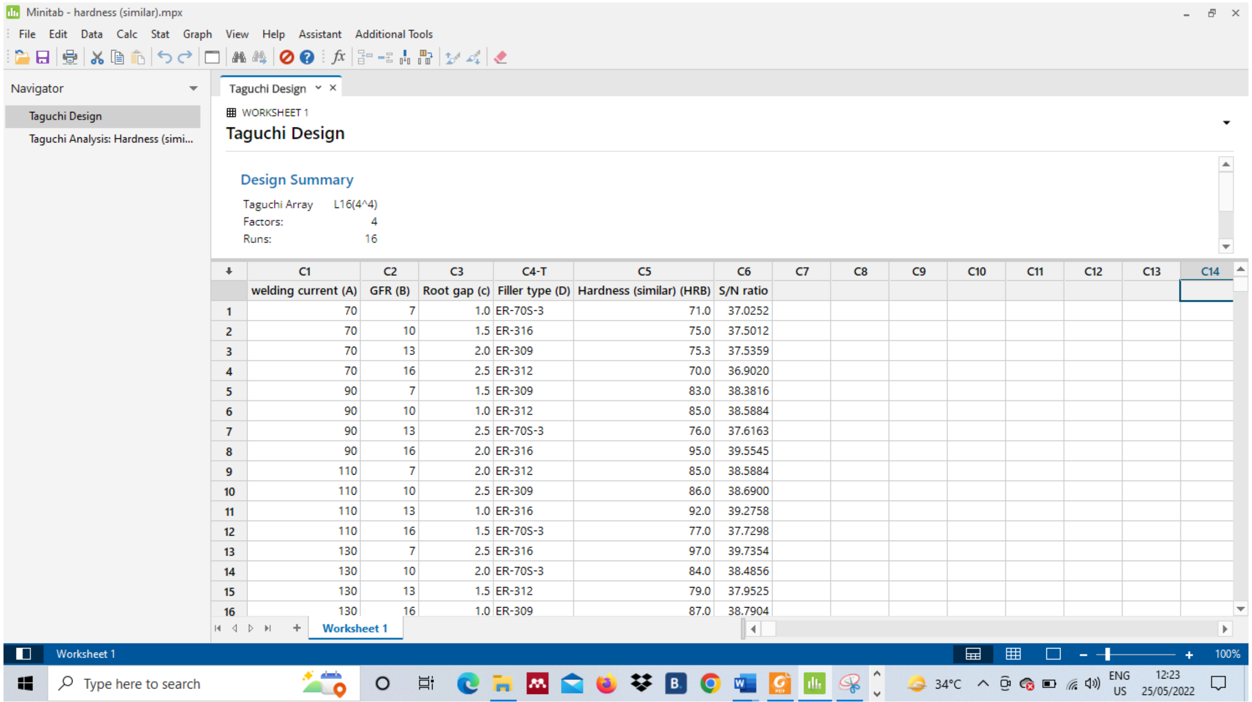

Minitab - hardness (similar).mpx

Taguchi Design

Design Summary

Taguchi Array	L16(4^4)
Factors:	4
Runs:	16

	C1 welding current (A)	C2 GFR (B)	C3 Root gap (c)	C4-T Filler type (D)	C5 Hardness (similar) (HRB)	C6 S/N ratio
1	70	7	1.0	ER-70S-3	71.0	37.0252
2	70	10	1.5	ER-316	75.0	37.5012
3	70	13	2.0	ER-309	75.3	37.5359
4	70	16	2.5	ER-312	70.0	36.9020
5	90	7	1.5	ER-309	83.0	38.3816
6	90	10	1.0	ER-312	85.0	38.5884
7	90	13	2.5	ER-70S-3	76.0	37.6163
8	90	16	2.0	ER-316	95.0	39.5545
9	110	7	2.0	ER-312	85.0	38.5884
10	110	10	2.5	ER-309	86.0	38.6900
11	110	13	1.0	ER-316	92.0	39.2758
12	110	16	1.5	ER-70S-3	77.0	37.7298
13	130	7	2.5	ER-316	97.0	39.7354
14	130	10	2.0	ER-70S-3	84.0	38.4856
15	130	13	1.5	ER-312	79.0	37.9525
16	130	16	1.0	ER-309	87.0	38.7904

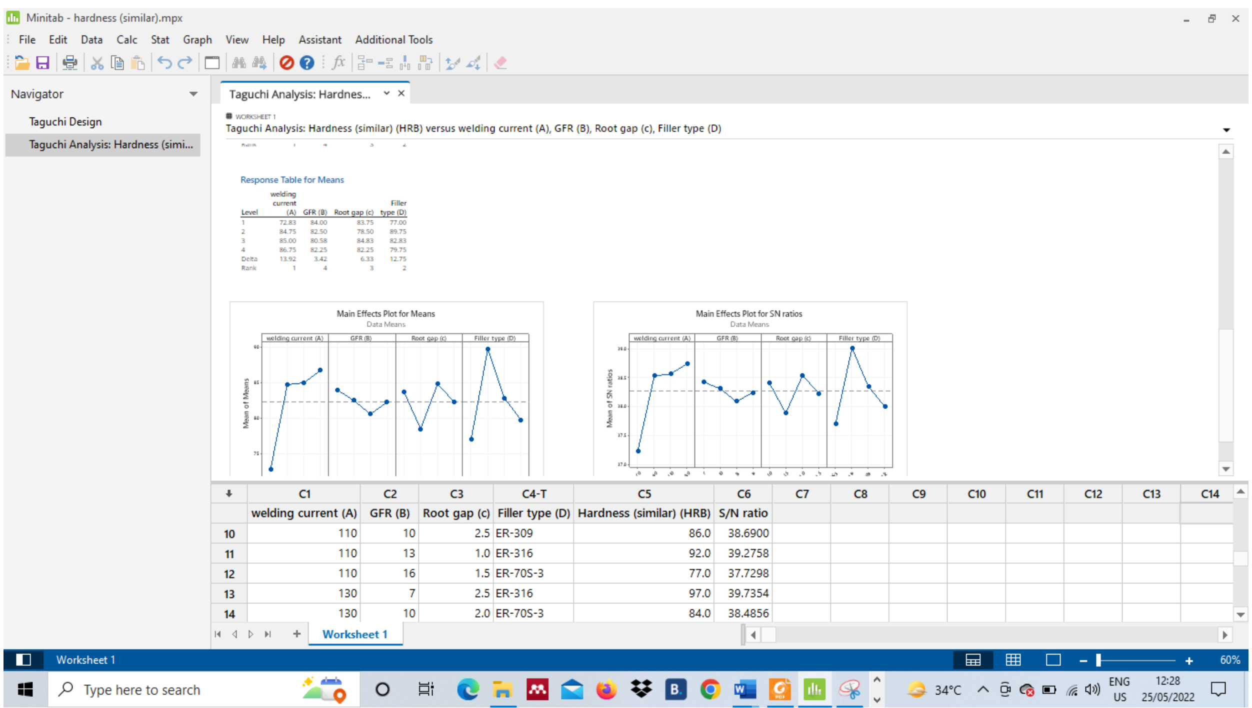

Taguchi Analysis: Hardness (similar) (HRB) versus welding current (A), GFR (B), Root gap (c), Filler type (D)

Response Table for Means

Level	welding current (A)	GFR (B)	Root gap (c)	Filler type (D)
1	72.83	84.00	83.75	77.00
2	84.75	82.50	78.50	89.75
3	85.00	80.58	84.83	82.83
4	86.75	82.25	82.25	79.75
Delta	13.92	3.42	6.33	12.75
Rank	1	4	3	2

	C1 welding current (A)	C2 GFR (B)	C3 Root gap (c)	C4-T Filler type (D)	C5 Hardness (similar) (HRB)	C6 S/N ratio
10	110	10	2.5	ER-309	86.0	38.6900
11	110	13	1.0	ER-316	92.0	39.2758
12	110	16	1.5	ER-70S-3	77.0	37.7298
13	130	7	2.5	ER-316	97.0	39.7354
14	130	10	2.0	ER-70S-3	84.0	38.4856

Appendix 3: Desirability function Analysis for similar and dissimilar metals

Similar welding optimization

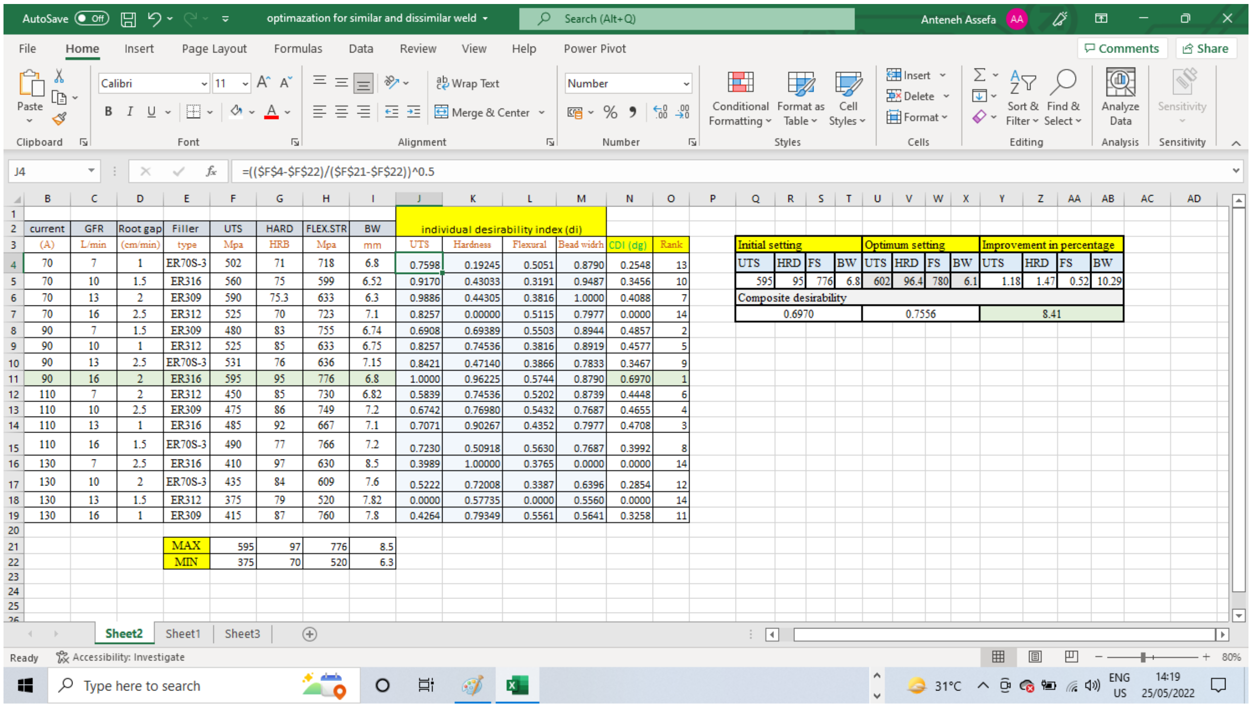

J4: =((F4-F22)/(F21-F22))^0.5

current	GFR	Root gap	Filler	UTS	HARD	FLEX.STR	BW	individual desirability index (di)					
(A)	L/min	(cm/min)	type	Mpa	HRB	Mpa	mm	UTS	Hardness	Flexural	Bead widrh	CDI (dg)	Rank
70	7	1	ER70S-3	502	71	718	6.8	0.7598	0.19245	0.5051	0.8790	0.2548	13
70	10	1.5	ER316	560	75	599	6.52	0.9170	0.43033	0.3191	0.9487	0.3456	10
70	13	2	ER309	590	75.3	633	6.3	0.9886	0.44305	0.3816	1.0000	0.4088	7
70	16	2.5	ER312	525	70	723	7.1	0.8257	0.00000	0.5115	0.7977	0.0000	14
90	7	1.5	ER309	480	83	755	6.74	0.6908	0.69389	0.5503	0.8944	0.4857	2
90	10	1	ER312	525	85	633	6.75	0.8257	0.74536	0.3816	0.8919	0.4577	5
90	13	2.5	ER70S-3	531	76	636	7.15	0.8421	0.47140	0.3866	0.7833	0.3467	9
90	16	2	ER316	595	95	776	6.8	1.0000	0.96225	0.5744	0.8790	0.6970	1
110	7	2	ER312	450	85	730	6.82	0.5839	0.74536	0.5202	0.8739	0.4448	6
110	10	2.5	ER309	475	86	749	7.2	0.6742	0.76980	0.5432	0.7687	0.4655	4
110	13	1	ER316	485	92	667	7.1	0.7071	0.90267	0.4352	0.7977	0.4708	3
110	16	1.5	ER70S-3	490	77	766	7.2	0.7230	0.50918	0.5630	0.7687	0.3992	8
130	7	2.5	ER316	410	97	630	8.5	0.3989	1.00000	0.3765	0.0000	0.0000	14
130	10	2	ER70S-3	435	84	609	7.6	0.5222	0.72008	0.3387	0.6396	0.2854	12
130	13	1.5	ER312	375	79	520	7.82	0.0000	0.57735	0.0000	0.5560	0.0000	14
130	16	1	ER309	415	87	760	7.8	0.4264	0.79349	0.5561	0.5641	0.3258	11
			MAX	595	97	776	8.5						
			MIN	375	70	520	6.3						

Initial setting				Optimum setting				Improvement in percentage			
UTS	HRD	FS	BW	UTS	HRD	FS	BW	UTS	HRD	FS	BW
595	95	776	6.8	602	96.4	780	6.1	1.18	1.47	0.52	10.29
Composite desirability											
0.6970				0.7556				8.41			

Dissimilar welding optimization

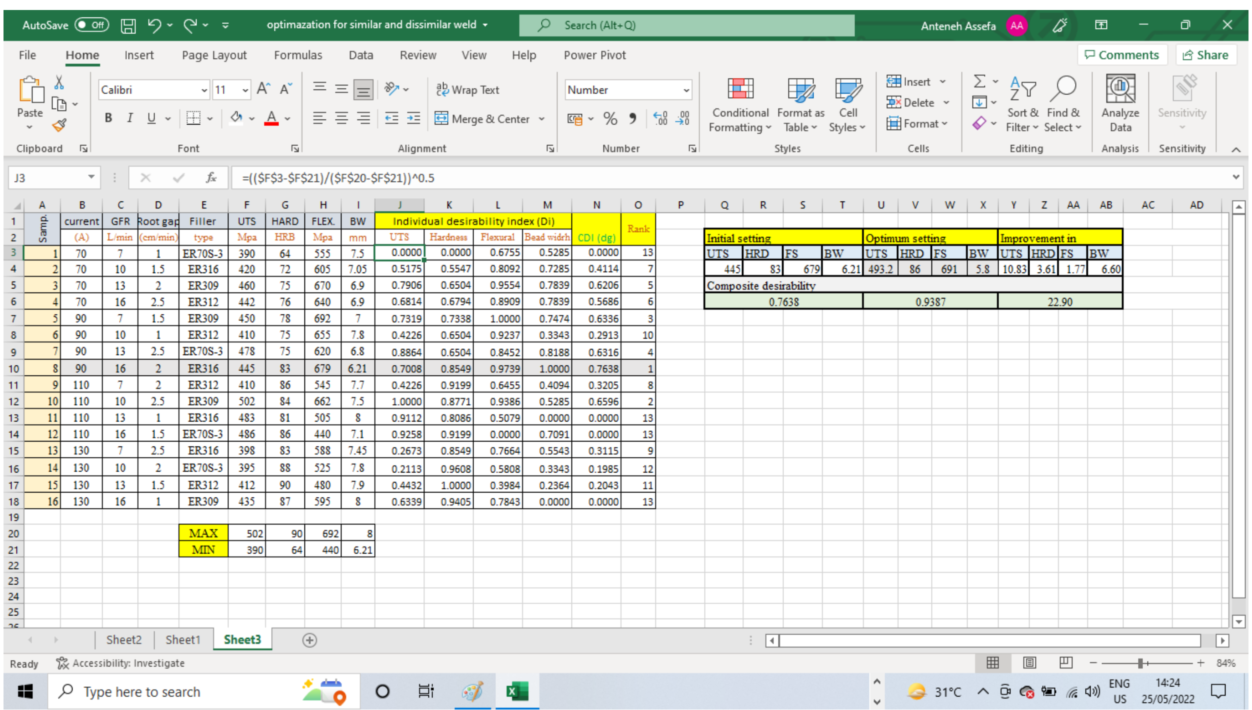

J3: =((F3-F21)/(F20-F21))^0.5

Samp.	current	GFR	Root gap	Filler	UTS	HARD	FLEX.	BW	Individual desirability index (Di)					Rank
	(A)	L/min	(cm/min)	type	Mpa	HRB	Mpa	mm	UTS	Hardness	Flexural	Bead widrh	CDI (dg)	
1	70	7	1	ER70S-3	390	64	555	7.5	0.0000	0.0000	0.6755	0.5285	0.0000	13
2	70	10	1.5	ER316	420	72	605	7.05	0.5175	0.5547	0.8092	0.7285	0.4114	7
3	70	13	2	ER309	460	75	670	6.9	0.7906	0.6504	0.9554	0.7839	0.6206	5
4	70	16	2.5	ER312	442	76	640	6.9	0.6814	0.6794	0.8909	0.7839	0.5686	6
5	90	7	1.5	ER309	450	78	692	7	0.7319	0.7338	1.0000	0.7474	0.6336	3
6	90	10	1	ER312	410	75	655	7.8	0.4226	0.6504	0.9237	0.3343	0.2913	10
7	90	13	2.5	ER70S-3	478	75	620	6.8	0.8864	0.6504	0.8452	0.8188	0.6316	4
8	90	16	2	ER316	445	83	679	6.21	0.7008	0.8549	0.9739	1.0000	0.7638	1
9	110	7	2	ER312	410	86	545	7.7	0.4226	0.9199	0.6455	0.4094	0.3205	8
10	110	10	2.5	ER309	502	84	662	7.5	1.0000	0.8771	0.9386	0.5285	0.6596	2
11	110	13	1	ER316	483	81	505	8	0.9112	0.8086	0.5079	0.0000	0.0000	13
12	110	16	1.5	ER70S-3	486	86	440	7.1	0.9258	0.9199	0.0000	0.7091	0.0000	13
13	130	7	2.5	ER316	398	83	588	7.45	0.2673	0.8549	0.7664	0.5543	0.3115	9
14	130	10	2	ER70S-3	395	88	525	7.8	0.2113	0.9608	0.5808	0.3343	0.1985	12
15	130	13	1.5	ER312	412	90	480	7.9	0.4432	1.0000	0.3984	0.2364	0.2043	11
16	130	16	1	ER309	435	87	595	8	0.6339	0.9405	0.7843	0.0000	0.0000	13
				MAX	502	90	692	8						
				MIN	390	64	440	6.21						

Initial setting				Optimum setting				Improvement in			
UTS	HRD	FS	BW	UTS	HRD	FS	BW	UTS	HRD	FS	BW
445	83	679	6.21	493.2	86	691	5.8	10.83	3.61	1.77	6.60
Composite desirability											
0.7638				0.9387				22.90			

Appendix 4: EQOUTIP 2 Portable hardness testing machine & Vickers indenter

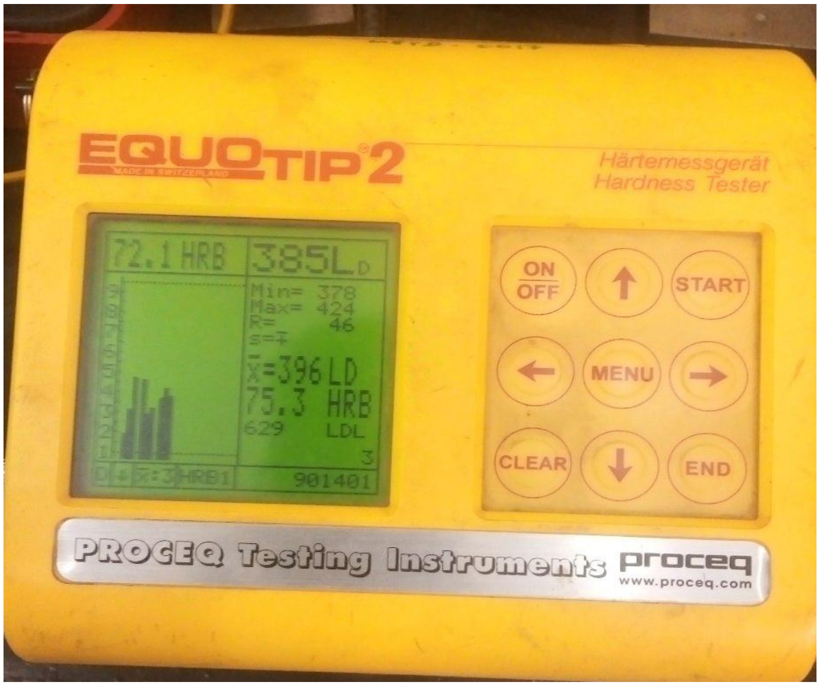

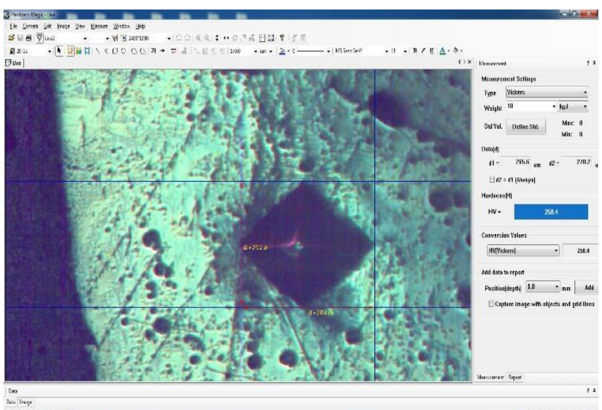

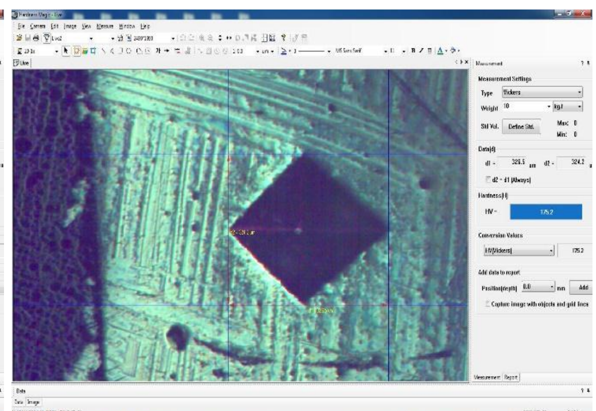

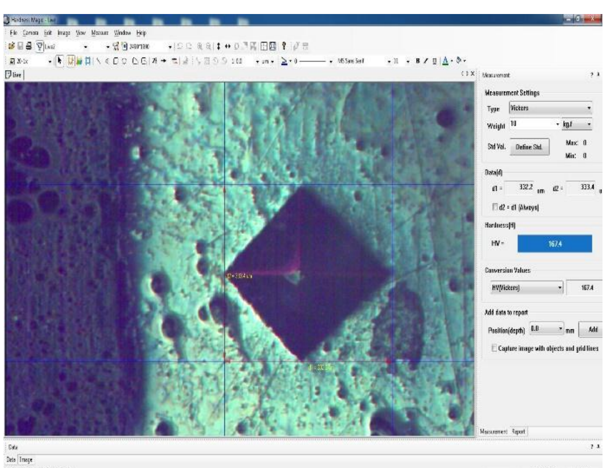

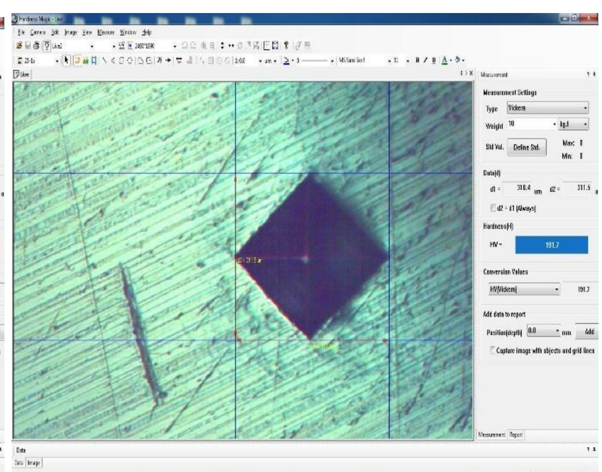

Appendix 5: NDT Testing apparatus

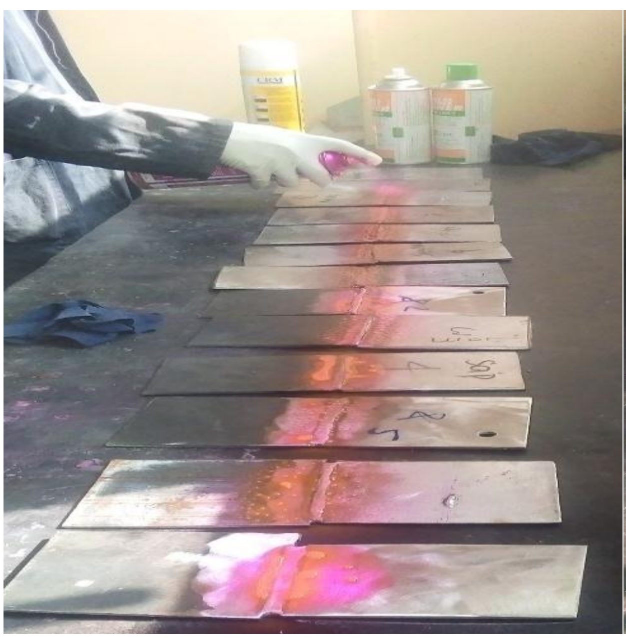

Appendix 6: Universal testing machine used for tensile and flexural strength.

@ Ethiopian conformity assessment enterprise & **@ Ethiopian Technical institute**